

CRITICAL CARE

Characteristic pattern of pleural effusion in electrical impedance tomography images of critically ill patients

T. Becher*, M. Bußmeyer, I. Lautenschläger, D. Schädler, N. Weiler and I. Frerichs

Department of Anaesthesiology and Intensive Care Medicine, University Medical Centre Schleswig-Holstein, Campus Kiel, Kiel, Germany

*Corresponding author. E-mail: tobias.becher@uksh.de

Abstract

Background: Electrical impedance tomography (EIT) is increasingly used for continuous monitoring of ventilation in intensive care patients. Clinical observations in patients with pleural effusion show an increase in out-of-phase impedance changes. We hypothesised that out-of-phase impedance changes are a typical EIT finding in patients with pleural effusion and could be useful in its detection.

Methods: We conducted a prospective observational study in intensive care unit patients with and without pleural effusion. In patients with pleural effusion, EIT data were recorded before, during, and after unilateral drainage of pleural effusion. In patients with no pleural effusion, EIT data were recorded without any intervention. EIT images were separated into four quadrants of equal size. We analysed the sum of out-of-phase impedance changes in the affected quadrant in patients with pleural effusion before, during, and after drainage and compared it with the sum of out-of-phase impedance changes in the dorsal quadrants of patients without pleural effusion.

Results: We included 20 patients with pleural effusion and 10 patients without pleural effusion. The median sum of out-of-phase impedance changes was 70 (interquartile range 49–119) arbitrary units (a.u.) in patients with pleural effusion before drainage, 25 (12–46) a.u. after drainage ($P < 0.0001$) and 11 (6–17) a.u. in patients without pleural effusion ($P < 0.0001$ vs pleural effusion before drainage). The area under the receiver operating characteristics curve was 0.96 (95% limits of agreement 0.91–1.01) between patients with pleural effusion before drainage and those without pleural effusion.

Conclusions: In patients monitored with EIT, the presence of out-of-phase impedance changes is highly suspicious of pleural effusion and should trigger further examination.

Keywords: critical care; pleural effusion; thoracocentesis; tomography

Editor's key points

- Electrical impedance tomography has several potential applications in patients with respiratory failure.
- In this small study, differences in out-of-phase impedance on electrical impedance tomography were found between patients with and without a pleural effusion.
- There were also differences before and after drainage of an effusion.
- Electrical impedance tomography could be useful in detecting pleural effusion in intensive care patients.

Electrical impedance tomography (EIT) is a relatively new, non-invasive, and radiation-free imaging modality which can serve for a variety of purposes in critically ill patients.¹ Possible clinical applications include assessment of ventilation distribution,^{2,3} detection of alveolar recruitment, derecruitment, overdistension,^{4,5} tidal recruitment,⁶ assessment of regional respiratory mechanics in controlled mechanical ventilation,⁷ assisted spontaneous breathing,⁸ quantification of ventilation heterogeneity,^{9,10} and individual adjustment of ventilator settings to improve lung-protective ventilation.¹¹

EIT is increasingly used in patients with or at risk for respiratory failure.¹² Typically, lung aeration during inspiration leads to an increase in impedance in the ventilated lung areas, followed by a similar decrease in impedance during expiration. However, in some patients, regional out-of-phase impedance changes can be observed. These are characterised by a seemingly paradoxical decrease in impedance in some areas of the EIT image during inspiration, followed by an increase in impedance during expiration (Fig. 1).

Clinical observations in patients with pleural effusion and previous studies^{13,14} suggest that out-of-phase impedance changes may occur when areas of high ventilation-related impedance change, such as the lungs,¹⁵ are in close proximity to areas of low ventilation-related impedance change, such as the heart or fluid accumulations. This is most likely caused by an overshoot phenomenon introduced by the algorithms used for EIT image reconstruction^{1,16,17} that may occur under these circumstances.¹⁴

This is typically the case in patients with pleural effusion (Fig. 2). While previous studies have assessed the effects of pleural aspiration on lung re-aeration and re-ventilation,¹⁸ to our knowledge the diagnostic value of out-of-phase impedance changes in the detection of pleural effusion has not been investigated.

We hypothesised that out-of-phase impedance changes in the dependent image quadrants are a typical finding in patients with pleural effusion and could be useful for the detection of pleural effusion in critically ill patients undergoing monitoring with EIT.

Methods

We conducted an observational study in three mixed surgical and medical intensive care units (ICUs). Patients were enrolled between January 2015 and June 2016.

EIT monitoring was initiated as per clinical decision by the attending intensivist in patients with acute respiratory failure or who were considered as being at risk for developing acute respiratory failure, taking into account clinical parameters such as gas exchange and impairment of respiratory mechanics.

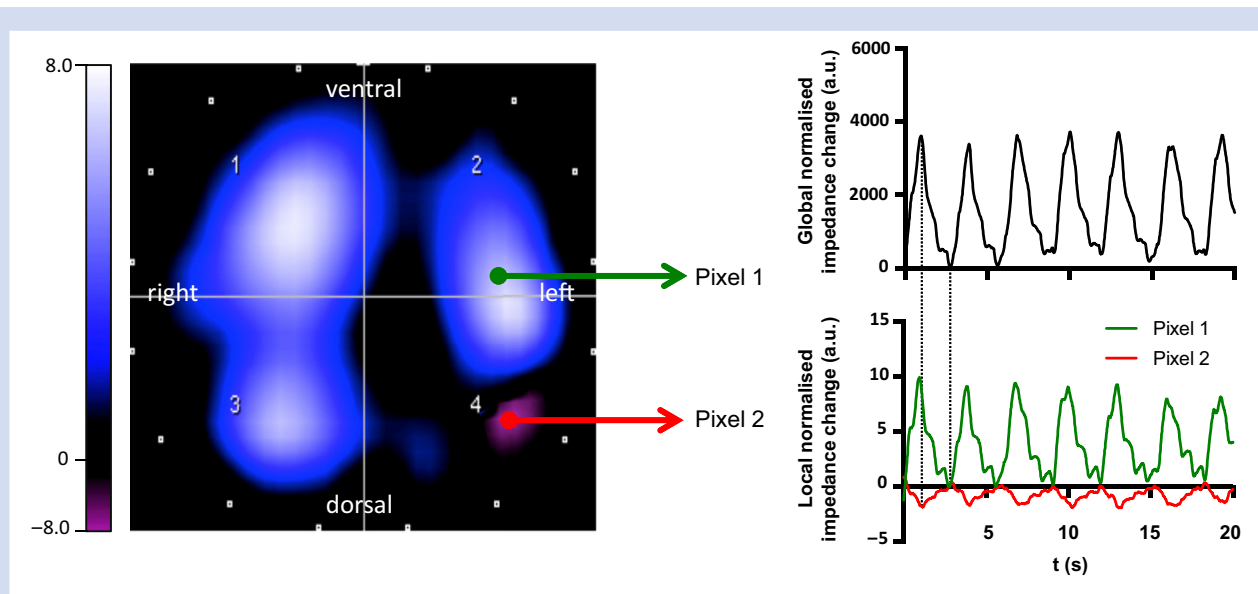


Fig 1. In-phase (pixel 1) and out-of-phase (pixel 2) impedance changes in a representative patient suffering from left-sided pleural effusion. Left: tidal image, illustrating the pixel differences between the time points of end-expiration (global impedance minimum) and end-inspiration (global impedance maximum). Out-of-phase impedance changes are shown in purple colour. Right: time course of global (top) and local (bottom) relative impedance changes for the same patient over a period of 20 s. Pixel 1 shows a typical 'in-phase' behaviour with the global electrical impedance tomography (EIT) signal, whereas pixel 2 shows 'out-of-phase' behaviour that may be a typical finding in patients with pleural effusion. a.u., arbitrary units.

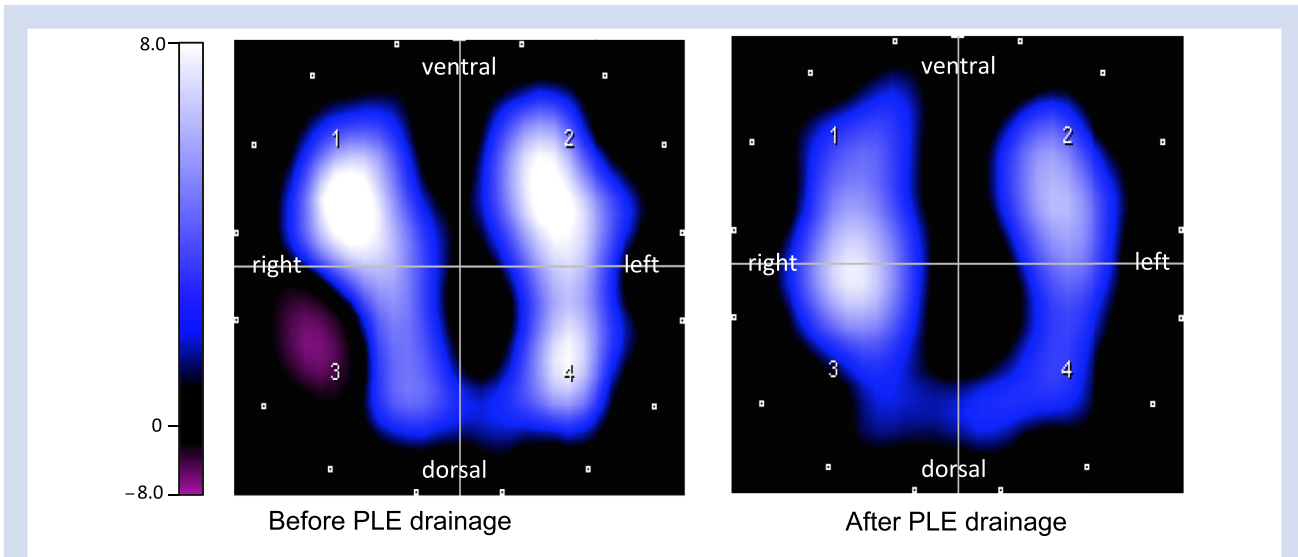


Fig 2. Electrical impedance tomography (EIT) images of tidal ventilation in a patient with pleural effusion in the right posterior quadrant before (left) and after (right) the placement of a pigtail catheter and aspiration of 500 ml of pleural effusion. Out-of-phase impedance changes (purple colour) are evident before pleural aspiration (left). PLE, pleural effusion.

All patients were screened with ultrasound for evidence of pleural effusion on a daily basis. Ultrasound examinations were carried out according to routine clinical practice by the intensivist in charge. In general, this involved systematic bilateral assessment of the juxtadiaphragmatic pleural spaces with a 4 MHz convex probe. The decision to initiate drainage was based solely on the results of the ultrasound examination and on the attending intensivist's clinical judgement, who decided whether the sonographically estimated size of the effusion was large enough to allow safe thoracocentesis. EIT data were not taken into account for this decision.

All consecutive patients aged more than 18 yr with EIT monitoring and a clinical indication for drainage were enrolled in the pleural effusion group. Patients aged more than 18 yr with EIT monitoring in whom presence of a pleural effusion had been excluded sonographically by an experienced sonographer or who had undergone computed tomography (CT) for other reasons on the same day and showed no signs of pleural effusion, were enrolled in the control group.

Patients were excluded if there was uncertainty regarding the presence of pleural effusion, if a sonographically confirmed effusion was too small for drainage, or if the attending intensivist decided against drainage for other clinical reasons (Fig. 3).

Because of the observational study design, a waiver of informed consent was granted by the Ethics Committee of the Medical Faculty of the Christian-Albrechts-University Kiel (D513/13).

In the pleural effusion group, $\text{PaO}_2/\text{FiO}_2$ ratio and PaCO_2 were obtained from the last blood gas sample obtained before pleural drainage for baseline assessment and from the first blood gas sample obtained after pleural drainage for comparison with baseline. In the control group, $\text{PaO}_2/\text{FiO}_2$ ratio and PaCO_2 were obtained from the last blood gas sample before the start of recording of EIT data. Basic patient characteristics, such as age, height, weight, and simplified acute physiology (SAPS) II score were extracted from the electronic patient record.

Recording of EIT data

EIT data were acquired at a scan rate of 50 images per second using the PulmoVista 500 device (Dräger, Lübeck, Germany). The 16 electrode belt was attached to the patient's chest circumference at the level of the 4th–5th intercostal space, measured in the parasternal line.

In the pleural effusion group, a pigtail catheter for pleural drainage was introduced according to routine clinical practice by the ICU physician in charge. Before the start of pleural effusion drainage, EIT data were recorded during 1 min of normal tidal breathing or ventilation. EIT data were recorded continuously during drainage and 1 min after completion of drainage.

For insertion of the pigtail catheter, patients were positioned in the supine, semi recumbent, or sitting position, as indicated by the physician in charge. The patient's body position remained unchanged during the drainage procedure.

In the control group, 1 min of normal tidal breathing was recorded with EIT without any intervention with the patient in the supine or semi recumbent position.

Analysis of EIT data

EIT data were analysed off-line using the EIT Data Analysis Tool 6.1 (Dräger) and Microsoft Excel 2010 (Microsoft, Seattle, WA, USA). The beginning and end of inspiration and expiration were detected from the global impedance waveform using the software's breath detection algorithm. The relative impedance values were calculated for every time point and image pixel as the difference between the current impedance and the reference impedance, divided by the reference impedance. Because it is a ratio, the resulting pixel values are commonly expressed in arbitrary units (a.u.)¹. For every image pixel, we calculated the difference between the pixel value at end-inspiration and the preceding end-expiration. These pixel values were displayed as a tidal variation image. For data

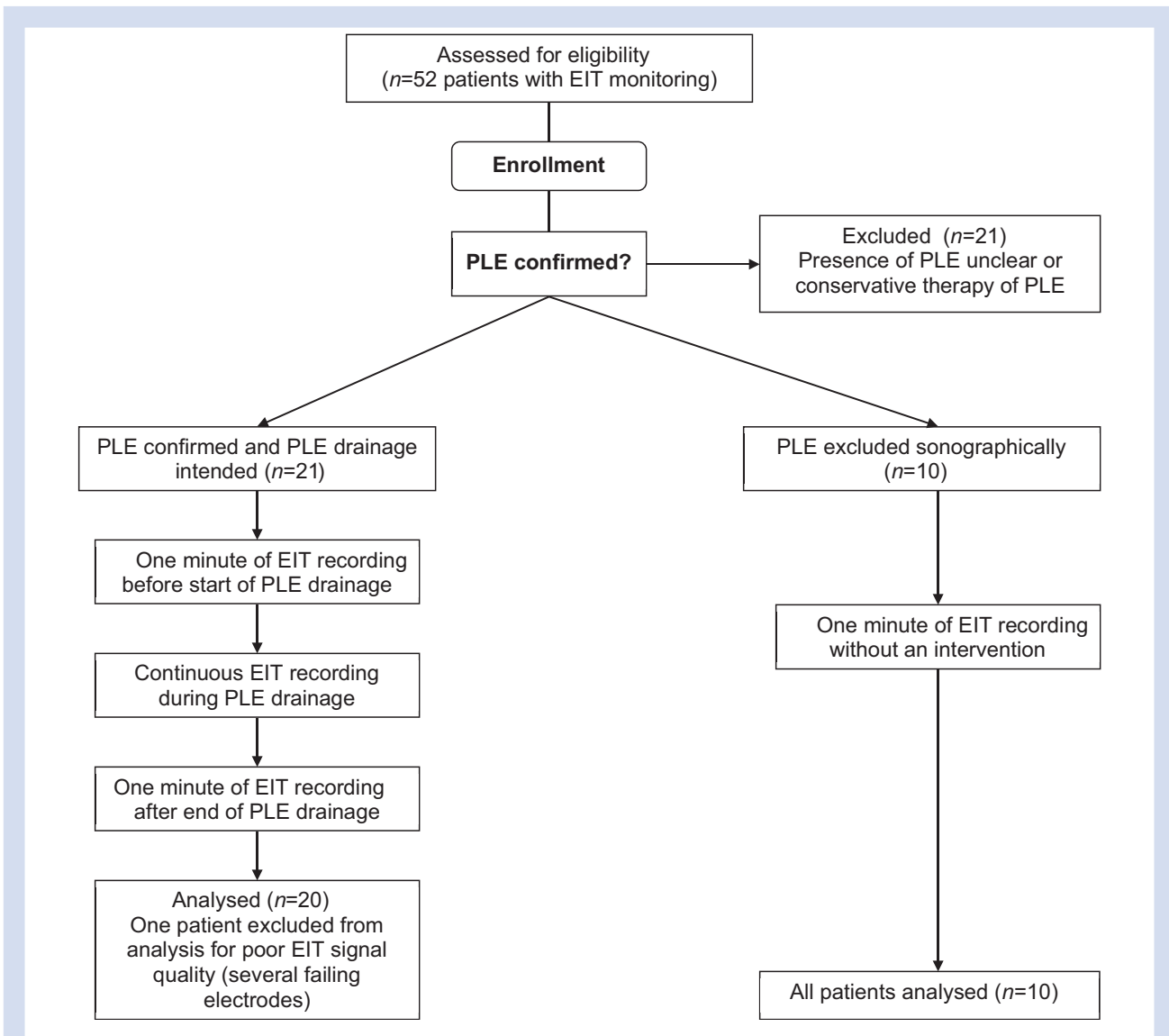


Fig 3. Flow chart of patients. Patients undergoing monitoring with electrical impedance tomography (EIT) were screened for presence of pleural effusion (PLE) requiring intervention and subsequently assigned to the PLE group if PLE requiring intervention was present or to the control group if presence of PLE was excluded by lung ultrasound or computed tomography. If presence of PLE remained unclear or a small PLE was detected without the need for an intervention, patients were excluded from the analysis.

analysis, the tidal image was divided into four quadrants of equal size, comprising 16×16 image pixels each (Fig. 1). The overall sum of tidal impedance changes was calculated for the whole image and each quadrant. To calculate the sum of in-phase impedance changes, we included only the values from pixels with tidal impedance changes >0 . For out-of-phase impedance changes, only values from pixels with tidal impedance changes <0 were included.

In patients with pleural effusion, the sums of in-phase and out-of-phase impedance changes were calculated for the affected dorsal quadrants. In control patients, the sums of in-phase and out-of-phase impedance changes were calculated for both dorsal quadrants separately. For graphical representation (Fig. 5) and to facilitate visual comparison of results with in-phase impedance changes (Fig. 4), the resulting sums of

out-of-phase impedance changes in the affected quadrants were multiplied with a factor of -1 .

In patients with pleural effusion, the changes in end-expiratory lung impedance (EELI) in comparison with baseline (before start of drainage) were assessed after 25%, 50%, 75%, and 100% of drainage for both the dorsal lung quadrant on the side of drainage ('affected side') and the contralateral lung quadrant ('unaffected side').

Statistical analysis

Statistical analysis was performed using GraphPad Prism 6.0 (GraphPad Software, La Jolla, CA, USA). Sample size was chosen to detect a 50% difference in out-of-phase impedance changes between the pleural effusion group and the control

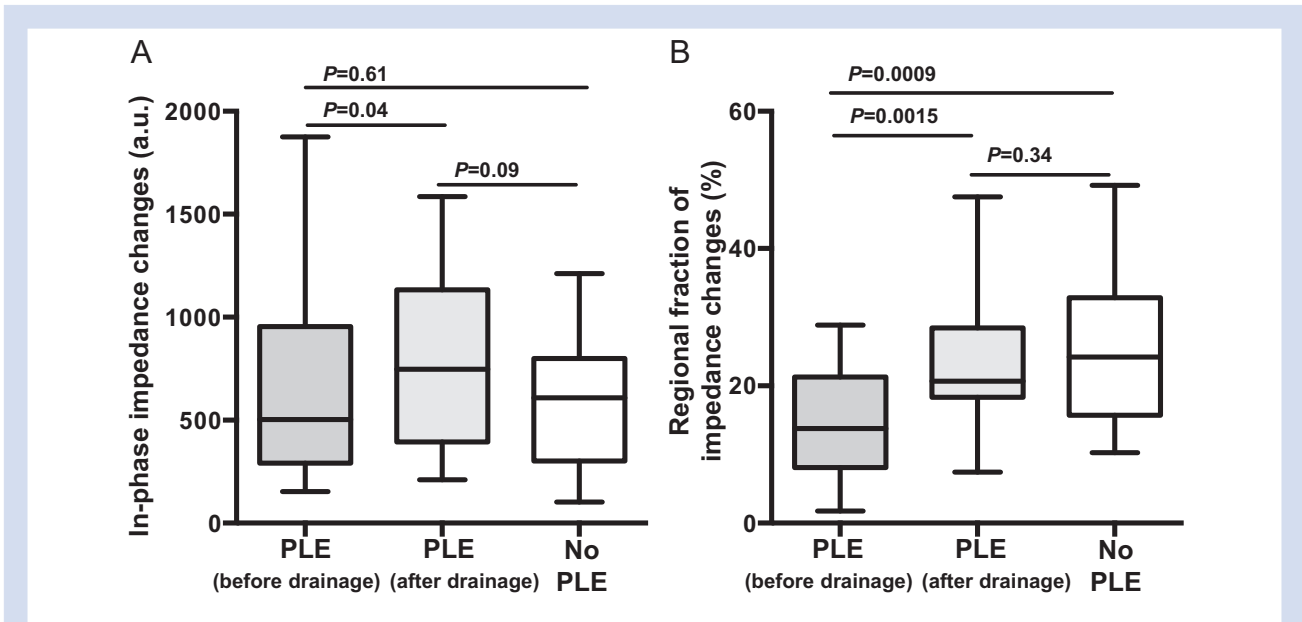


Fig 4. (A) Sum of in-phase impedance changes in the affected lung quadrant of patients with pleural effusion (PLE) before and after drainage and in the dorsal lung quadrants of control patients, expressed in arbitrary units (a.u.). (B) Percentage of impedance changes in the affected lung quadrants of patients with PLE before and after drainage and in the dorsal lung quadrants of control patients.

group with statistical power of 0.8 and $\alpha=0.05$. All data sets were tested for normal distribution with the D’Agostino Pearson omnibus normality test. Results are reported as mean (standard deviation) for normally distributed variables and as median (25th–75th percentile) for not normally distributed variables. Group comparisons were performed by the independent samples t-test or the paired t-test for normally distributed variables and by the Mann–Whitney test or Wilcoxon matched pairs test for not normally distributed

variables. The diagnostic performance for discrimination between groups was assessed by calculating the area under the receiver operating characteristics curve (AUC). Changes in EELI after 25%, 50%, 75%, and 100% of drainage were assessed using two-way analysis of variance for repeated measures with ‘percentage drained’ as one factor and ‘side’ (affected vs unaffected) as the other factor. In a *post hoc* analysis, the correlation between the volume of effusion drained and the sum of out-of-phase impedance changes, and the correlation

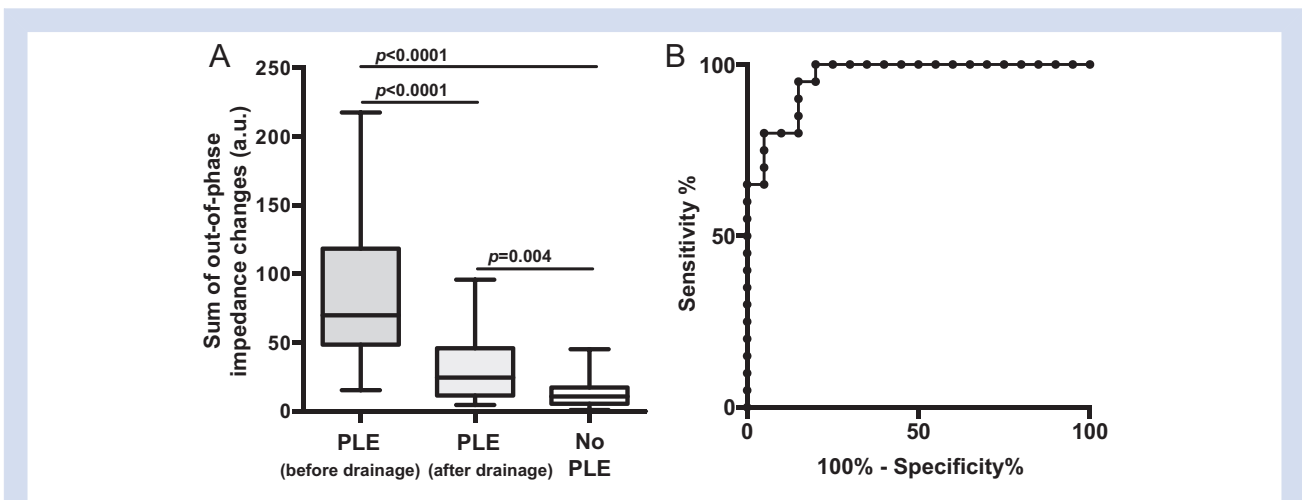


Fig 5. (A) Sum of out-of-phase impedance changes in the affected lung quadrant of patients with pleural effusion (PLE) before and after drainage and in the dorsal lung quadrants of control patients, expressed in arbitrary units (a.u.). (B) Receiver-operating-characteristics curve for discrimination between patients with PLE and control patients using the sum of out-of-phase impedance changes. Area under the curve=0.96 (95% limits of agreement 0.91–1.01).

between the sum of out-of-phase impedance changes and the dorsal ventilation-related impedance changes were assessed by calculating the Pearson correlation coefficient (r).

Results

A total of 52 patients undergoing imaging with EIT were screened for eligibility. Twenty-one patients were not analysed because the presence of a pleural effusion could not be excluded, but there was no clinical indication for drainage. One patient was excluded from the analysis for poor EIT image quality. A total of 20 patients with pleural effusion and 10 control patients were included and analysed (Fig. 3).

We found no significant differences in age, SAPS II, gas exchange, and other basic patient characteristics between the analysed patients with and without pleural effusion (Table 1).

In the control group, six out of 10 patients were in the supine position and four out of 10 patients were in the semi recumbent position during EIT data recording. In the pleural effusion group, 12 out of 20 patients were in the supine position, five out of 20 patients were in the semi recumbent position, and three out of 20 patients were in the sitting position during pleural effusion drainage. The patient position was not changed throughout the recordings.

In patients with pleural effusion, a median of 700 (600–900) ml of pleural fluid was drained after introducing the pigtail catheter.

Arterial blood gas samples were obtained 120 (79) min before drainage of the effusion and 146 (72) min after drainage. $\text{PaO}_2/\text{FiO}_2$ ratio increased from 37.6 (12.7) kPa before drainage to 46.2 (13.9) kPa after drainage ($P=0.03$). PaCO_2 showed a small

but statistically significant reduction from 5.7 (0.9) to 5.4 (1) kPa ($P=0.01$).

The median sum of in-phase impedance changes in the affected dorsal quadrants of patients with an effusion was 504 (292–955) a.u. before drainage and 747 (395–1133) a.u. after drainage ($P=0.04$). In control patients, the sum of in-phase impedance changes was 609 (301–800) a.u. and did not differ significantly from patients with pleural effusion before and after drainage (Fig. 4A).

The overall percentage of ventilation-related impedance changes was 14 (8)% in the affected dorsal quadrant in patients with a pleural effusion before drainage which increased significantly to 22 (10)% after drainage ($P=0.0015$). In the dorsal quadrants of control patients, the percentage of ventilation-related impedance changes was 26 (12)%, significantly higher than in pleural effusion patients before drainage ($P=0.0009$) but not significantly different from patients after drainage ($P=0.34$) (Fig. 4B).

The sum of out-of-phase impedance changes was 70 (49–119) a.u. in patients with pleural effusion before drainage and 25 (12–46) a.u. after drainage ($P<0.0001$). In the control group, the median sum of out-of-phase impedance changes was 11 (6–17) a.u. ($P<0.0001$ vs pleural effusion before drainage, Fig. 5A).

For out-of-phase impedance changes, the AUC for discrimination between patients with a pleural effusion (before drainage) and patients without an effusion was 0.96 (95% limits of agreement 0.91–1.01, Fig. 5B). For a cut-off value of 36 a.u., we found a sensitivity and specificity of 0.85 and 0.95, respectively.

We found a trend towards a negative correlation between the sum of out-of-phase impedance changes and dorsal ventilation, which was not statistically significant ($r=-0.38$; $P=0.10$; Fig. 6A).

There was a significant positive correlation between the amount of fluid drained and the sum of out-of-phase impedance changes ($r=0.63$, $P<0.01$; Fig. 6B).

There was a significant increase in EELI during drainage in both the affected and the unaffected quadrant during drainage ($P<0.0001$). There was no significant difference between affected and unaffected quadrant at 25% drainage, but a significant difference with higher increase in EELI on the affected side at 50%, 75%, and 100% drainage ($P<0.001$; Supplementary Fig. S1).

Discussion

Our findings show that out-of-phase impedance changes are common in patients with a pleural effusion and generate the hypothesis that the sum of out-of-phase impedance changes may allow to distinguish between patients with and without pleural effusion with high diagnostic accuracy. Furthermore, we demonstrated that the sum of out-of-phase impedance changes is reduced significantly after initial drainage, without reaching the low level observed in patients without pleural effusion.

The sum of in-phase impedance changes in the affected quadrant of patients with pleural effusion did not differ from the one observed in control patients, whereas there was a small but statistically significant difference in the percentage of ventilation-related impedance changes in the affected quadrant in comparison with control patients. This seemingly contradictory finding can easily be explained by the presence of out-of-phase impedance changes: While out-of-phase

Table 1 Basic patient characteristics. SAPS, simplified acute physiology score¹⁹; PaO_2 , arterial partial pressure of oxygen; FiO_2 , fraction of inspired oxygen; PaCO_2 , arterial partial pressure of carbon dioxide; PIP, peak inspiratory pressure; SB, spontaneous breathing; PSV; pressure-support ventilation; BIPAP, biphasic positive airway pressure; ARDS, acute respiratory distress syndrome; PLE, pleural effusion; n.a., not available. Values are expressed as mean (range) for age and mean (standard deviation) for all other variables.

Parameter	PLE	No PLE	p
Age (years)	66 (21-84)	67 (52-87)	0.88
Height (cm)	172 (9)	172 (8)	0.78
Weight (kg)	72 (18)	78 (15)	0.35
SAPS II	37 (15)	41 (11)	0.42
$\text{PaO}_2/\text{FiO}_2$ (kPa)	37.6 (12.7)	33.7 (11.4)	0.43
PaCO_2 (kPa)	5.7 (0.9)	6.5 (1.6)	0.22
Tidal Volume (ml)	575 (133)	597 (80)	0.67
Respiratory Rate (1/min)	18 (6)	17 (5)	0.61
PEEP (cmH ₂ O)	8 (2)	10 (4)	0.30
PIP (cmH ₂ O)	19 (5)	21 (4)	0.39
Ventilation mode (n)			
SB	9/20	3/10	n.a.
PSV	6/20	4/10	n.a.
BIPAP	5/20	3/10	n.a.
Main diagnosis (n)			
ARDS	9/20	5/10	n.a.
Sepsis	5/20	3/10	n.a.
Trauma	1/20	1/10	n.a.
Other	5/20	1/10	n.a.

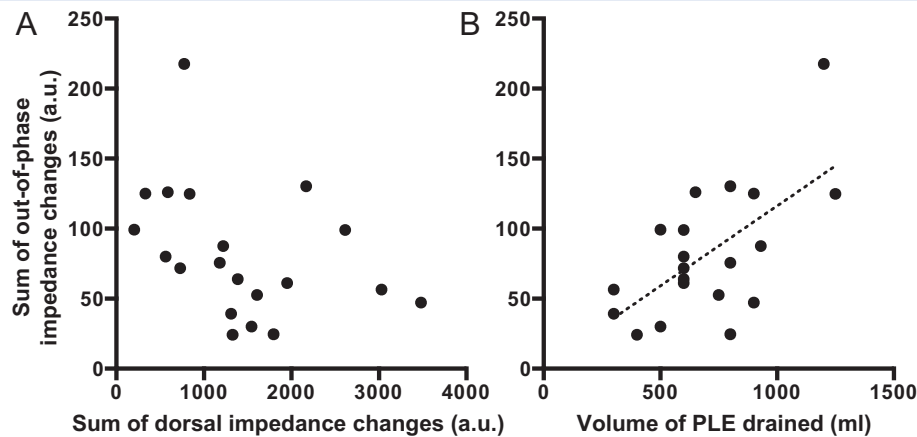


Fig 6. (A) Correlation between the sum of out-of-phase impedance changes and the overall (in-phase and out-of-phase) sum of dorsal ventilation-related impedance changes ($r=-0.38$, $P=0.10$). (B) Correlation between overall amount of pleural fluid drained and out-of-phase impedance changes ($r=0.63$; $P<0.01$). a.u., arbitrary units; PLE, pleural effusion.

impedance changes are excluded when calculating the sum of in-phase impedance changes, the percentage of impedance changes measures the overall sum of in-phase and out-of-phase impedance changes in a quadrant, divided by the sum of in-phase and out-of-phase impedance changes in the whole EIT image. This finding implies that the lower percentage of impedance changes in the quadrant with an effusion is mainly caused by out-of-phase impedance changes, which are reversed when draining a significant amount of fluid. This phenomenon could lead to an underestimation of the true quantity of ventilation in quadrants with a pleural effusion.

Reasons for out-of-phase impedance changes in pleural effusion

In patients with a pleural effusion, the ventilated lung, which constitutes an area of high ventilation-related impedance change, and the effusion, which constitutes an area of relatively low ventilation-related impedance change, are typically located only a few millimetres apart. The EIT image reconstruction algorithms, including the Newton–Raphson algorithm that is used in PulmoVista 500, cannot precisely follow step changes in conductivity. In areas with step changes in conductivity, this may lead to the observed overshoot (or ringing) phenomenon^{1,16,17} and seemingly paradoxical ‘out-of-phase’ impedance changes.¹⁴

Differential diagnosis of out-of-phase impedance changes

There are other possible causes of out-of-phase impedance changes that need to be considered when applying EIT in clinical practice. As discussed in the previous paragraph, out-of-phase impedance changes seem to occur when areas of low impedance are in close proximity to areas of high impedance, such as the ventilated lung. Apart from pleural effusion, in some patients this phenomenon can be detected at the boundary of the cardiac area. This can easily be distinguished from an effusion by means of its anatomical location. While impedance phenomena related to the cardiac area are located

medially and in the anterior quadrants of the EIT image, those caused by pleural effusion are typically located laterally and in the posterior quadrants of the EIT image in supine or semi-recumbent patients (Supplementary Fig. S2a and d).

Placing the EIT belt below the 6th intercostal space frequently causes the upper abdominal organs to be included in the EIT plane, causing out-of-phase impedance changes around the EIT image circumference (Supplementary Fig. S2b). As the upper abdominal organs constitute an area of low impedance in comparison with the ventilated lung, this is probably caused by the same overshoot phenomenon that may cause out-of-phase impedance changes in patients with pleural effusion. Placement of the EIT belt below the 6th intercostal space should generally be avoided because of a possible loss in sensitivity to ventilation-related phenomena.¹⁴

Artefacts arising from coughing or external chest compression (Supplementary Fig. S2c) are other possible reasons for out-of-phase impedance changes. Small areas of out-of-phase impedance change have been described previously near the midline of EIT images at the non-ventilated chest side during one-lung ventilation²⁰ or in a preterm neonate with a large pneumothorax.²¹ Occasionally, out-of-phase impedance changes occur as a combination in both cardiac area and pleural effusion (Fig. S2d). In most cases, artefacts can easily be identified from the typical ‘patchy’ pattern of impedance changes (Supplementary Fig. S2c).

In some patients with moderate to severe acute respiratory distress syndrome under assisted mechanical ventilation, a short and transient decrease in impedance in the non-dependent lung regions can be observed, a phenomenon which has been attributed to ‘Pendelluft’ caused by strong spontaneous breathing efforts.²² A ‘Pendelluft’ phenomenon has also been described in patients after single-lung transplantation.²³ This phenomenon differs from the out-of-phase impedance changes in pleural effusion in two ways. First, it is very transient, so the regional decrease in impedance during early inspiration is followed by an increase in impedance during ongoing inspiration in the same region. In contrast, the out-of-phase impedance changes described in this paper appear to ‘mirror’ the global in-phase impedance signal and do

therefore persist during the whole time course of inspiration. This is expected for the overshoot mechanism that has been postulated as a reason for out-of-phase impedance changes in effusion. Second, 'Pendelluft' during spontaneous efforts appears to occur predominantly in the non-dependent lung regions, whereas out-of-phase impedance changes during pleural effusion naturally occur in the dependent lung regions.

A small amount of out-of-phase impedance changes was present in control patients as well (Fig. 5) and could possibly be explained by some of the abovementioned phenomena, for example, parts of the upper abdominal organs entering the EIT image plane.

Reaeration during pleural effusion drainage

We found a highly significant increase in EELI after effusion drainage on both the affected and unaffected sides of the dorsal hemithorax. This increase is presumably caused by reaeration of formerly non-aerated lung tissues and by the decrease in highly conductive pleural fluid. Distinguishing between these two effects may be difficult in clinical routine and may impair the assessment of end-expiratory lung aeration with EIT during pleural fluid drainage.

Nevertheless, our results also showed a significant increase in regional ventilation-related (in-phase) impedance changes in the quadrants of fluid drainage, which should not be affected by pleural effusion to the same extent as EELI. Therefore, even though the increase in EELI must be interpreted with caution during drainage, the concomitant increase in regional ventilation implies that drainage led to some lung reaeration in the affected dorsal quadrants.

Correlation between volume of pleural effusion and out-of-phase impedance changes

The relatively low correlation ($r=0.63$) between the volume of pleural effusion drained and the sum of out-of-phase impedance changes could be explained by some variability in the spatial relationship between the EIT electrode plane and the main location of pleural effusion. Depending on the individual patient's anatomy and pathophysiology, the pleural effusion may have entered the electrode plane to a variable extent. In some patients, the effusion may have been located mainly within the electrode plane, whereas in other patients, only a relatively small part of the effusion may have been in this plane.

Clinical significance

Pleural effusions are common in ICU patients and are associated with impaired gas exchange, restrictive respiratory mechanics, and marked dyspnoea in spontaneously breathing patients. In patients with a pleural effusion, pleural drainage leads to improvements in oxygenation, relief of dyspnoea and, to a variable extent, improved respiratory mechanics.²⁴

While CT remains the gold standard for the detection of pleural effusion, lung ultrasound has a high diagnostic accuracy and is therefore an excellent radiation-free alternative. In comparison with lung ultrasound, conventional supine chest radiography has a relatively poor diagnostic accuracy in the detection of pleural effusions in ICU patients.²⁵

Both lung ultrasound and CT cannot be applied continuously for monitoring purposes. In patients undergoing continuous ventilation monitoring with EIT, the observation of

out-of-phase impedance changes in the dorsal quadrants should trigger the diagnosis of possible pleural effusion, which should lead to further examination and validation with lung ultrasound. If a diagnosis of pleural effusion is confirmed and pleural drainage is performed, EIT can be used to continuously monitor re-aeration and relief of pleural effusion. However, the overall clinical significance of EIT in the detection and treatment of pleural effusion remains to be established.

Limitations

Our study has some important limitations. We used ultrasound as a reference method for excluding pleural effusion in the majority of patients in the control group, which may be less sensitive for the detection of pleural effusion than CT. However, the examinations were all carried out by an intensivist experienced in lung ultrasound, which should limit observer-dependent bias.

The dorsal lung quadrants were chosen for analysis both for pleural effusion and control patients because we assumed that they would contain the majority of fluid in patients with a pleural effusion. This may not necessarily have been the case in the three patients who were investigated in the sitting position, yet to improve comparability and to avoid any disturbance caused by cardiac-related out-of-phase impedance changes, we decided to investigate the dorsal lung quadrants in all patients.

We investigated a mixed population of patients, some of whom were on mechanical ventilation. The sample size was relatively small, but regarding the large effect of a pleural effusion on out-of-phase impedance changes, sufficiently powered to show clear and statistically significant results. A larger study using CT scans as a reference method would be desirable to confirm our results and to establish the relationship between the sum of out-of-phase impedance changes and the absolute size of an effusion, measured with CT.

Also, we analysed a 'convenience sample', which limits the generalisation of our results. Therefore, our study should be regarded as 'hypothesis-generating' with respect to the accuracy of EIT in diagnosing pleural effusion. Nevertheless, to allow critical appraisal of our results and to limit the risk of bias, we strive to adhere to the Standards for Reporting Diagnostic Accuracy²⁶ guideline within this paper.

Currently, the calculation of the sum of out-of-phase impedance changes cannot be performed online on the EIT device but rather after download of data to a computer with dedicated EIT data analysis software. Nevertheless, out-of-phase changes are displayed graphically on the 'Ventilation' screen of the EIT device (Figs 1 and 2, Supplementary Fig. S2) which allows at least a semi-quantitative bedside assessment. This online display could therefore be helpful in making a 'suspected diagnosis' that would then require further confirmation with other imaging methods.

As EIT is still a relatively new imaging modality, there are currently no generally accepted recommendations concerning which patients might benefit from EIT monitoring. Therefore, the initiation of EIT monitoring was based on the attending physician's individual decision in our study. This might be considered a limitation to the generalisability of our findings.

Conclusions

In conclusion, out-of-phase impedance changes are a typical finding in patients with pleural effusion and decrease

significantly with drainage. In patients under monitoring with EIT, the presence of out-of-phase impedance changes in dependent lung quadrants is highly suspicious of pleural effusion and should trigger further examination.

Authors' contributions

Designed the study: T.B., I.F., N.W.

Acquired and analysed the data: M.B., T.B., I.F., I.L., D.S.

Interpreted the data: T.B., M.B., I.F., N.W.

Drafted the manuscript: T.B.

Gave intellectual input to the manuscript and approved the final version of the manuscript: all authors.

Acknowledgements

The authors are indebted to E. Teschner (Drägerwerk AG & Co. KGaA, Lübeck, Germany) for his continuous valuable input and support.

Declaration of interest

T.B. has received speaking fees and reimbursement of travel expenses from Heinen & Löwenstein, Bad Ems, Germany and from Drägerwerk AG & Co. KGaA, Lübeck, Germany. I.F. has received speaking fees and reimbursement of congress and travel expenses from Drägerwerk AG & Co. KGaA. D.S. has received speaking fees and reimbursement of travel expenses from Drägerwerk AG & Co. KGaA. M.B., N.W. and I.L. declare no conflict of interests relevant to this paper.

Funding

Department of Anaesthesiology and Intensive Care Medicine, University Medical Centre Schleswig-Holstein, Campus Kiel, Germany.

Supplementary material

Supplementary data related to this article can be found at <https://doi.org/10.1016/j.bja.2018.02.030>.

References

- Frerichs I, Amato MB, van Kaam AH, et al. Chest electrical impedance tomography examination, data analysis, terminology, clinical use and recommendations: consensus statement of the TRanslational EIT developmeNt stuDy group. *Thorax* 2017; **72**: 83–93
- Radke OC, Schneider T, Heller AR, Koch T. Spontaneous breathing during general anesthesia prevents the ventral redistribution of ventilation as detected by electrical impedance tomography: a randomized trial. *Anesthesiology* 2012; **116**: 1227–34
- Mauri T, Bellani G, Confalonieri A, et al. Topographic distribution of tidal ventilation in acute respiratory distress syndrome: effects of positive end-expiratory pressure and pressure support. *Crit Care Med* 2013; **41**: 1664–73
- Costa EL, Borges JB, Melo A, et al. Bedside estimation of recruitable alveolar collapse and hyperdistension by electrical impedance tomography. *Intensive Care Med* 2009; **35**: 1132–7
- Meier T, Luepschen H, Karsten J, Leibecke T, Grossherr M, Gehring H. Assessment of regional lung recruitment and derecruitment during a PEEP trial based on electrical impedance tomography. *Intensive Care Med* 2008; **34**: 543–50
- Muders T, Luepschen H, Zinserling J, et al. Tidal recruitment assessed by electrical impedance tomography and computed tomography in a porcine model of lung injury. *Crit Care Med* 2012; **40**: 903–11
- Zick G, Elke G, Becher T, et al. Effect of PEEP and tidal volume on ventilation distribution and end-expiratory lung volume: a prospective experimental animal and pilot clinical study. *PLoS One* 2013; **8**: e72675
- Becher TH, Bui S, Zick G, et al. Assessment of respiratory system compliance with electrical impedance tomography using a positive end-expiratory pressure wave maneuver during pressure support ventilation: a pilot clinical study. *Crit Care* 2014; **18**: 679
- Zhao Z, Moller K, Steinmann D, Frerichs I, Guttman J. Evaluation of an electrical impedance tomography-based Global Inhomogeneity Index for pulmonary ventilation distribution. *Intensive Care Med* 2009; **35**: 1900–6
- Becher T, Vogt B, Kott M, Schadler D, Weiler N, Frerichs I. Functional regions of interest in electrical impedance tomography: a secondary analysis of two clinical studies. *PLoS One* 2016; **11**: e0152267
- Wolf GK, Gomez-Laberge C, Rettig JS, et al. Mechanical ventilation guided by electrical impedance tomography in experimental acute lung injury. *Crit Care Med* 2013; **41**: 1296–304
- Frerichs I, Becher T, Weiler N. Electrical impedance tomography imaging of the cardiopulmonary system. *Curr Opin Crit Care* 2014; **20**: 323–32
- Blaser D, Pulletz S, Becher T, et al. Unilateral empyema impacts the assessment of regional lung ventilation by electrical impedance tomography. *Physiol Meas* 2014; **35**: 975–83
- Karsten J, Stueber T, Voigt N, Teschner E, Heinze H. Influence of different electrode belt positions on electrical impedance tomography imaging of regional ventilation: a prospective observational study. *Crit Care* 2016; **20**: 3
- Geddes LA, Baker LE. The specific resistance of biological material—a compendium of data for the biomedical engineer and physiologist. *Med Biol Eng* 1967; **5**: 271–93
- Adler A, Arnold JH, Bayford R, et al. GREIT: a unified approach to 2D linear EIT reconstruction of lung images. *Physiol Meas* 2009; **30**: S35–55
- Yasin M, Bohm S, Gaggero PO, Adler A. Evaluation of EIT system performance. *Physiol Meas* 2011; **32**: 851–65
- Alves SH, Amato MB, Terra RM, Vargas FS, Caruso P. Lung re-aeration and re-ventilation after aspiration of pleural effusions. A study using electrical impedance tomography. *Ann Am Thorac Soc* 2014; **11**: 186–91
- Le Gall JR, Lemeshow S, Saulnier F. A new simplified acute physiology score (SAPS II) based on a European/North American multicenter study. *JAMA* 1993; **270**: 2957–63
- Pulletz S, Elke G, Zick G, et al. Performance of electrical impedance tomography in detecting regional tidal volumes during one-lung ventilation. *Acta Anaesthesiol Scand* 2008; **52**: 1131–9
- Miedema M, Frerichs I, de Jongh FH, van Veenendaal MB, van Kaam AH. Pneumothorax in a preterm infant

- monitored by electrical impedance tomography: a case report. *Neonatology* 2011; **99**: 10–3
22. Yoshida T, Torsani V, Gomes S, et al. Spontaneous effort causes occult pendelluft during mechanical ventilation. *Am J Respir Crit Care Med* 2013; **188**: 1420–7
 23. Ramanathan K, Mohammed H, Hopkins P, et al. Single-lung transplant results in position dependent changes in regional ventilation: an observational case series using electrical impedance tomography. *Can Respir J* 2016; **2016**: 2471207
 24. Walden AP, Jones QC, Matsa R, Wise MP. Pleural effusions on the intensive care unit; hidden morbidity with therapeutic potential. *Respirology* 2013; **18**: 246–54
 25. Xirouchaki N, Magkanas E, Vaporidi K, et al. Lung ultrasound in critically ill patients: comparison with bedside chest radiography. *Intensive Care Med* 2011; **37**: 1488–93
 26. Bossuyt PM, Reitsma JB, Bruns DE, et al. For the STARD Group. STARD 2015: an updated list of essential items for reporting diagnostic accuracy studies. *Br Med J* 2015; **351**: h5527

Handling editor: J.P. Thompson

Center of Ventilation—Methods of Calculation using Electrical Impedance Tomography and the Influence of Image Segmentation

V. Sobota¹ and K. Roubik¹

¹ Faculty of Biomedical Engineering, Czech Technical University in Prague, Kladno, Czech Republic

Abstract— Electrical impedance tomography (EIT) is a promising non-invasive, radiation-free imaging modality. Using EIT-derived index Center of Ventilation (CoV), ventral-to-dorsal shifts in distribution of lung ventilation can be assessed. The methods of CoV calculation differ among authors and so does the segmentation of EIT images from which the CoV is calculated. The aim of this study is to compare the values of CoV obtained using different algorithms, applied in variously segmented EIT images. An animal trial (n=4) with anesthetized mechanically ventilated pigs was conducted. In one animal, acute respiratory distress syndrome (ARDS) was induced by repeated whole lung lavage. Incremental steps in positive end-expiratory pressure (PEEP), each with a value of 5 cmH₂O (or 4 cmH₂O in the ARDS model), were performed to reach total PEEP level of 25 cmH₂O (or 22 cmH₂O in the ARDS model). EIT data were acquired continuously during this PEEP trial. From each PEEP level, 30 tidal variation (TV) images were used for analysis. Functional regions of interest (ROI) were defined based on the standard deviation (SD) of pixel values, using threshold 15%–35% of maximum pixel SD. The results of this study show that there might be statistically significant differences between the values obtained using different methods for calculation of CoV. The differences occurred in healthy animals as well as in the ARDS model. Both investigated algorithms are relatively insensitive to the image segmentation.

Keywords— center of ventilation, center of gravity, electrical impedance tomography, EIT, region of interest

I. INTRODUCTION

Electrical impedance tomography (EIT) is an imaging modality that provides information about regional lung ventilation. It is based on the application of small alternating currents using skin electrodes attached to the patient's chest and the consequent measurement of resulting voltages. It can offer a non-invasive, radiation-free bedside alternative to computed tomography in monitoring of tidal volume (V_T) distribution and lung aeration inhomogeneity [1].

Due to the physical principle used, EIT images suffer from low spatial resolution [2], [3] and the information provided

by EIT is rather complex and may be difficult to interpret [3]. Therefore, several indices and measures were developed to assess lung ventilation [4].

One of the most widely used indices in EIT data processing is called Center of Ventilation (CoV) and was introduced for the first time in 1998 by Frerichs et al. [5]. It describes shifts in distribution of lung ventilation in ventral-to-dorsal direction. In that study, it was defined as a weighted mean of geometrical centers of the right and the left lung. In 2006, the same research group presented a modified approach for its calculation where CoV was calculated separately for both left and right lung [6].

Since CoV has proven to be a useful index in assessment of regional lung ventilation, it was adopted by many research groups [7]–[12]. However, the definitions of CoV are not consistent among these studies. Some authors define CoV as a weighted mean of the row sums [7], [9], [11], [12]. Van Heerde et al. defined CoV as “the point where the sum of fractional ventilation was 50% of the summed fractional ventilation” [8] and Blankman et al. computed it as a ratio between dorsal and total fractional ventilation [10]. Similarly to CoV, Center of Gravity (CoG) index was introduced in 2007 as a weighted mean of image row sums [13].

Unfortunately, different definitions of CoV are not the only inconsistency in its use. Segmentation of EIT images from which the CoV is calculated also varies. Initially, circular mask was applied to the EIT image and the resulting area was divided into several regions of interest (ROI) [6], [8]. However, some authors use functional segmentation of the images, defined as 20% of maximum regression coefficient obtained between global and local relative impedance [11] or as 20% of the maximum standard deviation (SD) of the pixel value in certain time period [12]. Finally, there are studies where CoV was calculated without any previous image segmentation [9].

As there are different definitions of CoV published, used together with various EIT image segmentation, we hypothesized that the resulting CoV values and thus the evaluation of regional lung ventilation may differ.

The aim of this study is to compare the values of CoV obtained using different methods of its computation, applied in variously segmented images.

II. METHODS

The study protocol was approved by the Institutional Review Board of the First Faculty of Medicine, Charles University in Prague (FFM CU) and is in accordance with Act No. 246/1992 Coll., on the protection of animals against cruelty. The measurements were performed at an accredited animal laboratory of the FFM CU.

Four crossbred Landrace female pigs (*Sus scrofa domestica*) with a body weight of 48 ± 2 kg were used in this study.

A. Anesthesia and preparation

The animals were premedicated with azaperone (2 mg/kg IM). Anesthesia was initiated with ketamine hydrochloride (20 mg/kg IM) and atropine sulphate (0.02 mg/kg IM), followed by boluses of morphine (0.1 mg/kg IV) and propofol (2 mg/kg IV). A cuffed endotracheal tube (I.D. 7.5 mm) was used for intubation. Anesthesia was maintained with propofol (8 to 10 mg/kg/h IV) in combination with morphine (0.1 mg/kg/h IV) and heparin (40 U/kg/h IV). To suppress spontaneous breathing, myorelaxant pipecuronium bromide (4 mg boluses every 45 min) was administered during mechanical lung ventilation. Initially, rapid infusion of 1 000 mL of saline was administered intravenously, followed by a continuous IV administration of 250 mL/h to reach and maintain central venous pressure of 6 to 7 mmHg.

Mixed venous blood oxygen saturation and continuous cardiac output were measured by Vigilance (Edwards Lifesciences, Irvine, CA, USA) monitor. Arterial blood gases, i.e. arterial partial pressure of oxygen, carbon dioxide (PaCO_2) and pH, were continuously measured by CDI 500 (Terumo, Tokyo, Japan). The arterio-venous extracorporeal circuit for CDI 500 monitor was established between the femoral artery and the femoral vein using a mechanical blood pump (peristaltic roller pump with a blood flow set to 400 mL/min).

In one animal, repeated whole lung lavage (normal saline, 30–40 mL/kg, 37°C) was performed to induce the surfactant deficiency similar to acute respiratory distress syndrome (ARDS) [8].

B. Ventilation

Conventional ventilator Hamilton G5 (Hamilton Medical AG, Bonaduz, Switzerland) was used in the CMV mode with the following setting: respiratory rate 18 bpm, FiO_2 21%, I:E 1:2 with initial positive end-expiratory pressure (PEEP) of 5 cmH₂O and pressure limit set to 40 cmH₂O. The initial V_T was set to 8.5 mL/kg of the actual body weight and was titrated to reach normocapnia (PaCO_2 40 ± 3 mmHg). During the study protocol four increasing PEEP steps of 5 cmH₂O

were performed in animals with healthy lungs and three increasing PEEP steps of 4 cmH₂O with initial value of 10 cmH₂O were performed in the ARDS model. Each PEEP level was maintained at least for 3 minutes.

C. EIT measurements

EIT system PulmoVista 500 (Dräger Medical, Lübeck, Germany) was used for data acquisition. The electrode belt (size S) was attached to the chest of the animal at the level of the 6th intercostal space. The frequency of the applied current was set to 110 kHz with amplitude of 9 mA. EIT images were recorded continuously with a frame rate of 50 Hz during the entire PEEP maneuver.

D. Data Processing

The acquired data were pre-processed in Dräger EIT Data Analysis Tool 6.1 (Dräger Medical, Lübeck, Germany). Baseline frame was set automatically for each animal as a frame that corresponds with the global minimum of impedance waveform. Reconstructed data were processed in MATLAB 2014b (MathWorks, Natick, MA, USA).

At each PEEP level, EIT data from 30 consecutive breaths were used for analysis. The breaths were selected in the phases where the values of end-expiratory lung impedance were the most stable. Tidal variation (TV) images were calculated as a difference between end-inspiratory and end-expiratory EIT images. In consequence, 30 TV images were obtained for each PEEP level.

Functional ROI was defined based on the standard deviation (SD) of individual pixel values in time [12], [14]. Six threshold levels ranging from 15% to 40% of maximum pixel SD with 5% step were used for image segmentation. For each set of 30 TV images, a common ROI was applied. The index called Center of Gravity (CoG) was defined as a weighted mean of row sums obtained from TV image [13]:

$$\text{CoG} = \frac{1}{N+1} \cdot \frac{\sum_{x=1}^N \sum_{y=1}^N y \cdot TV_{xy}}{\sum_{x=1}^N \sum_{y=1}^N TV_{xy}} \quad (1)$$

where N stands for both the number of pixel rows and pixel columns in the TV image ($N = 32$ for EIT images provided by PulmoVista 500) and TV_{xy} stands for the value of the pixel with coordinates x, y .

For the purposes of this study, Center of Ventilation (CoV) index was defined as a vertical coordinate that divides the sum of fractional ventilation in two equal halves [8] (Fig. 1). Our implementation of the algorithm for calculation of CoV can be summarized as follows:

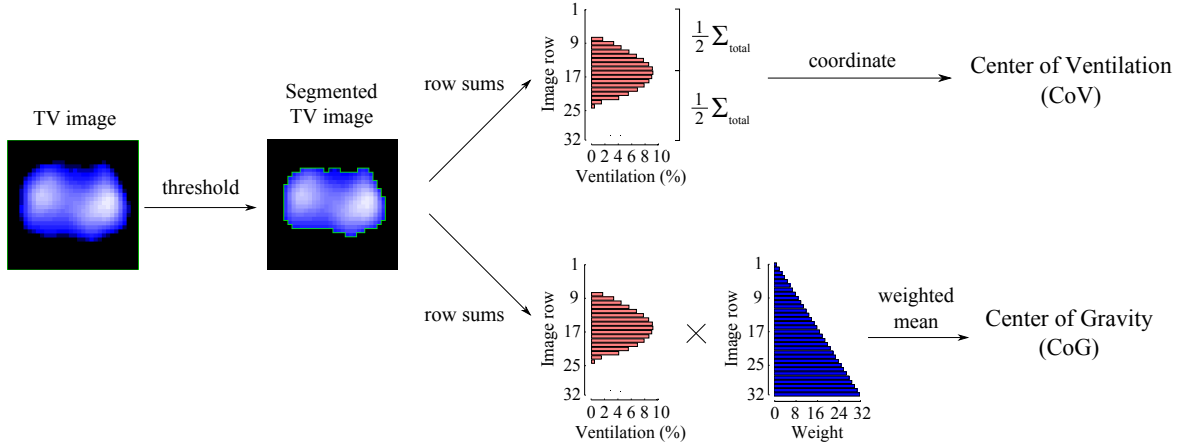


Fig. 1: Computation of Center of Ventilation (CoV) and Center of Gravity (CoG). Tidal variation (TV) images were segmented and a region of interest (ROI) was defined. Row sums were calculated from the segmented TV image. CoV was calculated as a coordinate that divides row sums in two equal halves. CoG was calculated as a weighted mean of image row sums.

1. Normalize the pixel values in the TV image:

$$TV_{xy}^* = \frac{TV_{xy}}{\sum_{x=1}^N \sum_{y=1}^N TV_{xy}} \cdot 100 \quad (2)$$

where TV_{xy}^* expresses the value of the original pixel TV_{xy} as a percentage of the total sum of the TV image.

2. Calculate row sums of the normalized TV image and save them into the array \mathbf{r} .
3. Find the highest index $n \in \mathbb{N}$ for which holds:

$$\sum_{i=1}^n \mathbf{r}_i \leq 50 \quad (3)$$

4. Calculate the ratio k :

$$k = \frac{50 - \sum_{i=1}^n \mathbf{r}_i}{r_n} \quad (4)$$

5. Calculate the value of CoV:

$$\text{CoV} = \frac{n + k + 0.5}{N + 1} \quad (5)$$

For calculation of both CoV and CoG, a coordinate system with the top left pixel represented by coordinates $x = 1$, $y = 1$ was used. In the following text the abbreviations “CoV” and “CoG” refer to the indices described above and the unabbreviated term “Center of Ventilation” represents the index in general.

Paired two-tailed t-test was used for evaluation of statistical differences between CoV and CoG. The values of both indices obtained at different PEEP levels were visualized as a box plot.

III. RESULTS

EIT data from 4 animals were studied. The highest PEEP step was omitted in two subjects due to their hemodynamic instability. In total 510 TV images were analyzed.

In general, the values of CoV were significantly higher ($p < 0.05$) than the corresponding values of CoG in all subjects. As shown in Table 1, there were four cases where the difference between CoV and CoG was not statistically significant and three cases where the mean value of CoG was higher than the corresponding mean value of CoV.

Box plots were created for each animal to visualize the effect of image segmentation upon values of both CoV and CoG. Figure 2 shows typical values of these indices during incremental PEEP steps. Both CoV and CoG move dorsally when a higher PEEP level is applied. When calculated from segmented TV images, variation in values of both indices decreases with higher threshold.

The effect of image segmentation upon the values of CoV and CoG is rather small when the indices are calculated from mean TV image, as illustrated in Fig. 3 and 4. The influence of PEEP upon both indices is much higher when compared to the changes caused by application of different image segmentation thresholds.

IV. DISCUSSION

The results of this study show, that in general, there is a statistically significant difference between the values obtained using different methods for calculation of Center of Ventilation. Both presented algorithms for its calculation show relatively low sensitivity to lung segmentation.

Table 1: The differences CoV–CoG (mean \pm SD). Statistically insignificant differences (paired t-test, $p > 0.05$) are marked as *. The cases where the mean value of CoG is higher than the value of CoV are marked as †. Repeated whole lung lavage was performed in pig 4.

Pig	PEEP level (cmH ₂ O)	Threshold (% of max. SD)					
		15	20	25	30	35	40
1	5	0.290 \pm 0.049	0.315 \pm 0.043	0.361 \pm 0.045	0.392 \pm 0.053	0.509 \pm 0.047	0.509 \pm 0.040
	10	0.477 \pm 0.089	0.434 \pm 0.046	0.387 \pm 0.028	0.383 \pm 0.057	0.308 \pm 0.048	0.308 \pm 0.043
	15	0.348 \pm 0.112	0.193 \pm 0.058	0.166 \pm 0.012	0.191 \pm 0.027	0.090 \pm 0.027	0.090 \pm 0.027
	20	0.507 \pm 0.333	0.034 \pm 0.179*	0.062 \pm 0.054	0.098 \pm 0.036	0.047 \pm 0.036	0.047 \pm 0.031
	25	1.131 \pm 0.434	0.539 \pm 0.374	0.088 \pm 0.243*	0.066 \pm 0.093	0.057 \pm 0.051	0.057 \pm 0.049
2	5	0.770 \pm 0.122	0.823 \pm 0.112	0.908 \pm 0.110	0.845 \pm 0.101	0.719 \pm 0.091	0.719 \pm 0.086
	10	1.158 \pm 0.063	1.174 \pm 0.054	0.972 \pm 0.050	0.635 \pm 0.056	0.513 \pm 0.055	0.513 \pm 0.044
	15	0.851 \pm 0.056	0.314 \pm 0.023	0.186 \pm 0.026	0.138 \pm 0.025	0.080 \pm 0.021	0.080 \pm 0.019
	20	0.507 \pm 0.017	0.093 \pm 0.026	0.026 \pm 0.028	−0.001 \pm 0.030 ^{†*}	−0.039 \pm 0.029 [†]	−0.039 \pm 0.033 [†]
3	5	0.193 \pm 0.122	0.186 \pm 0.121	0.181 \pm 0.118	0.186 \pm 0.117	0.052 \pm 0.122	0.052 \pm 0.110*
	10	0.498 \pm 0.098	0.448 \pm 0.098	0.407 \pm 0.103	0.355 \pm 0.105	0.221 \pm 0.107	0.221 \pm 0.102
	15	0.647 \pm 0.106	0.532 \pm 0.063	0.358 \pm 0.050	0.320 \pm 0.055	0.198 \pm 0.057	0.198 \pm 0.059
	20	0.460 \pm 0.233	0.307 \pm 0.159	0.246 \pm 0.067	0.240 \pm 0.040	0.146 \pm 0.041	0.146 \pm 0.036
4	10	0.304 \pm 0.206	0.351 \pm 0.199	0.234 \pm 0.129	0.166 \pm 0.078	0.106 \pm 0.081	0.106 \pm 0.084
	14	0.528 \pm 0.255	0.497 \pm 0.231	0.385 \pm 0.176	0.341 \pm 0.138	0.264 \pm 0.127	0.264 \pm 0.113
	18	1.116 \pm 0.474	1.088 \pm 0.479	0.930 \pm 0.448	0.730 \pm 0.392	0.449 \pm 0.312	0.449 \pm 0.237
	22	1.338 \pm 0.376	1.197 \pm 0.387	1.051 \pm 0.380	0.742 \pm 0.324	0.311 \pm 0.220	0.311 \pm 0.134

Although statistically significant, the differences between the values of CoV and CoG presented in this study are mostly at the edge of clinical relevance or even negligible. However, as shown in Fig. 5, there might be considerable differences in some subjects.

When functional ROI is applied to TV image, the variation in values of both CoV and CoG and the difference between their mean values decrease with an increasing threshold of lung segmentation. This is mainly due to the fact that the pixels with low change of relative impedance in time represent poorly ventilated lung regions or tissues that does not participate in ventilation at all. When these pixels are excluded from the ROI, only the lung regions that substantially contribute to ventilation are used for the calculation. In consequence, this may result in cases where CoV and CoG switch their positions when a high segmentation threshold is applied, as shown in Table 1. Similarly, the mean difference between CoV and CoG values substantially decreases when large insufficiently ventilated lung regions are omitted from the calculation because of the use of high segmentation threshold, as shown in the values of the ARDS model in Table 1.

Contrary to the effect of lung segmentation, when incremental PEEP steps are performed, the lung area that is pre-

dominantly ventilated moves dorsally. Therefore, the changes of both CoV and CoG values caused by PEEP setting are more pronounced.

For the purposes of this study we expressed both CoV and CoG in percentage as we consider this as the most common way [6]–[9], [12]. However, the expression as a value from the interval $(1, N)$, where N stands for the number of image row is also possible and correct [13].

To enable the comparison of two different approaches for calculation of Center of Ventilation, we modified the published algorithms to provide the value of 50% for a homogeneous image and also for images that are symmetrical along vertical axis. Both algorithms are also shift invariant for the structures that are symmetrical along vertical axis (top row of Fig. 5). Therefore, the biggest differences between CoV and CoG occur for the images with a strong horizontal asymmetry as shown in the bottom row of Fig. 5.

We used the abbreviation “CoV” for the method presented by van Heerde et al. [8] as it is in our opinion closer to the original idea of geometrical center of ventilation [5], [6]. The methods for calculation of this index presented in [7], [9], [11], [12] are closer to the idea of Center of Gravity index [13]. Therefore, abbreviation “CoG” was used for this

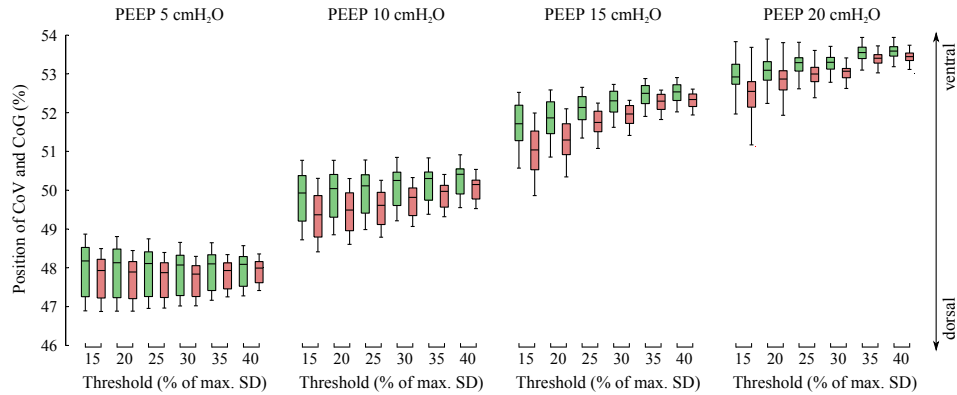


Fig. 2: Values of Center of Ventilation (red) and Center of Gravity (green) calculated from EIT images that were segmented using thresholds in the range of 15% – 40% of maximum pixel standard deviation (SD). The data obtained at four different PEEP levels are presented as box-and-whisker plot (minimum – lower quartile – median – upper quartile – maximum).

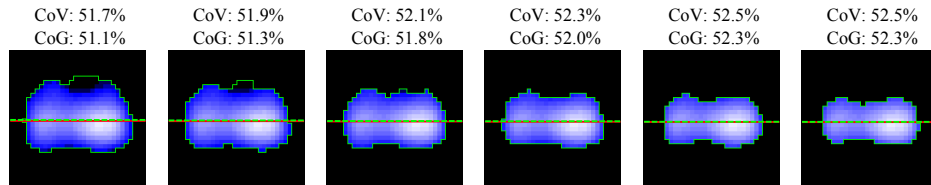


Fig. 3: Thresholding effect upon mean tidal variation (TV) image in the range from 15% to 40% in 5% steps (fig 3, PEEP 15 cmH₂O). The position of Center of Ventilation (CoV) and Center of Gravity (CoG) is depicted with red solid line and green dashed line, respectively. The pixel values of the image were obtained as a mean of 30 consecutive TV images.

method. In this study we did not evaluate the method presented by Blankman et al. [10].

Segmentation of TV images based on SD values of individual pixels is one of the most common approaches used for definition of functional ROI [14]. For this method, there is a recommended range of threshold values from 20% to 35% of maximum pixel SD. In this study we used threshold values ranging from 15% to 40% to assess also the effect of ROIs that are produced by setting of the threshold criteria outside the recommended range.

V. CONCLUSION

This study shows that there is a statistically significant difference between the values provided by the two studied methods for calculation of Center of Ventilation. The differences occurred in healthy animals as well as in the model of lung injury. In consequence, assessment of ventral-to-dorsal shifts in lung ventilation may be compromised. However, both algorithms that were evaluated are relatively insensitive to the segmentation of EIT images.

ACKNOWLEDGEMENTS

The authors thank the employees of the animal laboratory of the Department of Physiology, FFM CU, where the animal trial was performed. The study was supported by grants VG20102015062 and SGS14/216/OHK4/3T/17.

The authors declare that they have no conflict of interest.

REFERENCES

1. Frerichs I., Hinz J., Herrmann P., et al. Detection of local lung air content by electrical impedance tomography compared with electron beam CT *J Appl Physiol.* 2002;93:660-666.
2. Holder D.S.. *Electrical Impedance Tomography: methods, history and applications.* Philadelphia: Institute of Physics Pub. 2005.
3. Putensen C., Wrigge H., Zinslerling J.. Electrical impedance tomography guided ventilation therapy *Curr Opin Crit Care.* 2007;13:344-350.
4. Adler A., Amato M.B., Arnold J.H., et al. Whither lung EIT: Where are we, where do we want to go and what do we need to get there? *Physiol Meas.* 2012;33:679-694.
5. Frerichs I., Hahn G., Golisch W., Kurpitz M., Burchardi H., Hellige G.. Monitoring perioperative changes in distribution of pulmonary ventilation by functional electrical impedance tomography *Acta Anaesthesiol Scand.* 1998;42:721-726.
6. Frerichs I., Dargaville P.A., Van Genderingen H., Morel D.R., Rimensberger P.C.. Lung volume recruitment after surfactant administration

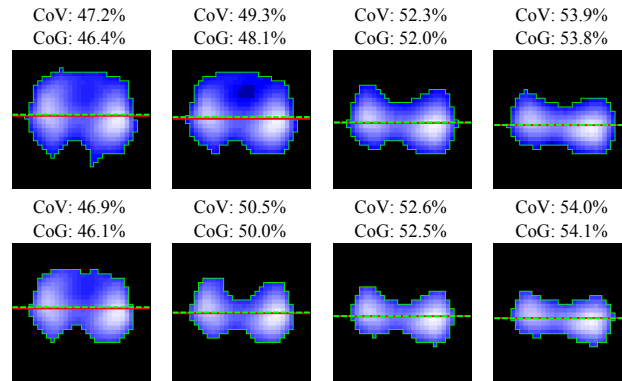


Fig. 4: The effect of PEEP and lung segmentation upon mean tidal variation (TV) images. Distribution of ventilation at four PEEP levels (from left to right, 5 to 20 cmH₂O with a step of 5 cmH₂O). Top row: thresholding set to 20% of maximum SD, bottom row: threshold set to 35% of maximum SD. The position of Center of Ventilation (CoV) and Center of Gravity (CoG) is depicted with red solid line and green dashed line, respectively. The pixel values of the image were obtained as a mean of 30 consecutive TV images.

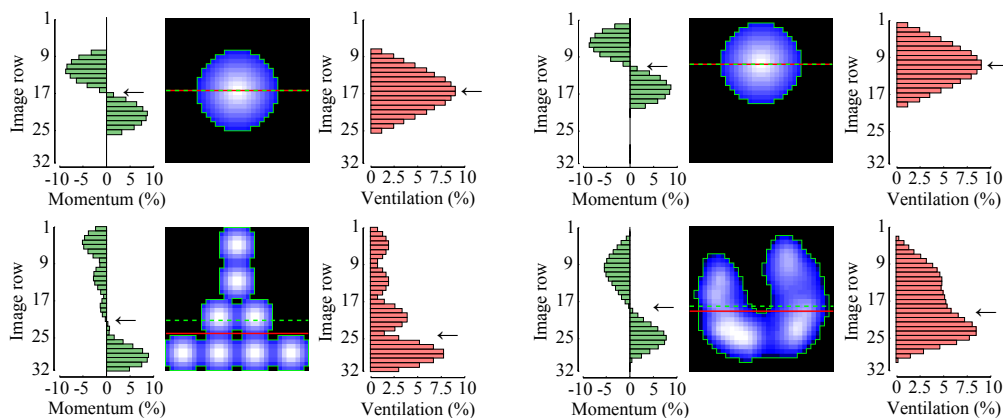


Fig. 5: The position of Center of Ventilation (CoV) and Center of Gravity (CoG) for the image structures that are symmetrical (top row) and asymmetrical (bottom row) along vertical axis. For each image, the left bar graph represents the distribution of momentum (weighted means) along vertical axis and the right bar graph shows the row sums in the normalized tidal variation (TV) image. The right bottom image is an example of TV image obtained in a spontaneously breathing healthy volunteer. The position of CoV and CoG is depicted with red solid line and green dashed line, respectively.

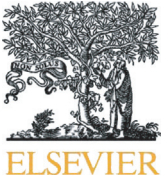
modifies spatial distribution of ventilation *Am J Respir Crit Care Med.* 2006;174:772-779.

- Schibler A., Yuill M., Parsley C., Pham T., Gilshenan K., Dakin C.. Regional ventilation distribution in non-sedated spontaneously breathing newborns and adults is not different *Pediatr Pulmonol.* 2009;44:851-858.
- Van Heerde M., Roubik K., Kopelent V., Kneyber M.C.J., Markhorst D.G.. Spontaneous breathing during high-frequency oscillatory ventilation improves regional lung characteristics in experimental lung injury *Acta Anaesthesiol Scand.* 2010;54:1248-1256.
- Radke O.C., Schneider T., Heller A.R., Koch T.. Spontaneous breathing during general anesthesia prevents the ventral redistribution of ventilation as detected by electrical impedance tomography: A randomized trial *Anesthesiology.* 2012;116:1227-1234.
- Blankman P., Hasan D., Erik G.J., Gommers D.. Detection of 'best' positive end-expiratory pressure derived from electrical impedance tomography parameters during a decremental positive end-expiratory pressure trial *Crit Care.* 2014;18.
- Zhao Z., Frerichs I., Pulletz S., Müller-Lisse U., Möller K.. The influence of image reconstruction algorithms on linear thorax EIT image

analysis of ventilation *Physiol Meas.* 2014;35:1083-1093.

- Schaefer M.S., Wania V., Bastin B., et al. Electrical impedance tomography during major open upper abdominal surgery: A pilot-study *BMC Anesthesiol.* 2014;14.
- Luepschen H., Meier T., Grossherr M., Leibecke T., Karsten J., Leonhardt S.. Protective ventilation using electrical impedance tomography *Physiol Meas.* 2007;28:S247-S260.
- Pulletz S., Van Genderingen H.R., Schmitz G., et al. Comparison of different methods to define regions of interest for evaluation of regional lung ventilation by EIT *Physiol Meas.* 2006;27:S115.

Author: Vladimír Sobota
 Institute: Faculty of Biomedical Engineering,
 Czech Technical University in Prague
 Street: Sitna Sq. 3105
 City: Kladno
 Country: Czech Republic
 Email: vladimir.sobota@fbmi.cvut.cz



Effects of pleural effusion drainage in the mechanically ventilated patient as monitored by electrical impedance tomography and end-expiratory lung volume: A pilot study

Ales Rara^{a,b,*}, Karel Roubik^b, Tomas Tyll^{a,b}

^a Department of Anaesthesia and Intensive Care, Military University Hospital Prague, Czech Republic

^b Department of Biomedical Technology, Faculty of Biomedical Engineering, Czech Technical University in Prague, Czech Republic



ARTICLE INFO

Available online xxxx

Keywords:

Electrical impedance
Tomography
Mechanical ventilation
Pleural effusion
Thoracocentesis

ABSTRACT

Purpose: In patients with pleural effusion (PLE) monitored by Electrical Impedance Tomography (EIT) an increase in end-expiratory lung impedance (EELI) is observed following evacuation of the PLE. We aimed at differentiating the effect of fluid removal from lung re-aeration and describe the change in ventilation distribution.

Materials and methods: Mechanically ventilated patients were monitored by EIT during PLE evacuation. End-expiratory lung volume (EELV) was measured concurrently. We included a calibration maneuver consisting of an increase in positive end-expiratory pressure (PEEP) by 5 cm H₂O. The ratio $\Delta\text{EELI}/\Delta\text{EELV}$ was used to compare changes of EELI and EELV in response to the calibration maneuver and PLE evacuation. At the same time we assessed distribution of ventilation using changes in tidal variation.

Results: PLE removal resulted in a 6-fold greater increase in $\Delta\text{EELI}/\Delta\text{EELV}$ when compared to the calibration maneuver ($r = 0.84, p < .05$). We observed a relative increase in ventilation in the area of the effusion (mean 7.1%, $p < .006$) and an overall shift of ventilation to the dorsal fraction of the lungs (mean 8%, $p < .0002$).

Conclusions: The increase in EELI in the EIT image after PLE removal was primarily due to the removal of the conductive effusion fluid.

© 2020 Elsevier Inc. All rights reserved.

1. Introduction

Critically ill patients frequently have a disorder of the distribution and volume of body fluids, one manifestation of which is pleural effusion (PLE) formation [1]. According to observational studies 50% to 60% of mechanically ventilated patients develop pleural effusion [2]. PLE may affect pulmonary mechanics and gas exchange, but the consequences are variable and individual. They are determined by anatomical conditions, coexisting pathologies of the pulmonary parenchyma, and the rate of effusion development. The impact of PLE on the clinical outcomes of critically ill patients is unclear and thus the clinical value of fluid evacuation is uncertain [3,4]. The reference method for PLE diagnosis is computed tomography (CT). However, in the intensive care unit ultrasound is routinely used as an excellent and reliable means of assessing the lungs, pleural cavities and PLE [5]. The accuracy of ultrasound in PLE detection is 93% when compared to CT [6].

Electrical impedance tomography (EIT) is a well-known diagnostic method that provides a planar view of the conductivity of the evaluated environment. It is a bed-side, non-invasive, inexpensive, and radiation-free

imaging modality that offers real-time information about the investigated area [7,8]. In clinical practice functional EIT (fEIT) is typically used [8]. fEIT calculates changes in tissue conductivity between a set baseline and the current time frame. Therefore only relative impedance changes expressed in arbitrary units (A.U.) are observable and areas of constant impedance (like pleural effusion) are not easily analyzed. The use of EIT to monitor ventilation and the effect of treatment interventions is common [8-10].

The first study on the effect of changes of thoracic fluid content on thoracic electrical impedance was published over 40 years ago [11] but those dealing with EIT and the presence or the removal of PLE are rare [10,12-15]. A recent study showed a possible diagnostic tool that could help detect pleural effusion using out-of-phase impedance changes [16]. After removal of pleural effusion a significant increase of end-expiratory lung impedance (ΔEELI) has been observed in spontaneously ventilating as well as mechanically ventilated patients [16,17]. The clinical value of such information is uncertain however, because ΔEELI could result not only from increased aeration of lung tissue which was previously compressed by the effusion but also from the removal of the conductive fluid itself.

The aerated lung tissue in ventilated patients corresponds to end-expiratory lung volume (EELV) and its manipulation through changes in positive end-expiratory pressure (PEEP) which is commonly used as a means of improving oxygenation and ventilation mechanics. In

* Corresponding author at: Department of Anaesthesia and Intensive Care, Military University Hospital Prague, U Vojenské nemocnice 1200, Prague, Czech Republic.
E-mail address: raraales@uvn.cz (A. Rara).

other words, changes in EELV correspond to variations in lung aeration. In several trials a good to moderate correlation between Δ EELI and change in end-expiratory lung volume (Δ EELV) was described [18,19].

For these reasons we designed a study that combines EIT monitoring with concurrent EELV measurement before, during and after elimination of pleural effusion in mechanically ventilated patients. Our objective was to determine whether EIT could be used for assessment of lung re-aeration after PLE evacuation. Concurrently we attempted to determine the relative contribution of lung aeration and fluid removal on the change in EELI.

2. Material and methods

We performed a prospective interventional study in the intensive care unit (ICU) of The Military University Hospital in Prague. It was approved by the Ethics committee (RN 108/9–107/2016) and registered in [ClinicalTrials.gov](https://www.clinicaltrials.gov) (NCT03231072). The requirement for written informed consent was waived by the ethics committee. Patients were recruited from January 2017 to March 2018.

Once likely pleural effusion was identified in a patient on mechanical ventilation it was assessed by ultrasound, Ultrasonix Sonix Touch (Ultrasonix Medical Corporation, Richmond, Canada). If the distance from chest-wall to lung parenchyma was over 30 mm and the attending physician indicated fluid removal the patient could be enrolled in the study. We included patients in which the PLE developed in the course of acute disease. Patients suffering from pneumonia, ARDS, or those with lung contusion or lung tumor complications were excluded as well as those that would require excessive sedation or even muscle relaxation to ensure ventilator synchrony during measurement.

All patients were in the supine position with the upper half of the body elevated by 20° and were sedated with propofol and sufentanil. Patients received synchronized intermittent mandatory ventilation via a cuffed endotracheal tube using an Engström Carestation ventilator (GE Healthcare, Madison, Wisconsin) that enables measurement of end-expiratory lung volume (EELV) by oxygen wash-in/wash-out technique. Tidal volume was set to 6–7 ml/kg of ideal body weight. Other ventilator settings remained the same as before the study except for the EIT calibration maneuver (ECM), which was carried out by PEEP elevation of 5 cm H₂O for 5 min before and after PLE removal. EELV was measured before, during, and after each EIT calibration maneuver with six measurements in total. The point of drainage was identified by ultrasound and infiltrated with local anaesthetic (trimecaine), with consideration to the intended location of the EIT belt. The selection of drainage set or chest tube and its insertion was performed by the attending physician. The 16-electrode belt was placed at the level of the 4–6th intercostal space at the parasternal line and connected to the PulmoVista 500 system (Dräger Medical, Lübeck, Germany). EIT recording with a scan rate of 50 Hz was started and continued throughout the procedure (Fig. 1). As soon as fluid ceased to appear in the collection system, the drainage was considered to be complete for the purposes of our measurements. The procedure itself took one hour on average. The fluid was routinely examined according to the attending physician's orders. All interventions were completed without complications.

Analysis of the raw EIT data was done offline by Dräger EIT Data Analysis Tool 6.1. (Dräger Medical, Lübeck, Germany), Microsoft Excel 2010 (Microsoft, Seattle, WA, USA) and Matlab (MathWorks, Inc., Natick, Massachusetts, USA). The selection of the baseline for fEIT data reconstruction has a substantial effect on evaluation of EELI and thus EELV, therefore a single baseline for EIT data reconstruction was selected for each patient at a minimum impedance value during the EIT recording segment before fluid evacuation [20]. We used the default regions-of-interest (ROI) in layers and quadrants that the Dräger software offers, which were applied to the whole image. The end-expiratory lung impedance (EELI) was defined as the average of the end-expiratory global impedance values of 10 consecutive breaths in a specific time span. Ventilation was calculated using the tidal variation (TV) of impedance, defined by the software's

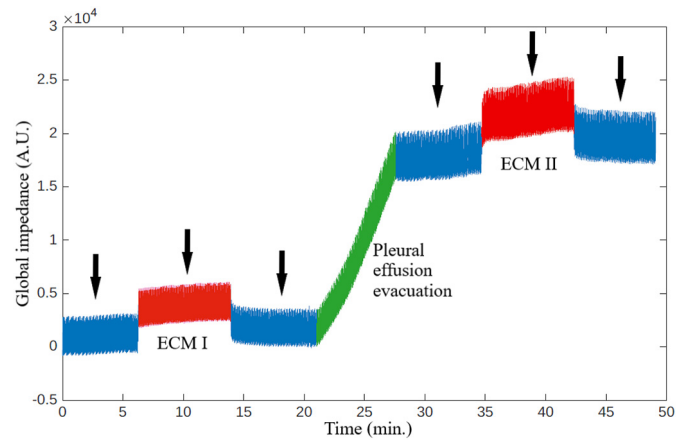


Fig. 1. EIT record of global impedance (i.e. end-expiratory lung impedance, EELI) of one patient during the entire course of measurement with study protocol events labeled. Black arrows—EELV measurement; Red sections—EIT calibration maneuvers (ECM I and II); Green section—evacuation of pleural effusion. (For interpretation of the references to colour in this figure legend, the reader is referred to the web version of this article.)

breath-detection algorithm as the average difference between the maximum and minimum impedance values achieved during the 10 measured breaths. The ventilation change (Δ TV) in a specific fraction of the lung or ROI was calculated as the relative change of TV in percent. The lung adjacent to the PLE was arbitrarily defined as ipsilateral.

3. Data analysis

Results were evaluated using a two-tailed Student's *t*-test for the comparison of two continuous variables. Normality of data was tested using the Kolmogorov-Smirnov test. Comparison of categorical variables was done using the chi-square test. Correlations between variables were assessed using Pearson's *r* coefficient. The limit of statistical significance was defined as *p* = .05. STATISTICA 13.5 software (TIBCO Software Inc., Palo Alto, CA, USA) was employed in statistical evaluation. Results are presented as mean ± standard deviation (SD).

4. Results

A total of 19 patients was included in the study. Of these, 4 were additionally excluded due to interference with the ventilator despite sedation and 2 discarded during data processing for inconsistent measurements and poor EIT image quality. There were 8 women and 5 men in the evaluated group, other characteristics are detailed in [Table 1](#).

Table 1
Basic patient characteristics.

Parameter	
Age (years)	64 ± 15 (32–82)
Height (cm)	166 ± 11
Weight (kg)	64 ± 14
PEEP (cm H ₂ O)	7 ± 2
Tidal volume (ml)	476 ± 50
Pmax. (cm H ₂ O)	21 ± 5
Respiratory rate (per min.)	15 ± 2
Effusion site left (n)	7
Main diagnosis (n)	
Sepsis	6
Trauma	2
Abdominal tumor resection	3
Other	2

PEEP—positive end-expiratory pressure; P-max—peak inspiratory pressure; n—number of patients. Values are expressed as mean ± standard deviation with range for age only.

Table 2
Changes in EELI and EELV, summary.

	EIT calibration maneuver I	EIT calibration maneuver II	PLE evacuation
Δ EELI (A.U.)	2244 \pm 1216	3495 \pm 2462	6947 \pm 3436
Δ EELV (ml)	423 \pm 136	385 \pm 115	240 \pm 107
Δ EELI/ Δ EELV (A.U./ml)	5.5 \pm 2.8	9.2 \pm 6.2	35.2 \pm 22.6

EIT calibration maneuver I and II (PEEP increase by 5 cm H₂O) prior to and after fluid evacuation; Δ EELI—change in expiratory lung impedance; Δ EELV—end-expiratory lung volume change; PLE—pleural effusion.

Results are presented as mean \pm standard deviation.

4.1. Global ventilation

An overview of Δ EELV and Δ EELI measurements is given in Table 2. The volume of drained fluid was 625 \pm 204 ml, with a range of 380–1100 ml. After PLE removal we observed a Δ EELI of 6947 \pm 3436 A.U. and at the same time a Δ EELV of 240 \pm 107 ml. There was a correlation of drained volume to Δ EELV ($r = 0.60, p < .05$) as well as to Δ EELI ($r = 0.52, p < .05$). Δ EELI was inversely proportional to chest circumference ($r = -0.70, p < .05$) and grew in the area where the PLE was localised (Fig. 2). We found no effect of PLE drainage on airway resistance or dynamic compliance.

We calculated the ratio Δ EELI/ Δ EELV (A.U./ml) to follow the association between Δ EELI and Δ EELV during the EIT calibration maneuver and after PLE removal and compared the values for both cases. Results are in Table 2. The ratio of Δ EELI/ Δ EELV (A.U./ml) after evacuation of the fluid was on average 6.4 times greater than during ECM I and, as shown in Fig. 3, the ratios were correlated ($r = 0.84, p < .05$).

The global TV before PLE evacuation was 2546 \pm 963 A.U., after the withdrawal of the fluid it was 2915 \pm 1093 A.U. corresponding to an increase of TV in 12 patients (429 \pm 340 A.U.), in 1 patient a decrease was observed. The change in global TV in response to both calibration maneuvers was variable (from -800 to $+500$ A.U.).

4.2. Local ventilation

There was a relative increase of TV of 7.1% \pm 7.6% ($p < .006$) in quadrant ROI 3 or 4 where the maximum of the PLE was previously localised. In 11 patients we observed an overall increase in ipsilateral lung ventilation up to 10% of TV, but in 2 cases the trend was reversed (7.3 and 4.4%, respectively). The lateral redistribution of TV after PLE removal however, was not statistically significant ($p = .92$).

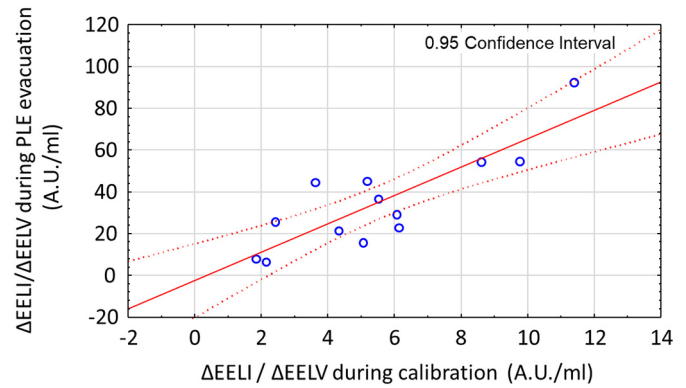


Fig. 3. The correlation between Δ EELI/ Δ EELV ratio (A.U./ml) during EIT calibration maneuver I and after pleural effusion evacuation.

Concerning anteroposterior ventilation distribution, after PLE evacuation there was a shift of TV to the dorsal lung fraction, i.e. layers ROI 3 and 4, of 8% \pm 5.5% ($p < .0002$), after ECM I 9% \pm 5.5% ($p < .0002$) and ECM II 4% \pm 2.7% ($p < .0002$).

Layers ROI 2 and 3 represent the middle parts of the lungs which initially contained 78.8% \pm 6.8% of global TV, followed by a small decrease after effusion removal of 2.7% \pm 3.5% ($p < .03$) shifting towards ROI 4.

5. Discussion

We showed that the increase in global impedance following effusion evacuation does not fully correspond to the improvement of lung aeration but is largely influenced by the removal of the conductive pleural fluid. Therefore, the functional EIT itself is not a suitable tool for evaluating the impact of PLE evacuation on lung aeration.

The increase of EELV immediately after effusion evacuation was about one third of the volume of the evacuated effusion, which is similar to earlier published data [21]. Although the increase in EELV was more pronounced during the calibration maneuvers the change in EELI per unit change in EELV, i.e. the ratio Δ EELI/ Δ EELV, was 4–6 times greater after effusion evacuation (Table 1). If the observed change in EELI after effusion evacuation corresponded only to changes in lung tissue aeration—as with the calibration maneuver—the corresponding increase in EELV would be larger than the effusion volume. The strong influence of the removal of conductive material is supported by the fact that EIT

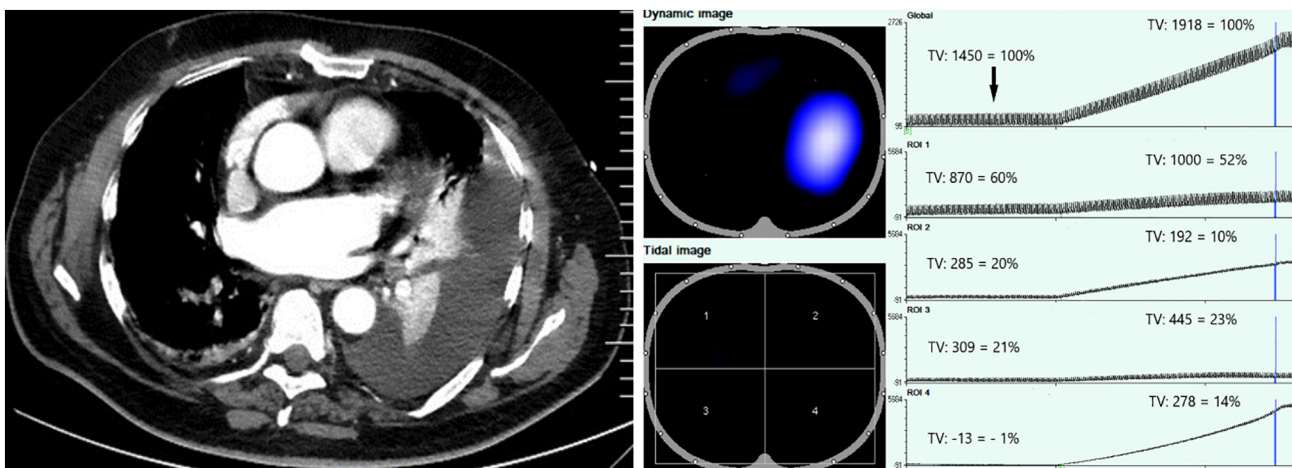


Fig. 2. Left: CT scan, left-sided pleural effusion, patient with urosepsis. Right: the same patient, EIT record, before and during evacuation of PLE, PulmoVista 500 system, modified. Region-of-interest (ROI) in quadrants. Black arrow—time of tidal variation (TV) distribution (%) in ROI before evacuation. Vertical blue line—time of the dynamic image in the upper left corner and corresponding TV distribution (%) in ROI after PLE evacuation. (For interpretation of the references to colour in this figure legend, the reader is referred to the web version of this article.)

is very sensitive to even a small evacuated fluid volume and a steep increase of impedance was visible in the area that anatomically corresponded to the PLE site (Fig. 2).

According to global tidal variation we observed mainly an increase in ventilation after PLE removal while in the course of calibration maneuvers this trend was not apparent. This is probably due to the fact that PEEP elevation influences more the whole lung and the response at the cross section of EIT belt is therefore quite variable.

Our results further showed a significant increase in ventilation in the quadrants previously occupied by the effusion. This may indicate definite lung re-aeration [16] but a concurrent dorsal shift of already ventilated lung tissue cannot be distinguished. The effusion evacuation led to a small shift in ventilation to the dorsal fraction of the lungs but the maximum ventilated regions (layers ROI 2 and 3) of the lungs remained almost unchanged. Interestingly, we did not observe a statistically significant shift of ventilation towards the ipsilateral lung.

These changes may contribute to the discussion of the clinical importance of PLE removal because the main outcome criteria such as mortality or length of ICU stay are not significantly influenced [26]. If removal of effusion does not substantially alter the ventilation distribution, then the area of the lung exposed to positive pressure during mechanical ventilation is almost the same after PLE evacuation and the incidence of ventilator induced lung injury (VILI) should not be affected.

The observed ventilation redistribution can also be explained by the fact that the EIT image is made up of the volume of tissue extending ± 10 cm from the tomographic plane depending on the EIT type [27] and thus also shows parts of the lungs where there is less or no surrounding exudate. The belt position could be important as well in patients whose diaphragm level is unusual due to high intraabdominal pressure [28].

A trend towards increased aeration (EELI) was apparent during ECM II (Fig. 1) and remained in the final phase of the EIT record. We could expect a more pronounced increase of EELI several hours apart but this would require further research. It is likely that performing the classic recruitment maneuver following effusion evacuation would result in greater aeration of previously compressed lung tissue and greater participation in ventilation. It could therefore be convenient to include some form of distension routinely after PLE removal that could improve aeration and thus further improve oxygenation.

The actual underlying pathology and pleural fluid characteristics may have an effect on lung expansion and residual fluid volume. The re-expansion corresponds with Δ EELV which was included in our measurements and in this sense the results (the ratio Δ EELI/ Δ EELV) takes into account the degree of re-expansion.

This study is to our knowledge the first to combine the use of EIT and EELV measurements during PLE evacuation to evaluate the effect of fluid removal and lung aeration. Ensuring synchrony with the ventilator and maintaining constant ventilatory parameters were prerequisites for consistent measurement, particularly of EELV and its changes.

EELV was used in this study as a surrogate of lung aeration changes. To calibrate EELV measurement using EIT, the PEEP maneuvers were conducted. Several studies confirmed the linear relationship between EELV measured by an independent method with EELI measured by EIT and induced by PEEP maneuvers [18] and suggest EIT as a suitable method for PEEP-induced EELV measurement [19]. Even though several authors documented that the EELV/PEEP relationship might not always be linear [22] and might be affected by the position of the EIT belt [23], the PEEP maneuvers can be used for EELV measurement calibration, especially when the PEEP changes used for calibration are small [24,25].

It turned out that the second calibration maneuver led to smaller Δ EELV than the first one (Table 2). After the PLE evacuation the lung partly re-expanded and EELV increased by one third of the volume of the drained fluid (240 ± 107 ml). We can therefore assume that the recruitable volume of the lungs that could be influenced by moderate PEEP elevation (i.e. ECM) was reduced and so was Δ EELV during the second calibration maneuver.

Our study has several limitations. Above all, it should be noted that EELV is a global ventilation parameter, while EIT measurements are focused only on the cross-section within the wide plane of the belt. The re-aeration could be scanned but not quantified by ultrasound. The most accurate method for assessing regional re-aeration would probably be to compare the CT scan at the EIT belt level. Secondly, the small patient group had to be further reduced to assure consistent data for evaluation. Finally, patients were monitored only for a short time after the evacuation of most effusions and lacked long-term follow up for comparison and measurement of residual effusion volume and lung re-expansion.

6. Conclusion

In summary, the influence of pleural effusion evacuation on lung aeration in mechanically ventilated patients cannot be effectively evaluated by EIT alone. The steep increase of end-expiratory lung impedance in the course of pleural effusion evacuation was largely caused by the loss of conductive electrolyte (i.e. the pleural effusion) adjacent to the EIT belt. Improved aeration of lung tissue had only a relatively minor effect.

Funding

This work was supported by the Department of Anaesthesia and Intensive Care, Military University Hospital Prague, Czech Republic and Czech Technical University in Prague, Czech Republic, grant SGS20/202/OHK4/3T/17.

Acknowledgements

The authors thank to O. Bradac for statistical analysis, M. Müller for data processing in MatLab and M. Pochop for language corrections.


References

- Miserochchi G. Physiology and pathophysiology of pleural fluid turnover, (in eng). *Eur Respir J* Jan 1997;10(1):219–25.
- Walden AP, Garrard CS, Salmon J. Sustained effects of thoracocentesis on oxygenation in mechanically ventilated patients, (in eng). *Respirology* Aug 2010;15(6):986–92. <https://doi.org/10.1111/j.1440-1843.2010.01810.x>.
- Goligher EC, Leis JA, Fowler RA, Pinto R, Adhikari NK, Ferguson ND. Utility and safety of draining pleural effusions in mechanically ventilated patients: a systematic review and meta-analysis, (in eng). *Crit Care* 2011;15(1):R46. <https://doi.org/10.1186/cc10009>.
- Razazi K, et al. Pleural effusion during weaning from mechanical ventilation: a prospective observational multicenter study, (in eng). *Ann Intensive Care* Nov 2018;8(1):103. <https://doi.org/10.1186/s13613-018-0446-y>.
- Balik M, et al. Ultrasound estimation of volume of pleural fluid in mechanically ventilated patients, (in eng). *Intensive Care Med* Feb 2006;32(2):318–21. <https://doi.org/10.1007/s00134-005-0024-2>.
- Walden AP, Jones QC, Matsa R, Wise MP. Pleural effusions on the intensive care unit: hidden morbidity with therapeutic potential, (in eng). *Respirology* Feb 2013;18(2):246–54. <https://doi.org/10.1111/j.1440-1843.2012.02279.x>.
- Costa ELV, Lima RG, Amato MBP. Electrical impedance tomography. *Curr Opin Crit Care* 2009;15(1):18–24.
- Leonhardt S, Lachmann B. Electrical impedance tomography: the holy grail of ventilation and perfusion monitoring?, (in eng). *Intensive Care Med* Dec 2012;38(12):1917–29. <https://doi.org/10.1007/s00134-012-2684-z>.
- Kobylanski J, Murray A, Brace D, Goligher E, Fan E. Electrical impedance tomography in adult patients undergoing mechanical ventilation: a systematic review, (in eng). *J Crit Care* 10 2016;35:33–50. <https://doi.org/10.1016/j.jccr.2016.04.028>.
- Frerichs I, et al. Chest electrical impedance tomography examination, data analysis, terminology, clinical use and recommendations: consensus statement of the Transnational EIT development study group, (in eng). *Thorax* 01 2017;72(1):83–93. <https://doi.org/10.1136/thoraxjnl-2016-208357>.
- Denniston JC, Baker LE. Measurement of pleural effusion by electrical impedance, (in eng). *J Appl Physiol* May 1975;38(5):851–7.
- Petersen JR, Jensen BV, Drabaek H, Viskum K, Mehlsen J. Electrical impedance measured changes in thoracic fluid content during thoracocentesis. *Clin Physiol (Oxford, England)* 1994;14(4):459–66.
- Arad M, Zlochiver S, Davidson T, Shoenfeld Y, Adunsky A, Abboud S. The detection of pleural effusion using a parametric EIT technique, (in eng). *Physiol Meas* Apr 2009;30(4):421–8. <https://doi.org/10.1088/0967-3334/30/4/006>.

- [14] Campbell JH, Harris ND, Zhang F, Brown BH, Morice AH. Clinical applications of electrical impedance tomography in the monitoring of changes in intrathoracic fluid volumes, (in eng). *Physiol Meas* May 1994;15(Suppl 2a):A217–22. <https://doi.org/10.1088/0967-3334/15/2a/027>.
- [15] Bläser D, et al. Unilateral empyema impacts the assessment of regional lung ventilation by electrical impedance tomography, (in eng). *Physiol Meas* Jun 2014;35(6): 975–83. <https://doi.org/10.1088/0967-3334/35/6/975>.
- [16] Becher T, Bußmeyer M, Lautenschläger I, Schädler D, Weiler N, Frerichs I. Characteristic pattern of pleural effusion in electrical impedance tomography images of critically ill patients, (in eng). *Br J Anaesth* Jun 2018;120(6):1219–28. <https://doi.org/10.1016/j.bja.2018.02.030>.
- [17] Alves SH, Amato MB, Terra RM, Vargas FS, Caruso P. Lung re-aeration and re-ventilation after aspiration of pleural effusions. A study using electrical impedance tomography, (in eng). *Ann Am Thorac Soc* Feb 2014;11(2):186–91. <https://doi.org/10.1513/AnnalsATS.201306-1420C>.
- [18] Hinz J, et al. End-expiratory lung impedance change enables bedside monitoring of end-expiratory lung volume change, (in eng). *Intensive Care Med* Jan 2003;29(1): 37–43. <https://doi.org/10.1007/s00134-002-1555-4>.
- [19] Grivans C, Lundin S, Stenqvist O, Lindgren S. Positive end-expiratory pressure-induced changes in end-expiratory lung volume measured by spirometry and electric impedance tomography, (in eng). *Acta Anaesthesiol Scand* Oct 2011;55(9): 1068–77. <https://doi.org/10.1111/j.1399-6576.2011.02511.x>.
- [20] Roubik K, Sobota V, Laviola M. Selection of the baseline frame for evaluation of electrical impedance tomography of the lungs. Presented at the 2015 Second International Conference on Mathematics and Computers in Sciences and in Industry (MCSI), Siema; 2015.
- [21] Razavi K, et al. Effects of pleural effusion drainage on oxygenation, respiratory mechanics, and hemodynamics in mechanically ventilated patients, (in eng). *Ann Am Thorac Soc* Sep 2014;11(7):1018–24. <https://doi.org/10.1513/AnnalsATS.201404-1520C>.
- [22] Markhorst DG, Groeneveld AB, Heethaar RM, Zonneveld E, Van Genderingen HR. Assessing effects of PEEP and global expiratory lung volume on regional electrical impedance tomography, (in eng). *J Med Eng Technol* 2009;33(4):281–7. <https://doi.org/10.1080/03091900802451240>.
- [23] Bikker IG, Leonhardt S, Bakker J, Gommers D. Lung volume calculated from electrical impedance tomography in ICU patients at different PEEP levels, (in eng). *Intensive Care Med* Aug 2009;35(8):1362–7. <https://doi.org/10.1007/s00134-009-1512-6>.
- [24] Sobota V, Müller M, Roubík K. Intravenous administration of normal saline may be misinterpreted as a change of end-expiratory lung volume when using electrical impedance tomography. *Sci Rep* 2019;9(1):5775 2019/04/08 <https://doi.org/10.1038/s41598-019-42241-7>.
- [25] Sobota V, Roubik K. Center of Ventilation—Methods of Calculation Using Electrical Impedance Tomography and the Influence of Image Segmentation; 2016; 1258–63.
- [26] Fysh ETH, et al. Clinically significant pleural effusion in intensive care: a prospective multicenter cohort study, (in eng). *Crit Care Explor* Jan 2020;2(1):e0070. <https://doi.org/10.1097/CCE.000000000000070>.
- [27] *Electrical Impedance Tomography: The Realization of Regional Lung Monitoring*. Germany: Dräger Medical GmbH EIT Booklet; 2011.
- [28] Buzkova K, Muller M, Rara A, Roubik K, Tyll T. Ultrasound detection of diaphragm position in the region for lung monitoring by electrical impedance tomography during laparoscopy, (in eng). *Biomed Pap Med Fac Univ Palacky Olomouc Czech Repub* Mar 2018;162(1):43–6. <https://doi.org/10.5507/bp.2018.005>.

Rara, A., Roubik, K., Tyll, T. Effects of pleural effusion drainage in the mechanically ventilated patient as monitored by electrical impedance tomography and end-expiratory lung volume: A pilot study. *Journal of Critical Care*, 59, October 2020, pp. 76-80.

SCIENTIFIC REPORTS



OPEN

Intravenous administration of normal saline may be misinterpreted as a change of end-expiratory lung volume when using electrical impedance tomography

Vladimír Sobota^{1,2}, Martin Müller^{1,3} & Karel Roubík¹

Electrical impedance tomography (EIT) is a noninvasive imaging modality that allows real-time monitoring of regional lung ventilation. The aim of the study is to investigate whether fast saline infusion causes changes in lung impedance that could affect the interpretation of EIT data. Eleven pigs were anaesthetized and mechanically ventilated. A bolus of 500 mL of normal saline was administered rapidly. Two PEEP steps were performed to allow quantification of the effect of normal saline on lung impedance. The mean change of end-expiratory lung impedance (EELI) caused by the saline bolus was equivalent to a virtual decrease of end-expiratory lung volume (EELV) by 227 (188–250) mL and decremental PEEP step of 4.40 (3.95–4.59) cmH₂O (median and interquartile range). In contrast to the changes of PEEP, the administration of normal saline did not cause any significant differences in measured EELV, regional distribution of lung ventilation determined by EIT or in extravascular lung water and intrathoracic blood volume. In conclusion, EELI can be affected by the changes of EELV as well as by the administration of normal saline. These two phenomena can be distinguished by analysis of regional distribution of lung ventilation.

Electrical impedance tomography (EIT) is a noninvasive bedside imaging modality suitable for continuous monitoring of lung functions¹. Dividing the acquired images into regions of interest (ROIs), EIT provides information about regional distribution of lung ventilation^{2–4}. Using the global trend of end-expiratory lung impedance (EELI), changes in end-expiratory lung volume (EELV) can be estimated^{5,6}. EIT is considered to be an easy-to-use technique for PEEP optimization^{7–9}, as shown in Fig. 1. The decreasing trend of EELI represents a gradual alveolar derecruitment due to insufficient PEEP, while an increasing trend represents recruitment. A stable EELI value indicates the optimal PEEP level.

During our previous experiments in pigs with EIT measurements lasting several hours we observed a noticeable steady decrease of EELI values. This decrease could be falsely interpreted as a change of EELV that was not apparent. Importantly, we observed that the decreasing trend of EELI changed immediately after an interruption of intravenous fluid administration and was restored again when the fluid administration was re-established.

The effect of fluid balance on changes in electrical impedance of human body is well known and widely used in bioelectrical impedance analysis for determination of total body water^{10,11}. There are studies that described the effect of fluid accumulation in peritoneum^{12,13}, diuresis¹⁴ or intravenous fluid administration¹⁵ upon the changes of thoracic impedance as determined by EIT. However, to the best of our knowledge, there is no study dealing with the direct comparison of lung volume related changes in EIT with those caused by fluid administration.

The aims of the study are (1) to investigate whether the fast intravenous administration of normal saline affects EELI in healthy porcine lungs, (2) to compare these impedance changes with the impedance changes associated

¹Department of Biomedical Technology, Faculty of Biomedical Engineering, Czech Technical University in Prague, Kladno, Czech Republic. ²Department of Physiology, Maastricht University, Maastricht, The Netherlands.

³Department of Anaesthesiology and Intensive Care, First Faculty of Medicine, Charles University and Thomayer Hospital, Prague, Czech Republic. Correspondence and requests for materials should be addressed to V.S. (email: vladimir.sobota@fbmi.cvut.cz)

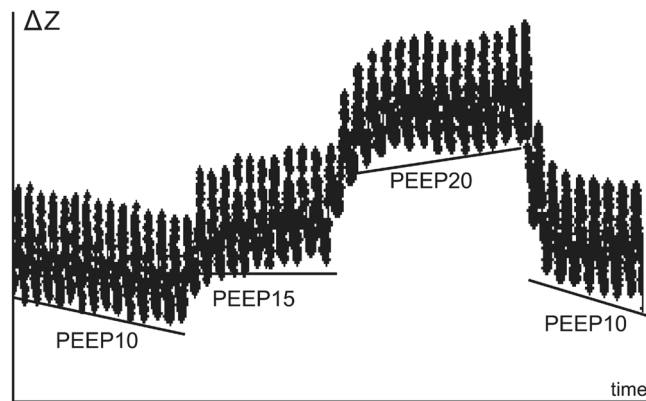


Figure 1. Optimization of positive end-expiratory pressure (PEEP) using electrical impedance tomography. Decreasing trend in end-expiratory lung impedance (EELI) indicates derecruitment while an increase of EELI indicates recruitment. Horizontal tracing indicates stable end-expiratory lung volume and corresponds with the optimal PEEP. Reproduced with permission⁷.

Parameter	Baseline values (Phase 1)	End values (Phase 6)	<i>p</i> Wilcoxon test
Expiratory tidal volume, mL	469 (426–494)	473 (424–498)	0.91
Respiratory rate*, b/min	20 (20–22)	20 (20–22)	—
Inspiratory to expiratory time ratio*	0.5	0.5	—
Fraction of inspired oxygen*, %	25 (25–30)	25 (25–30)	—
End-tidal carbon dioxide concentration, mmHg	43 (40–44)	42 (40–44)	0.12
Peripheral capillary oxygen saturation, %	98 (97–100)	98 (96–100)	0.91
Minute ventilation, L/min	9.2 (8.9–9.5)	9.3 (8.9–9.5)	0.47
Peak airway pressure, cmH ₂ O	23 (21–26)	25 (24–26)	0.07
Positive end-expiratory pressure*, cmH ₂ O	5	5	—
Compliance, ml/cmH ₂ O	32 (31–42)	31 (30–39)	0.07

Table 1. Ventilatory parameters during the study protocol. Data are presented as median and interquartile range (Q₁–Q₃). *Preset parameter.

with PEEP alterations, (3) to investigate whether the impedance changes caused by intravenous administration of normal saline can be distinguished from the impedance changes caused by PEEP alterations.

Materials and Methods

The prospective interventional animal study was performed in the accredited animal laboratory of the Department of Physiology, First Faculty of Medicine, Charles University in Prague, in accordance with Act No. 246/1992 Coll., on the protection of animals against cruelty that incorporates the relevant legislation of the European Community. The study was approved by the Institutional Animal Care and Use Committee of the First Faculty of Medicine, Charles University in Prague.

Animal preparation and monitoring. Eleven crossbred (Landrace × Large White) female pigs (*Sus scrofa domestica*) 3–4 months old with an average body weight of 48 kg (43–52 kg range) were involved in the study.

The animals received total intravenous anaesthesia with muscle relaxation. Mechanical lung ventilation was conducted using an Engström Carestation (GE Healthcare, Waukesha, WI, USA) ventilator in the volume-controlled mode. The pre-set and measured ventilatory parameters are described in Table 1. Detailed information regarding the anaesthesia and animal preparation is provided in the Supplementary Information.

EIT system PulmoVista 500 (Dräger Medical, Lübeck, Germany) was used for data acquisition. An electrode belt of size “S” (chest circumference from 70 to 85 cm) was attached to the animal chest, cranially to the level of diaphragm at PEEP of 5 cmH₂O. In most of the subjects, this position corresponded with the 6th intercostal space. Correct placement of the electrode belt was verified by chest X-ray. The frequency of the applied alternating current was set to 110 kHz and the EIT images were acquired with a frame rate of 50 Hz.

End-expiratory lung volume (EELV) was measured by FRC INview module of the Engström Carestation ventilator. The applied change of FiO₂ for the wash-in/wash-out measurement of EELV was 10%.

Haemodynamic monitoring was performed using Edwards LifeSciences monitor EV1000 (Edwards LifeSciences, Irvine, CA, USA). Cardiac output, extravascular lung volume (EVLW) and intrathoracic blood volume (ITBV) were measured using the technique of transpulmonary thermodilution (TPTD) with the PiCCO arterial catheter placed in *a. femoralis* and cold normal saline applied in *v. jugularis interna*. Maximum of six

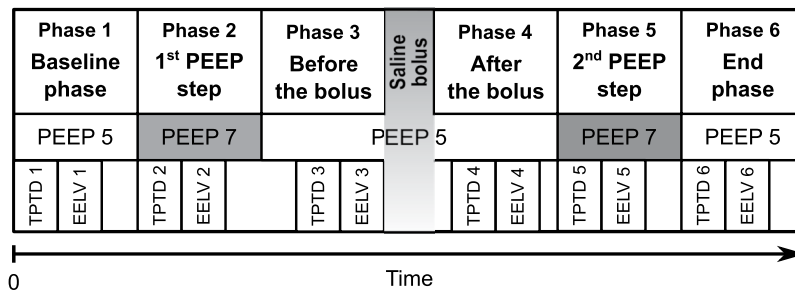


Figure 2. Timeline of the study protocol. TPTD1–TPTD6: individual transpulmonary thermodilution measurements; EELV1–EELV6: individual end-expiratory lung volume measurements.

boluses of normal saline were applied, 10 mL each. According to the EV1000 reference manual, three values of CO that did not differ more than by 10% were used for the evaluation.

Study protocol. After preparation, instrumentation and myorelaxation of an animal, calibration of the EIT system was performed and data acquisition was initiated. Recording of ventilatory data was initiated as well. A steady phase in a duration of approximately 30 minutes was introduced. The study protocol consisted of six phases and is described schematically in Fig. 2. Initial TPTD measurement was conducted at the beginning of the baseline phase. Incremental PEEP step from 5 to 7 cmH₂O was performed and the second TPTD measurement followed. PEEP was decreased back from 7 to 5 cmH₂O and TPTD was measured again. Consequently, a bolus of 500 mL of normal saline was administered using a pressure infusion bag. The duration of the administration was 6 minutes on average. Three minutes after the end of the saline administration a TPTD was measured, followed by the second incremental PEEP step from 5 to 7 cmH₂O. TPTD was measured again and PEEP was decreased back to the initial value. The last TPTD measurement was done during the end phase when the PEEP was set back to 5 cmH₂O. EELV measurements were performed always immediately after the measurements of TPTD.

Data analysis and statistics. EIT data were pre-processed using EIT Data Analysis Tool (Dräger Medical, Lübeck, Germany). For each animal, a reference frame (also referred to as a baseline frame) was selected from the initial baseline phase of the experiment and was used for the reconstruction of EIT images and impedance waveforms. The data were exported to MATLAB (Mathworks Inc., Natick, MA, USA) where further processing was performed.

For each breath cycle, tidal variation (TV) image was calculated as a difference between the end-inspiratory and the previous end-expiratory EIT image¹. Four horizontal regions of interest (ROIs) were determined in the TV images, numbered from 1 (ventral) to 4 (dorsal). Proportional ventilation was calculated for each ROI and was expressed as a percentage of the overall tidal impedance change. Mean values of proportional ventilation were calculated for each phase, considering the values from an interval of 60 seconds. Detailed description of the method for calculation of the differences in regional ventilation is provided in the Supplementary Information.

To quantify the changes in end-expiratory lung impedance caused by the administration of 500 mL of normal saline (ΔZ_{bolus}), the value of ΔZ_{bolus} was expressed both as an equivalent (i.e. virtual) change of end-expiratory lung volume ($\Delta \text{EELV}_{\text{bolus,equiv}}$) and an equivalent (virtual) change of positive end-expiratory pressure ($\text{PEEP}_{\text{bolus,equiv}}$). The values of $\Delta \text{EELV}_{\text{bolus,equiv}}$ were compared with reference EELV data measured using the FRC INview module of the ventilator. The calculation of $\text{PEEP}_{\text{bolus,equiv}}$ and $\Delta \text{EELV}_{\text{bolus,equiv}}$ is described in detail in the Supplementary Information.

The values are presented as median and interquartile range (Q_1 – Q_3) unless stated otherwise. The differences in regional ventilation, EELV, EVLW and ITBV were compared using Friedman's test with Tukey's post-hoc analysis. Wilcoxon's test was used for the comparison of the differences between the measured and the estimated EELV values, and for the comparison of initial and end values of ventilatory parameters. A p -value < 0.05 was considered statistically significant.

Results

All animals completed the full study protocol and were included in the data analysis. Decrease in end-expiratory lung impedance (EELI) was observed in all subjects when the bolus of normal saline was administered intravenously. A representative example of changes in EELI, the time course of regional ventilation in pre-defined ROIs and the corresponding values of applied PEEP are shown in Fig. 3.

The impedance change caused by the administration of the normal saline (ΔZ_{bolus}) was equivalent to a decrease of end-expiratory lung volume ($\Delta \text{EELV}_{\text{bolus,equiv}}$) by 227 mL (178–250 mL). Compared to this, the measured decrease of end-expiratory lung volume ($\Delta \text{EELV}_{\text{bolus,meas}}$) was only 52 mL (25–78 mL) and differed significantly from the values of $\Delta \text{EELV}_{\text{bolus,equiv}}$ as depicted in Fig. 4A. When expressed as a value of an equivalent (virtual) positive end-expiratory pressure ($\text{PEEP}_{\text{bolus,equiv}}$), the administration of normal saline was equivalent to the decrease of PEEP by 4.40 cmH₂O (3.95–4.59 cmH₂O).

The administration of saline bolus was not associated with any statistically significant difference in the regional distribution of lung ventilation and in EELV, as shown in Figs 4 and 5. Contrary to this, the PEEP steps performed

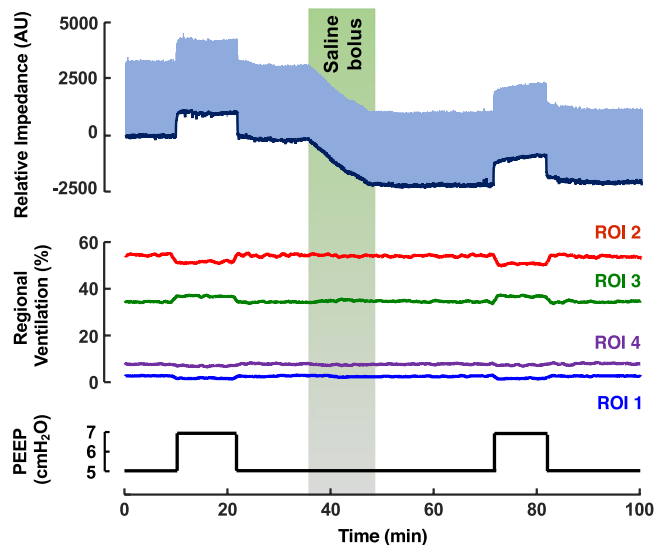


Figure 3. Typical changes of end-expiratory lung impedance and regional ventilation during the animal trial. Top graph: End-expiratory lung impedance (EELI) trend (dark blue) was determined as local minima of the relative impedance waveform (light blue). Middle graph: distribution of ventilation in the pre-defined regions of interest (ROIs). Bottom graph: time course of positive end-expiratory pressure (PEEP) during the trial.

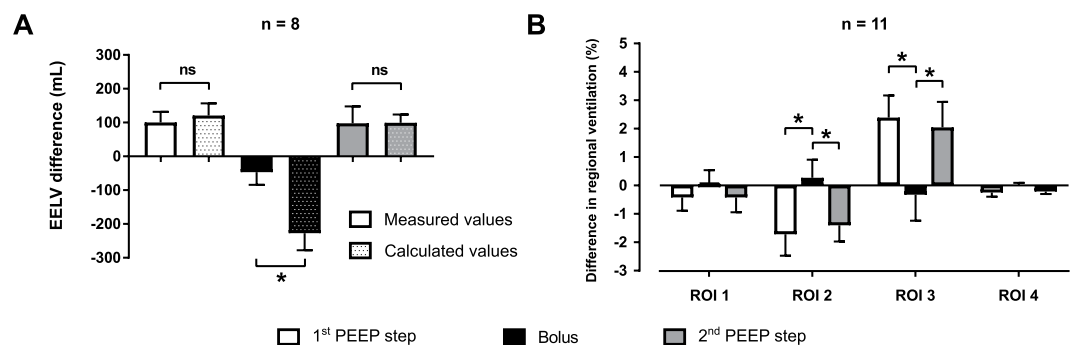


Figure 4. Changes in end-expiratory lung volume (EELV) and regional ventilation. (A) Ventilator-measured changes of EELV during the bolus of normal saline and induced by the PEEP steps together with the estimated EELV changes calculated from the EIT data. The solid black bar represents the decrease of EELV during the administration of normal saline ($\Delta\text{EELV}_{\text{bolus, meas}}$). The dotted black bar represents the respective change of EELV estimated from the EIT data ($\Delta\text{EELV}_{\text{bolus, equiv}}$). (B) Differences in regional ventilation caused by the PEEP steps and by the bolus of normal saline. Statistically significant differences (Wilcoxon's test for the EELV data, Friedman's test with Tukey's post hoc analysis for the regional ventilation data, $p < 0.05$) are denoted with *. The error bars represent standard deviation.

during the study protocol induced significant differences in the regional ventilation in ROI 2 and 3, as shown in Fig. 4B and in EELV, as shown in Fig. 5. The ventilatory parameters remained stable during the experiment, except for peak airway pressure and compliance in which statistically insignificant changes were observed (Table 1). No statistically significant differences were observed in the values of EVLW and ITBV measured by TPTD during the experiment, as shown in Fig. 6.

Discussion

The main finding of this study is that fast administration of normal saline significantly affects end-expiratory lung impedance (EELI) provided by EIT and thus can compromise assessment of end-expiratory lung volume. The study also shows that the administration of therapeutic volume of normal saline causes a decrease in EELI comparable to a decrease of PEEP by several cmH_2O . Nevertheless, the administration of normal saline does not affect regional distribution of lung ventilation in the pre-defined regions of interest.

Statistically significant shift of regional ventilation towards dorsal parts of lungs (increased proportional ventilation in ROI 3 and its decrease in ROI 2) was observed after the PEEP was increased by 2 cmH_2O . Compared to that, the application of normal saline was not associated with remarkable changes in the regional distribution of lung ventilation determined by EIT. This finding indicates that there was no redistribution of lung ventilation or regional differences of lung impedance when the saline was administered intravenously. PEEP-induced

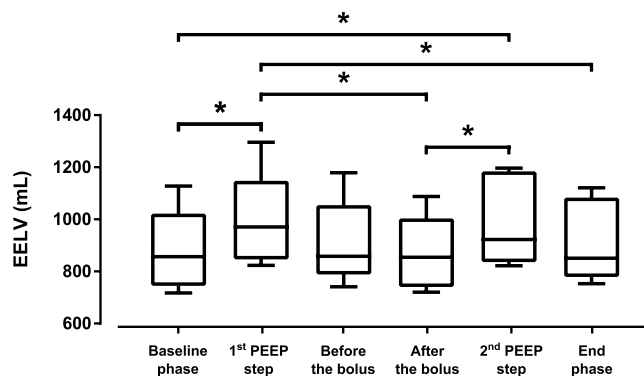


Figure 5. End-expiratory lung volume (EELV) measured by FRC INview module of the ventilator during the experiment. Statistically significant differences (Friedman's test with Tukey's post hoc analysis, $p < 0.05$) are denoted with *.

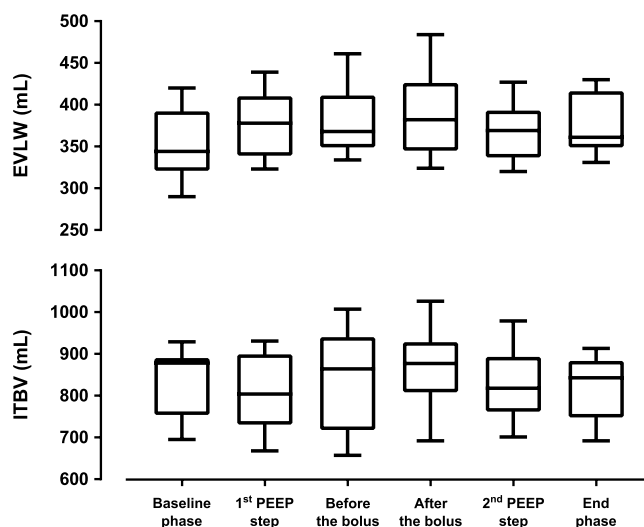


Figure 6. Extravascular lung water (EVLW) and intrathoracic blood volume (ITBV) during the experiment. No statistically significant differences were observed in the values of EVLW and ITBV (Friedman's test, $p > 0.05$).

increase of EELV led to an increase of regional lung ventilation in dependent parts of the lungs which is the main mechanism why PEEP optimisation represents a basic strategy for homogenisation of lung ventilation. Therefore, the EELI changes caused by the alterations of EELV can be distinguished from the changes of EELI caused by the administration of normal saline by analysing the regional differences in ventilation between dependent and non-dependent lung regions (ROIs).

Statistically significant differences in EELV were observed only when PEEP was modified. The application of normal saline did not result in statistically significant change of EELV when measured by the ventilator. Compared to that, the change of EELV estimated from the decrease of EELI differed significantly also during the application of the bolus of normal saline. This finding implies that administration of normal saline might be potentially misinterpreted as derecruitment, especially when regional ventilation is not taken into account.

A slight decrease of compliance and an increase of peak airway pressure were observed during the study. Though not statistically nor clinically significant, the authors speculate that these changes might be caused by a slight increase of the volume of intrathoracic water. This finding correlates with observed insignificant increase of EVLW. Moreover, gradual increase in the portion of atelectatic lung regions can be assumed at the end phase of the experiment due to the mechanical lung ventilation, muscle relaxation and anaesthesia¹⁶. Considering the magnitude of the observed changes in ventilatory parameters, the described finding may be also affected by the imprecision of the ventilator measurements.

No significant changes were observed in the values of EVLW and ITBV determined by transpulmonary thermomodulation. The decrease of EELI observed during the administration of normal saline thus can be explained by an increase of the compartment with higher electrical conductivity. The conductivity of lung tissue may be affected either by the volume of the administered fluid or by its electric properties. It has been described that hypertonic saline solution can be used as a contrast agent for EIT¹⁷. Our findings demonstrate that, compared to TPTD, EIT is more sensitive to identify changes in intrathoracic fluids when normal saline is administered.

The administered volumes of crystalloids per unit of body weight were considerably lower when compared to the volumes that are used for fluid therapy in clinical practice. For example, we used 10.64 mL/kg (9.90–10.99 mL/kg), while the guidelines of Surviving Sepsis Campaign recommend the fluid challenge of at least 30 mL/kg of crystalloids for the first three hours of the initial phase of the sepsis or septic shock treatment¹⁸. However, the mean dosing rate applied in our study (103 mL/kg/h) was substantially higher than the dosing rate recommended by the guidelines (>30 mL/kg within the first 3 hours, i.e. >10 mL/kg/h). Our main reason for the choice of the fast dosing rate and a short dosing time was to separate the effect of the saline administration from possible derecruitment, interferences or time instability of EIT¹⁹.

When studying the response time of the bolus administration upon the trend of end-expiratory lung impedance, we did not observe any remarkable time delay between the beginning of the saline administration and the onset of impedance change ΔZ_{bolus} .

The PEEP step of 2 cmH₂O was used because it is a common step used for PEEP titration^{20,21}. The aim of the performed PEEP steps in our protocol was to obtain changes of EELI that can be further used for conversion of ΔZ_{bolus} into the values of equivalent (virtual) PEEP step (PEEP_{bolus,equiv}). Large PEEP changes were avoided due to possible alterations of lung mechanics. Moreover, applying a small PEEP step allowed us to linearize the relationship between PEEP and EELI, which in general is non-linear²². The duration of PEEP steps was based on clinical studies that investigated the effect of PEEP on changes of EELV by means of EIT^{23,24}. Longer duration of the PEEP steps was not necessary because the levels of EELI became stable after several breath cycles.

There are several studies that investigated the effect of fluid-related interventions upon the changes in thoracic impedance^{12–15}. However, none of these studies compared the magnitude of the fluid-related impedance changes with the impedance changes caused by lung ventilation. Our study compares the impedance changes caused by administration of normal saline with those that are associated with alterations in end-expiratory lung volume. These changes were assessed quantitatively and were described in time domain as well as on a regional basis.

The results indicate that, compared to PEEP alterations, the administration of normal saline bolus does not affect regional distribution of lung ventilation when assessed by EIT. This finding is in agreement with the study of Bodenstern *et al.*¹⁵ who investigated the effect of volume interventions on pulmonary bioimpedance. The authors demonstrated that neither infusion of crystalloid or colloid, nor blood withdrawal cause changes in regional lung ventilation. However, changes in regional lung ventilation can be used for determination of extravascular lung water when small rotations of the subject are applied, as showed by Trepte *et al.*²⁵. Trepte *et al.* detected changes in tidal variations between left and right hemithorax in animals with induced lung injury when gravity-dependent redistribution of pulmonary oedema was created by lateral rotation of the animals along their longitudinal axis.

Using healthy animals as the subjects of the study, we assumed that the portion of ventilated lung was within the physiological limit and remained stable in the phases with constant PEEP values. To align the study closer to the real needs of clinical practice it would be appropriate to conduct the study in pathophysiological lung conditions such as acute respiratory distress syndrome^{26,27}. The effect of such conditions is not easy to predict. On one hand, increased permeability of the alveolar-capillary barrier could further induce extravasation of water in the interstitial and alveolar space with more pronounced and stable decrease of EELV and EELI and an increase of EVLW. On the other hand, the amount of intra-thoracic water might have already been increased during ARDS and thus the additional reduction of thoracic impedance caused by the fluid bolus may be minimised with a little or no change in EELI.

Seen from clinical perspective, the evaluation of lung recruitment and derecruitment that is based only on the information from EELI trends may be misleading when fluids are being administered intravenously. Therefore, assessment of changes in regional distribution of lung ventilation should be prioritized in such situations, since no effect of fluid administration on regional ventilation was observed in our study.

Limitations. The application of only one fluid type, its volume and infusion rate is a certain limitation of the study. To assure reliable quantification of the studied effect, we prioritized using one specific setting to achieve sufficient statistical power rather than investigating wider range of conditions, potentially resulting in underpowered study. Our previous study showed a linear decrease of EELI when either blood or Ringer's solution was administered intravenously²⁸. Such finding indicates that the administration of various fluid volumes would result in a linearly proportional decrease of EELI. Similarly, one may assume that application of different dosing rates would lead to the proportional change in the steepness of the EELI decrease. To fully explore the effect of fluid type, volume, infusion rate and different PEEP levels, more extensive randomized interventional trial would be necessary.

Conclusion

Fast intravenous administration of normal saline bolus causes significant changes in the values of end-expiratory lung impedance provided by electrical impedance tomography. The impedance changes induced by the bolus administration are comparable to the changes of EELV that would be caused by a decrease of PEEP in the order of several units of cmH₂O. The fast administration of the saline bolus has no effect on the distribution of regional lung ventilation. Seen from clinical perspective, the assessment of EELV changes that is based only on the information from EELI trend may be misleading when normal saline is administered intravenously.

Data Availability

The data generated and analysed during the current study will be made available from the corresponding author on reasonable request.

References

- Frerichs, I. *et al.* Chest electrical impedance tomography examination, data analysis, terminology, clinical use and recommendations: consensus statement of the Translational EIT development study group. *Thorax*. **72**, 83–93 (2017).
- Wrigge, H. *et al.* Electrical impedance tomography compared with thoracic computed tomography during a slow inflation maneuver in experimental models of lung injury. *Crit. Care Med.* **36**, 903–909 (2008).
- Wolf, G. K. *et al.* Reversal of dependent lung collapse predicts response to lung recruitment in children with early acute lung injury. *Pediatr. Crit. Care Med.* **13**, 509–515 (2012).
- Muders, T. *et al.* Tidal recruitment assessed by electrical impedance tomography and computed tomography in a porcine model of lung injury. *Crit. Care Med.* **40**, 903–911 (2012).
- Odenstedt, H. *et al.* Slow moderate pressure recruitment maneuver minimizes negative circulatory and lung mechanic side effects: evaluation of recruitment maneuvers using electric impedance tomography. *Intensive Care Med.* **31**, 1706–1714 (2005).
- Lowhagen, K., Lindgren, S., Odenstedt, H., Stenqvist, O. & Lundin, S. Prolonged moderate pressure recruitment manoeuvre results in lower optimal positive end-expiratory pressure and plateau pressure. *Acta Anaesthesiol. Scand.* **55**, 175–184 (2011).
- Erlandsson, K., Odenstedt, H., Lundin, S. & Stenqvist, O. Positive end-expiratory pressure optimization using electric impedance tomography in morbidly obese patients during laparoscopic gastric bypass surgery. *Acta Anaesthesiol. Scand.* **50**, 833–9 (2006).
- Becher, T. H. *et al.* Assessment of respiratory system compliance with electrical impedance tomography using a positive end-expiratory pressure wave maneuver during pressure support ventilation: a pilot clinical study. *Crit. Care*. **18**, 679 (2014).
- Blankman, P., Hasan, D., Erik, G. J. & Gommers, D. Detection of the 'best' positive end-expiratory pressure derived from electrical impedance tomography parameters during a decremental positive end-expiratory pressure trial. *Crit. Care*. **18**, R95 (2014).
- Kushner, R. F. & Schoeller, D. A. Estimation of total body water by bioelectrical impedance analysis. *Am. Journal Clin. Nutr.* **44**, 417–424 (1986).
- Tang, W., Ridout, D. & Modi, N. Assessment of total body water using bioelectrical impedance analysis in neonates receiving intensive care. *Arch. Dis. Child Fetal Neonatal. Ed.* **77**, F123–F126 (1997).
- Sadleir, R. J. & Fox, R. A. Detection and quantification of intraperitoneal fluid using electrical impedance tomography. *IEEE Trans. Biomed. Eng.* **48**, 484–491 (2001).
- Tucker, A. S., Ross, E. A., Paugh-Miller, J. & Sadleir, R. J. *In vivo* quantification of accumulating abdominal fluid using an electrical impedance tomography hemiarray. *Physiol. Meas.* **32**, 151–165 (2011).
- Noble, T. J., Harris, N. D., Morice, A. H., Milnes, P. & Brown, B. H. Diuretic induced change in lung water assessed by electrical impedance tomography. *Physiol. Meas.* **21**, 155–163 (2000).
- Bodenstein, M. *et al.* Influence of crystalloid and colloid fluid infusion and blood withdrawal on pulmonary bioimpedance in an animal model of mechanical ventilation. *Physiol. Meas.* **33**, 1225–1236 (2012).
- Laghi, F. & Tobin, M. J. Indications for mechanical ventilation in *Principles and practice of mechanical ventilation* (ed. Tobin, M. J.) 115 (The McGraw-Hill Companies, Inc., 2013).
- Frerichs, I. *et al.* Regional lung perfusion as determined by electrical impedance tomography in comparison with electron beam CT Imaging. *IEEE Trans. Med. Imaging*. **18**, 6 (2002).
- Rhodes, A. *et al.* Surviving sepsis campaign: international guidelines for management of severe sepsis and septic shock: 2016. *Intensive Care Med.* **43**, 304–377 (2017).
- Frerichs, I. *et al.* Patient examinations using electrical impedance tomography – sources of interference in the intensive care unit. *Physiol. Meas.* **32**, L1–10 (2011).
- Costa, E. L. V. *et al.* Bedside estimation of recruitable alveolar collapse and hyperdistension by electrical impedance tomography. *Intensive Care Med.* **35**, 1132–1137 (2009).
- Karsten, J., Grusnick, C., Paarmann, H., Heringlake, M. & Heinze, H. Positive end-expiratory pressure titration at bedside using electrical impedance tomography in post-operative cardiac surgery patients. *Acta Anaesthesiol. Scand.* **59**, 723–732 (2015).
- Bikker, I. G., Leonhardt, S., Bakker, J. & Gommers, D. Lung volume calculated from electrical impedance tomography in ICU patients at different PEEP levels. *Intensive Care Med.* **35**, 1362–7 (2009).
- Grivans, C., Lundin, S., Stenqvist, O. & Lindgren, S. Positive end-expiratory pressure-induced changes in end-expiratory lung volume measured by spirometry and electric impedance tomography. *Acta Anaesthesiol. Scand.* **55**, 1068–1077 (2011).
- Markhorst, D. G., Groeneveld, A. B., Heethaar, R. M., Zonneveld, E. & van Genderingen, H. R. Assessing effects of PEEP and global expiratory lung volume on regional electrical impedance tomography. *J. Med. Eng. Technol.* **33**, 281–287 (2009).
- Trepte, C. J. C. *et al.* Electrical impedance tomography (EIT) for quantification of pulmonary edema in acute lung injury. *Crit. Care*. **20**, 18 (2016).
- Otáhal, M., Mlček, M., Vitková, I. & Kittnar, O. A novel experimental model of acute respiratory distress syndrome in pig. *Physiol. Res.* **65**, S643–S651 (2016).
- Pomprapa, A. *et al.* Automatic protective ventilation using the ARDSNet protocol with the additional monitoring of electrical impedance tomography. *Crit. Care*. **18**, R128 (2014).
- Suchomel, J. & Sobota, V. A model of end-expiratory lung impedance dependency on total extracellular body water. *J. Phys.: Conf. Ser.* **434**, 012011 (2013).

Acknowledgements

The authors thank to employees of the animal laboratory of the Department of Physiology, First Faculty of Medicine, Charles University in Prague, especially to Mikuláš Mlček, MD, PhD, for valuable help with animal preparation. The authors would also like to express their gratitude to Jana Vránová, PhD, Department of Medical Biophysics and Medical Informatics, 3rd Faculty of Medicine, Charles University, Prague, for her statistical advices, and to Thomas Bachman, Czech Technical University in Prague, Faculty of Biomedical Engineering, for reviewing the manuscript. This work was supported, in part, by grant OP VK CZ.1.07/2.3.00/30.0034 from the Ministry of Education, Youth and Sports of the Czech Republic and grant SGS17/026/OHK4/3T/17 from Czech Technical University in Prague. This project also received funding from the European Union's Horizon 2020 research and innovation programme under the Marie Skłodowska-Curie grant agreement No. 675351.

Author Contributions

V.S., M.M. and K.R. designed and carried out the study, acquired and analysed the data, interpreted the data and wrote the manuscript. All authors read and approved the final version of the manuscript.

Additional Information

Supplementary information accompanies this paper at <https://doi.org/10.1038/s41598-019-42241-7>.

Competing Interests: The authors declare no competing interests.

Publisher's note: Springer Nature remains neutral with regard to jurisdictional claims in published maps and institutional affiliations.



Open Access This article is licensed under a Creative Commons Attribution 4.0 International License, which permits use, sharing, adaptation, distribution and reproduction in any medium or format, as long as you give appropriate credit to the original author(s) and the source, provide a link to the Creative Commons license, and indicate if changes were made. The images or other third party material in this article are included in the article's Creative Commons license, unless indicated otherwise in a credit line to the material. If material is not included in the article's Creative Commons license and your intended use is not permitted by statutory regulation or exceeds the permitted use, you will need to obtain permission directly from the copyright holder. To view a copy of this license, visit <http://creativecommons.org/licenses/by/4.0/>.


© The Author(s) 2019

RESEARCH

Open Access



Optimal mean airway pressure during high-frequency oscillatory ventilation in an experimental model of acute respiratory distress syndrome: EIT-based method

Songqiao Liu¹ , Zhanqi Zhao^{2,3}, Li Tan^{1,4}, Lihui Wang¹, Knut Möller², Inéz Frerichs⁵, Tao Yu¹, Yingzi Huang¹, Chun Pan¹, Yi Yang¹ and Haibo Qiu^{1*}

Abstract

Background: High-frequency oscillatory ventilation (HFOV) may theoretically provide lung protective ventilation. The negative clinical results may be due to inadequate mean airway pressure (mPaw) settings in HFOV. Our objective was to evaluate the air distribution, ventilatory and hemodynamic effects of individual mPaw titration during HFOV in ARDS animal based on oxygenation and electrical impedance tomography (EIT).

Methods: ARDS was introduced with repeated bronchoalveolar lavage followed by injurious mechanical ventilation in ten healthy male pigs (51.2 ± 1.9 kg). Settings of HFOV were 9 Hz (respiratory frequency), 33% (inspiratory time) and 70 cmH₂O (Δ pressure). After lung recruitment, the mPaw was reduced in steps of 3 cmH₂O every 6 min. Hemodynamics and blood gases were obtained in each step. Regional ventilation distribution was determined with EIT.

Results: PaO₂/FiO₂ decreased significantly during the mPaw decremental phase ($p < 0.001$). Lung overdistended regions decreased, while recruitable regions increased as mPaw decreased. The optimal mPaw with respect to PaO₂/FiO₂ was 21 (18.0–21.0) cmH₂O, that is comparable to EIT-based center of ventilation (EIT-CoV) and EIT-collapse/over, 19.5 (15.0–21.0) and 19.5 (18.0–21.8), respectively ($p = 0.07$). EIT-CoV decreasing along with mPaw decrease revealed redistribution toward non-dependent regions. The individual mPaw titrated by EIT-based indices improved regional ventilation distribution with respect to overdistension and collapse ($p = 0.035$).

Conclusion: Our data suggested personalized optimal mPaw titration by EIT-based indices improves regional ventilation distribution and lung homogeneity during high-frequency oscillatory ventilation.

Keywords: Acute respiratory distress syndrome, High-frequency oscillatory ventilation, Electrical impedance tomography, Mean airway pressure, Titration

Background

Acute respiratory distress syndrome (ARDS) is common in ICU characterized by diffuse endothelial and epithelial injury, inflammatory pulmonary edema, small

lung, lung injury inhomogeneities and severe hypoxemia [1, 2]. Mechanical ventilation remains mainstay in the management of patients with ARDS [3]. Lung protective ventilation with low tidal volumes [4], positive end-expiratory pressure (PEEP) [5, 6] and prone position [7] may improve outcomes. Nevertheless, the mortality of ARDS patients remains high, up to 30–50% [8].

High-frequency oscillatory ventilation (HFOV) delivered high mean airway pressure (mPaw) and extremely

*Correspondence: haiboq2000@163.com

¹ Department of Critical Care Medicine, Zhongda Hospital, School of Medicine, Southeast University, Jiangsu Province, Nanjing 210009, China

Full list of author information is available at the end of the article

small tidal volumes to prevent alveolar derecruitment/overdistention as well as avoid the repeated opening/closing of individual alveolar [9]. Clinical trials [10] and large animal trials [11] have demonstrated that HFOV improves oxygenation, reduces lung inflammatory processes and histopathological damages, and attenuates oxidative lung injury compared with conventional mechanical ventilation (CMV).

Currently, clinical data do not support the use of HFOV in patients of ARDS. Two major multicenter, randomized trials (OSCAR and OSCILLATE) failed to show improvement on 30-day mortality in moderate-to-severe ARDS patients [12–14]. A meta-analysis found that HFOV might not improve outcome compared with CMV [15]. One possible reason may be the improper HFOV protocols applied and inadequate HFOV settings.

The optimal mPaw titration is still a challenge during HFOV. The selection of Paw is usually guided by a static P - V curve or based on the oxygenation index [9]; however, either computed tomography scanning [16] or frequent blood gas analysis is indispensable. Recently, a study showed that HFOV guided by transpulmonary pressure improved systemic hemodynamics, oxygenation, and lung overdistension compared with conventional HFOV in animals [17]. But the ventilation distribution and homogeneity remain unknown toward the methods mentioned above to titrate mPaw.

Electrical impedance tomography (EIT) might allow the clinician to better adjust these ventilatory settings. EIT is a bedside imaging technique that enables monitoring air distribution in the lungs [18]. Our previous study has showed the GI index may provide new insights into air distribution in CMV and may be used to guide ventilator settings [19, 20]. EIT might allow the clinician to better adjust ventilatory settings in HFOV. It is possible that HFOV would be safer and more effective with a more individualized approach to setting mPaw adjusted according to ventilation distribution bedside.

In the present study, our objective was to evaluate the air distribution, ventilatory, and hemodynamic effects of individual mPaw titration in HFOV based on oxygenation and EIT.

Methods

The study was approved by the Science and Technological Committee and the Animal Use and Care Committee of the Southeast University, School of Medicine, Nanjing, China. All animal procedures and protocols were performed according to the Guidance for the Care and Use of Laboratory Animals [21].

Animal preparation

A total of ten healthy male pigs (body weight 51.2 ± 1.9 kg, mean \pm SD) were included. Pigs were anesthetized with an intramuscular injection of ketamine hydrochloride (3 mg/kg), atropine (2 mg/kg) and fentanyl citrate (2 mg/kg), followed by a continuous intravenous infusion of propofol (1–2 mg/kg/h), fentanyl citrate (0.5–1.0 μ g/kg/h), midazolam (0.1 mg/kg/h), and atracurium (0.4 mg/kg/h). After the induction of anesthesia, the pigs were placed in supine position, on a thermo-controlled operation table to maintain body temperature at about 37.0 °C. With local anesthesia, a mid-line neck incision was performed and the trachea was secured using an 8-mm-ID endotracheal tube. The animals received conventional mechanical ventilation (Servo-i ventilator, Solna, Sweden) under volume-controlled mode (respiratory rate 30 breaths per minute; inspiration-to-expiration time ratio 1:2 and PEEP 5 cmH₂O; fraction of inspiration O₂ (FiO₂) and tidal volume (V_T) 0.4 and 6 ml/kg, respectively). A Swan–Ganz catheter (Arrow International, Reading, PA, USA) was inserted through the internal jugular vein to measure central venous pressure (CVP) and pulmonary arterial wedge pressure (PAWP). A thermistor-tipped PiCCO catheter (Pulsion Medical System, Munich, Germany) was advanced through the right femoral artery to monitor the mean arterial pressure (MAP) and cardiac output (CO). In addition, arterial blood samples were collected from a PiCCO catheter. A continuous infusion of a 5 ml/(kg h) balanced electrolyte solution was administered during the experiment, and MAP was maintained above 60 mmHg with rapid infusions of 0.9% saline solution at up to 20 ml/kg, if required.

Experimental protocol

After the initial animal preparation, the pigs were stabilized for 30 min and baseline measurements (T_{Baseline}) were taken. ARDS was induced by repeated bilateral bronchoalveolar lavage with 30 ml/kg of isotonic saline (38 °C). After stabilization, an arterial blood gas sample was obtained to verify that the ratio of partial pressure of arterial oxygen PaO₂ and FiO₂ decreased to less than 100 mmHg, followed by 1 h of injurious mechanical ventilation (PEEP 0 cmH₂O and distending pressure 35 cmH₂O in PCV). PaO₂/FiO₂ remained less than 100 mmHg for 30 min (T_{ARDS}) with an increase of FiO₂ to 1.0.

The mechanical ventilation mode was then switched to HFOV (FiO₂ 1.0; respiratory frequency 9 Hz; inspiratory time 33%; Δ pressure 70 cmH₂O), and a recruitment maneuver was performed (mPaw of 40 cmH₂O for 40 s) after 15-min HFOV ventilation. After recruitment, stepwise mPaw decrements were performed from 36 to

9 cmH₂O with a step of 3 cmH₂O decrease every 6 min. (Flowchart of the study is showed in Additional file 1: Figure S1). CVP, PAWP, MAP and CO were recorded at every pressure level. All blood gas measurements were performed using an automated blood gas analyzer (Nova M; Nova Biomedical, Waltham, MA, USA).

EIT measurements

Continuous EIT measurements started after tracheostomy (PulmoVista 500, Dräger Medical, Lübeck, Germany). An EIT electrode belt with 16 electrodes was placed around the thorax 5 cm above the xyphoid level and one reference ECG electrode was placed at the abdomen. The frequency of injected alternating current was selected automatically according to the noise spectrum. The images were continuously recorded and reconstructed at 40 Hz. The EIT data were reconstructed using a finite element method-based linearized Newton–Raphson reconstruction algorithm [22]. Baseline of the images was referred to the lowest impedance value measured during T_{ARDS} . Oscillatory impedance variations of every 5 s were averaged to present the ventilation distribution. One-minute period at the end of each mPaw step was used for further EIT analysis.

Mean paw titration strategies

mPaw optimization according to oxygenation

Optimal mPaw with respect to oxygenation was defined as mPaw in the step before the one at which PaO₂ dropped by > 10% compared to previous step (Additional file 1: Figure S2).

mPaw optimization according to EIT-based center of ventilation (EIT-CoV)

The center of ventilation (CoV) index showing the vertical distribution of ventilation was calculated [23, 24]:

$$CoV = \frac{\sum (y_i \times I_i)}{\sum I_i} \times 100\% \quad (1)$$

I_i denotes impedance value of pixel i . y_i is the pixel height and pixel i is scaled so the most ventral row is 0 and the most dorsal row is 1. Optimal mPaw with respect to EIT-CoV was defined as mPaw associated with the CoV values closest to 50%. EIT-based COV index higher than 50% at high mPaw steps indicated ventilation distribution toward gravity-dependent regions.

mPaw optimization according to EIT-based collapse–overdistension

Recruitable regions compared to the highest mPaw level and overdistended regions were calculated using a method that was published recently [24]. During the

analysis of HFOV in the present study, the oscillatory impedance variation was too small to confirm overdistension. Therefore, compared to the original method, the volume changes induced by mPaw changes were used. The differences of impedance between lower mPaw and higher mPaw were calculated. The regions with less than 20% changes were denoted as regions with limited volume changes. These regions with almost no pixels changes were considered to be overinflated, if they belonged to those image pixels that were showed in lung regions at lower mPaw step. Regions were considered to be recruitable if they were included in the lung regions at end-expiration at the highest mPaw step but not at the current mPaw step.

The lung regions at mPaw level n were defined as pixels with higher impedance value (I) than 20% of maximum changes compared to the lowest mPaw level r (reference level, the lowest mPaw level).

$$j \in \text{Lung if } I_j > 20\% \times \max(I_{n,i} - I_{r,i}), i \in [1, 1024] \quad (2)$$

Subsequently, the maximum differences of impedance ($I_{\max\text{-diff}}$) between lower mPaw (denoted as mPaw level n) and higher mPaw (mPaw level $n + 1$) were calculated.

$$I_{\max\text{-diff}} = \max(I_{n+1,i} - I_{n,i}), i \in [1, 1024] \quad (3)$$

The regions with less than 20% changes were denoted as regions with limited volume changes (for pixel k , $k \in i$, $I_k < 20\% \times I_{\max\text{-diff}}$). These regions k were compared to lung regions at mPaw level n (j_n). They were considered to be overinflated, if they belonged to lung regions at mPaw step n at the same time ($k \cap j_n$ intersection of set k and set j_n).

The numbers of pixels in these two regions were plotted against decremental mPaw. Optimal mPaw with respect to recruitable and overdistended regions was defined as the step where these two-pixel curves intersected. If the curves not intersected, mPaw with the lowest sum of recruitable and overdistended regions was selected. With the nature of this method, no values could be calculated for the lowest mPaw step, since the calculation required a comparison with a lower mPaw step (Eq. 3). Overdistension/recruitment ratio was defined as number of pixels in the overdistended regions over that in the recruitable regions.

Statistical analysis

Statistical analysis was performed with the MATLAB software package (MATLAB 7.2 statistic toolbox, The MathWorks Inc., Natick, MA, USA). Due to the limited number of subjects, results are presented as median \pm interquartile range. One-way Kruskal–Wallis

test was used to assess the significance of differences in Hemodynamics and oxygenation among different mPaw, and differences in optimal mPaw estimated with various criteria. A p value lower than 0.05 was considered statistically significant. Wilcoxon signed-rank test was applied for further comparison within groups and the significance levels were corrected for multiple comparisons using Holm's sequential Bonferroni method.

Results

ARDS was successfully induced by repeated bronchoalveolar lavages in all 10 pigs. The induction of ARDS led to a significant decrease in $\text{PaO}_2/\text{FiO}_2$ ($p < 0.001$).

Hemodynamics

MAP and CO increased while CVP and PAWP decreased along with the decremental mPaw trial. Hemodynamic data during the mPaw trial are plotted in Additional file 1: Table S1.

Titration of optimal mPaw by oxygenation

The effect of mPaw on the $\text{PaO}_2/\text{FiO}_2$ and partial pressure of arterial carbon dioxide (PaCO_2) during HFOV are shown in Additional file 1: Figure S2. During the decremental phase, significant decrease in $\text{PaO}_2/\text{FiO}_2$ and increase in PaCO_2 were found between the mPaw step of 18 cmH_2O and 15 cmH_2O ($p < 0.001$) (Additional file 1: Figure S2 left). The optimal mPaw calculated by individual animal with respect to $\text{PaO}_2/\text{FiO}_2$ was 21 (18.0–21.0) cmH_2O .

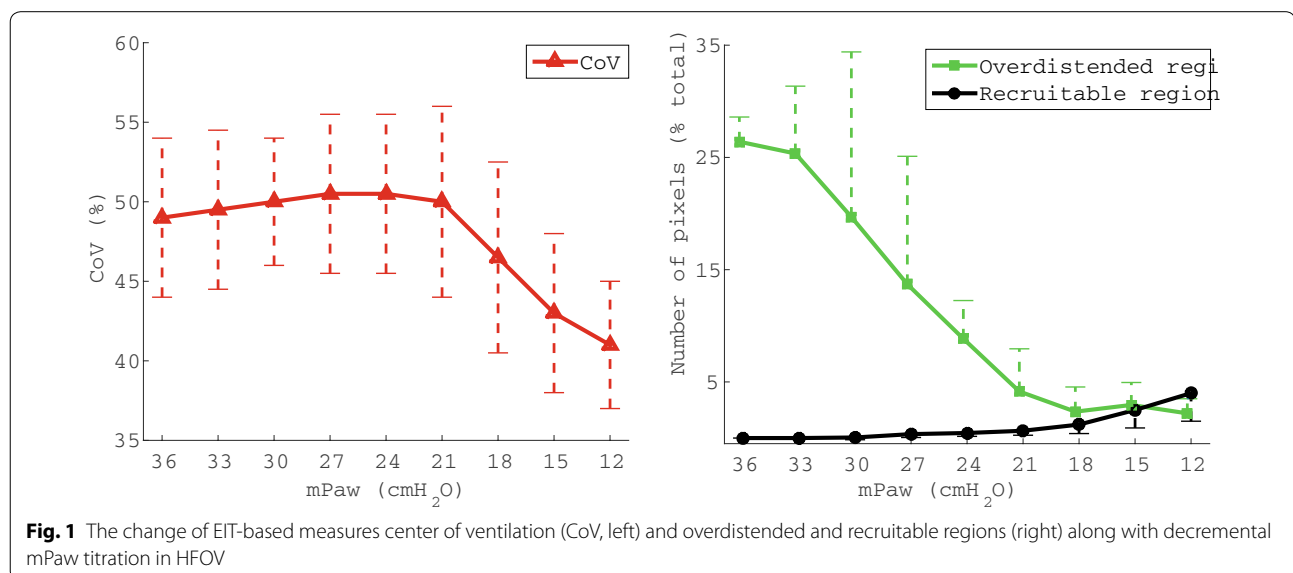
Optimal mPaw derived from regional ventilation distribution

CoV decreased along with mPaw decrease revealing a redistribution of ventilation toward non-dependent regions (Fig. 1, left). The optimal mPaw with respect to EIT-CoV in all pigs was 19.5 (15.0–21.0) cmH_2O and the values among individuals varied a lot.

EIT-derived overdistended regions decreased as mPaw decreased (Fig. 1, right, green circles). At the same time, recruitable regions increased (black stars). The optimal mPaw using the approach based on the calculated EIT-collapse/over was 19.5 (18.0–21.8) cmH_2O .

Optimal mPaw derived from different methods

The optimal mPaw with respect to $\text{PaO}_2/\text{FiO}_2$ was 21 (18.0–21.0) cmH_2O , that is comparable to EIT-based center of ventilation (EIT-CoV) and EIT-collapse/over, 19.5 (15.0–21.0) and 19.5 (18.0–21.8), respectively ($p = 0.07$). The differences between the selected mPaw according to oxygenation and according to "EIT-Cov" and "EIT-collapse/over" were compared with Bland–Altman plots (Fig. 2). The differences in mPaw selection between oxygenation and EIT-based methods could be as high as 6 cmH_2O in some pigs. The optimal mPaw settings derived from oxygenation, EIT-CoV and EIT-collapse/over were compared (Table 1). In Fig. 3, overdistended and recruitable regions at mPaw levels selected based on oxygenation were illustrated. In each pig, the optimal mPaw defined with oxygenation was given (x -axis). The mPaw titrated by EIT-based indices improved regional air distribution with respect to overdistension and collapse (comparison among 3 mPaw titration strategies, $p = 0.035$) (Table 2).



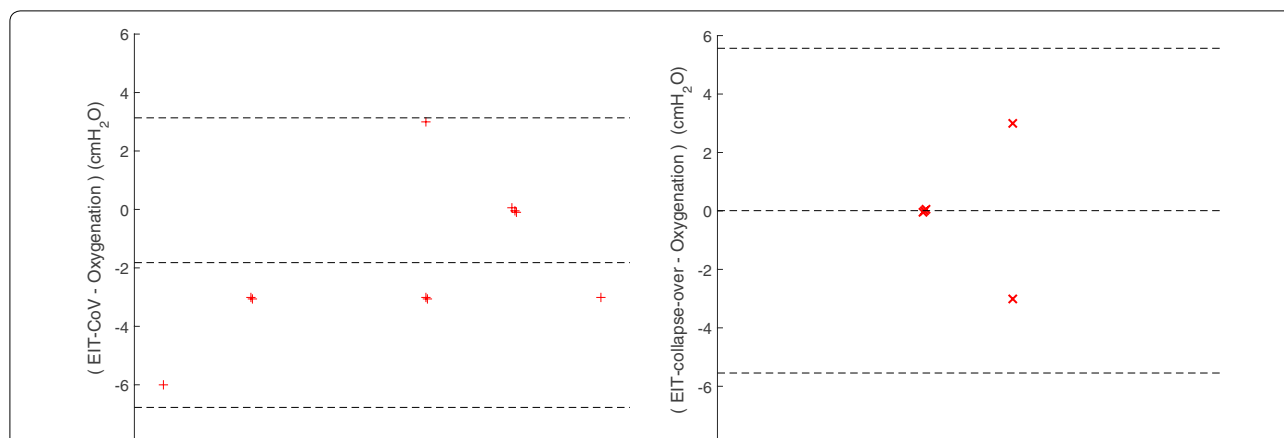


Fig. 2 Bland–Altman plots comparing optimal mPaw settings with EIT-CoV and oxygenation (left), with EIT-collapse-overdistended and oxygenation (right). EIT-CoV: EIT-based center of ventilation; EIT-collapse-overdistended: EIT-based overdistended and recruitable regions

Table 1 Selected mPaw according to oxygenation, EIT-CoV and EIT-regions

Pig number	mPaw (cmH ₂ O) selected by		
	Oxygenation	EIT-CoV	EIT-regions
1	18	15	18
2	21	18	18
3	21	18	21
4	24	21	18
5	21	21	24
6	18	12	18
7	21	21	21
8	18	15	18
9	18	21	21
10	21	21	24
Median (inter-quartile range)	21 (18.0–21.0)	19.5 (15.0–21.0)	19.5 (18.0–21.8)
F	3.115		
P	0.07		

Discussion

In the present study, novel EIT-based method titrating mPaw under HFOV was proposed and evaluated in ARDS model. The titration results were compared with oxygenation method and the effects on lung homogeneity were examined. We found that the individual mPaw titrated by EIT-based indices improved regional ventilation distribution with respect to overdistension and collapse and the suggested mPaw may not always match the ones proposed by oxygenation method.

HFOV may remain a tool in managing patients with severe ARDS and refractory hypoxemia and not the first-line treatment for ARDS patient. HFOV with high mPaw values applied in both two trials [25, 26] might contribute

to negative clinical outcome on ARDS patients and canceled out the positive effects. HFOV using Paw set according to a static *P–V* curve [16], oxygenation, mean airway pressure during CMV [27], and transpulmonary pressure [17] has been examined in clinical and animal studies, but the bedside monitoring base on ventilation distribution is lacking. In the present study, we provide new mPaw titration method in respect of regional ventilation distribution that improves lung homogeneity. The increased mPaw lead to more lung tissue hyperinflated, and the EIT-CoV decrease, which revealed redistribution toward non-dependent regions. A critical issue of this EIT-based method was the pre-defined threshold used to identify lung regions. Further studies are required to confirm if the threshold used in the present study is optimal for various subjects and conditions.

The reliability of EIT has been confirmed and EIT has been used in clinic setting and adjust of CMV. EIT has been used in PEEP titration and tidal volume setting by comparison with various conventional methods, such as CT [28], single-photon-emission computed tomography [29], positron emission tomography [30], and pneumotachography [31]. Previous studies have already shown that EIT was able to monitor ventilation distribution during HFOV in preterm infants and patients with chronic obstructive pulmonary disease [22, 32]. The optimal settings based on oxygenation were comparable to EIT-CoV and EIT-regional ventilation distribution. It was also observed that overdistended regions were large at the mPaw selected with oxygenation method in several pigs. PF ratio is an invasive method with a certain time delay in response to pressure changes. Although the average values between EIT-derived measures were not very different, individual differences could be large (up to 6 cmH₂O, Figs. 2 and 3). Hence, mPaw titration with

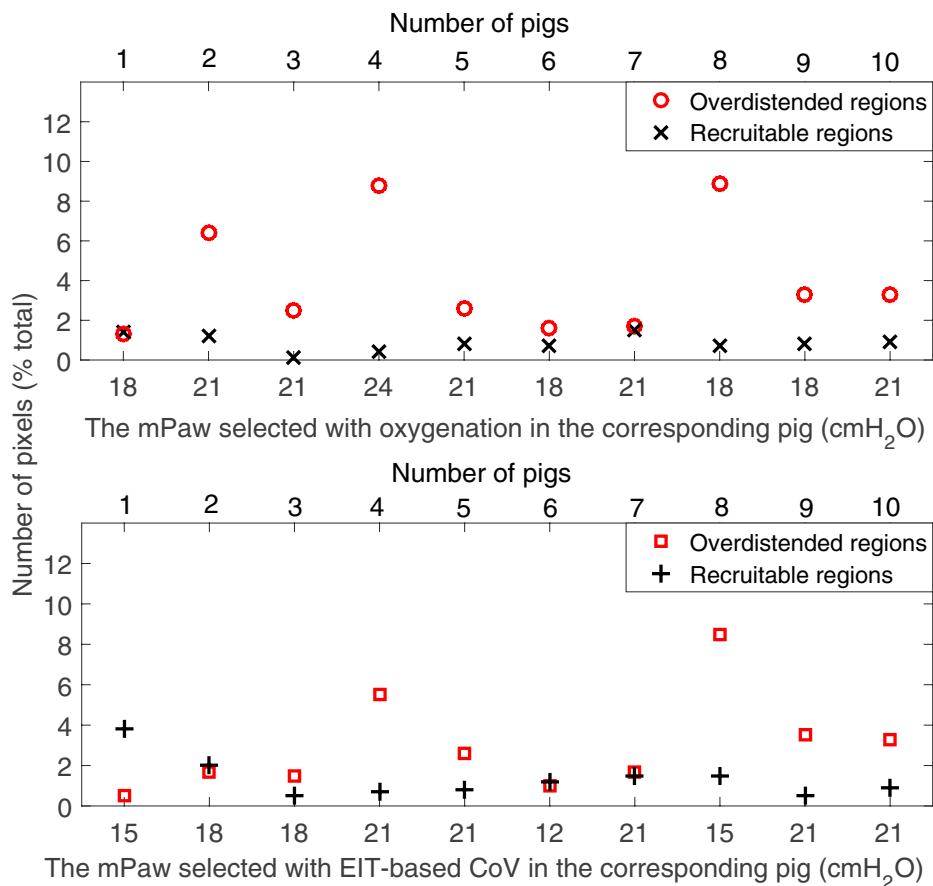


Fig. 3 The recruitable regions and overdistended regions in mPaw selected with oxygenation (left) and EIT-based CoV (right) in the individual pig. Number of pixels is presented as Black asterisk (recruitable lung region) and red circles (overdistended lung region) with the optimal mPaw were defined with oxygenation (Upper). The number of pixels is presented as black crosses (recruitable lung region) and red squares (overdistended lung region) with the optimal mPaw were defined with EIT-based center of ventilation index (lower x-axis) as well (lower)

Table 2 The effects of the 3 mPaw titration strategies on oxygenation, overdistension/recruitment and hemodynamics

mPaw titration strategies	Oxygenation	EIT-CoV	EIT-regions	F	p
PaO ₂ /FiO ₂ (mmHg)	210.8 ± 38.5	176.1 ± 47.7	204.7 ± 43.1	1.833	0.179
Overdistension/recruitment ratio	8.1 ± 7.9	5.3 ± 4.7	2.8 ± 2.1	4.985	0.035*
HR (BPM)	84.6 ± 30.5	82.2 ± 27.8	85.5 ± 28.9	0.0345	0.966
MAP (mmHg)	90.3 ± 33.8	92.5 ± 35.5	91.7 ± 34.1	0.0104	0.990
CVP (mmHg)	8.9 ± 2.8	8.1 ± 2.3	8.2 ± 3.0	1.879	0.183
PAWP (mmHg)	11.4 ± 2.9	10.9 ± 2.8	11.1 ± 3.1	0.774	0.457
CO (L/min)	4.6 ± 1.4	4.6 ± 1.5	4.5 ± 1.2	0.0155	0.985

Mean values and standard deviations are shown

HR heart rate, BPM breaths per minute, MAP mean arterial pressure, CVP measure central venous pressure, CO Cardiac output, PAWP pulmonary arterial wedge pressure

*p < 0.05

EIT-based indices improved regional ventilation distribution while titration aiming oxygenation was not always the case. Besides, it is worth to note that EIT is currently

the only bedside non-invasive tool to assess overdistension. Further investigation should be conducted in future clinical studies.

Our study has some limitations. First, as an experimental study, these data were obtained in animals and its clinical impact may be limited. Therefore, the optimal mPaw selected in the present study might be not suitable with that in ARDS patients. Second, HFOV should not be employed in the absence of well-trained expertise because of its complexity. Further validation study to assess the feasibility of such strategies in ARDS patients with proposed method should be conducted.

Conclusion

Our data provide personalized optimal mPaw titration in HFOV with EIT-based indices, which may provide a new insight of regional ventilation distribution and lung homogeneity during high-frequency oscillatory ventilation.

Supplementary information

Supplementary information accompanies this paper at <https://doi.org/10.1186/s13613-020-0647-z>.

Additional file 1: Figure S1. Flowchart of the study. **Figure S2.** PaO₂/FiO₂ (left) and PaCO₂ (right) during mPaw decrements trial after having fully recruited the lungs.

Additional file 2: Table S1. Hemodynamics characteristics during decremental HFOV mPaw (n = 10).

Abbreviations

ARDS: Acute respiratory distress syndrome; CO: Cardiac output; CoV: Center of ventilation; CT: Computed tomography; CVP: Central venous pressure; EELI: End-expiratory lung impedance; EIT: Electrical impedance tomography; FiO₂: Fraction of inspired oxygen; HFOV: High-frequency oscillatory ventilation; MAP: Mean arterial pressure; mPaw: Mean airway pressure; PaCO₂: Partial pressure of CO₂ in arterial blood; PaO₂: Partial pressure of O₂ in arterial blood; PAWP: Pulmonary arterial wedge pressure; PEEP: Positive end-expiratory pressure; VILI: Ventilator-induced lung injury; VT: Tidal volume.

Acknowledgements

Not applicable.

Authors' contributions

SL and HQ designed the study. SL, LT, TY, LW, YH, and CP performed the animal experiments and analyzed the data. ZZ developed the EIT method. YY, ZZ and HQ supervised the study and the analysis of results. SL, YY, HQ, and ZZ designed the concept of the manuscript and drafted the manuscript. All the authors (SL, ZZ, LT, LW, KM, IF, TY, YH, CP, YY, and HQ) contributed to the final drafting of the manuscript. All authors read and approved the final manuscript.

Funding

This work was supported by Jiangsu Province's Key Discipline/Laboratory of Medicine (No.ZDXKA2016025), Jiangsu Province's Key Provincial Talents Program (ZDRCA2016082), National Natural Science Foundation of China (81370180, Beijing, China), Natural Science Foundation of Jiangsu Province (H201432, Nanjing, Jiangsu, China).

Availability of data and materials

The datasets used and/or analyzed during the current study are available from the corresponding author on reasonable request.

Ethics approval and consent to participate

The study had the approval of the Science and Technological Committee and the Animal Use and Care Committee of the Southeast University, School of Medicine, Nanjing, China. The animals were handled according to the Helsinki convention for the use and care of animals.

Consent for publication

All authors have read this paper and agreed with the submission.

Competing interests

Inez Frerichs has received reimbursement of travel, meeting expenses and speaking fees from Swisstom and Dräger, respectively. Zhanqi Zhao receives a consulting fee from Dräger Medical. The remaining authors have disclosed that they do not have any potential conflicts of interest. The authors state that neither the study design, the results, the interpretation of the findings nor any other subject discussed in the submitted manuscript was dependent on support.

Author details

¹ Department of Critical Care Medicine, Zhongda Hospital, School of Medicine, Southeast University, Jiangsu Province, Nanjing 210009, China. ² Institute of Technical Medicine, Furtwangen University, Jakob-Kienzle Strasse 17, 78054 VS-Schwenningen, Germany. ³ Department of Biomedical Engineering, Fourth Military Medical University, Xi'an, China. ⁴ Department of Critical Care Medicine, Beijing Tongren Hospital, Capital Medical University, Beijing 100730, China. ⁵ Department of Anesthesiology and Intensive Care Medicine, University Medical Center of Schleswig-Holstein Campus Kiel, Arnold-Heller-Strasse 3, 24105 Kiel, Germany.

Received: 28 January 2019 Accepted: 26 February 2020

Published online: 06 March 2020

References

- Ashbaugh DG, Bigelow DB, Petty TL, Levine BE. Acute respiratory distress in adults. *Lancet*. 1967;2(7511):319–23.
- Force ADT, Ranieri VM, Rubenfeld GD, Thompson BT, Ferguson ND, Caldwell E, et al. Acute respiratory distress syndrome: the Berlin definition. *JAMA*. 2012;307(23):2526–33.
- Thompson BT, Chambers RC, Liu KD. Acute respiratory distress syndrome. *N Engl J Med*. 2017;377(6):562–72.
- Acute Respiratory Distress Syndrome N, Brower RG, Matthay MA, Morris A, Schoenfeld D, Thompson BT, et al. Ventilation with lower tidal volumes as compared with traditional tidal volumes for acute lung injury and the acute respiratory distress syndrome. *N Engl J Med*. 2000;342(18):1301–8.
- Guo L, Xie J, Huang Y, Pan C, Yang Y, Qiu H, et al. Higher PEEP improves outcomes in ARDS patients with clinically objective positive oxygenation response to PEEP: a systematic review and meta-analysis. *BMC Anesthesiol*. 2018;18(1):172.
- Chiumello D, Cressoni M, Carlesso E, Caspani ML, Marino A, Gallazzi E, et al. Bedside selection of positive end-expiratory pressure in mild, moderate, and severe acute respiratory distress syndrome. *Crit Care Med*. 2014;42(2):252–64.
- Guerin C, Reignier J, Richard JC, Beuret P, Gacouin A, Boulain T, et al. Prone positioning in severe acute respiratory distress syndrome. *N Engl J Med*. 2013;368(23):2159–68.
- Bellani G, Laffey JG, Pham T, Fan E, Brochard L, Esteban A, et al. Epidemiology, patterns of care, and mortality for patients with acute respiratory distress syndrome in intensive care units in 50 countries. *JAMA*. 2016;315(8):788–800.
- Chan KP, Stewart TE, Mehta S. High-frequency oscillatory ventilation for adult patients with ARDS. *Chest*. 2007;131(6):1907–16.
- Sud S, Sud M, Friedrich JO, Meade MO, Ferguson ND, Wunsch H, et al. High frequency oscillation in patients with acute lung injury and acute respiratory distress syndrome (ARDS): systematic review and meta-analysis. *BMJ*. 2010;340:c2327.
- Goffi A, Ferguson ND. High-frequency oscillatory ventilation for early acute respiratory distress syndrome in adults. *Curr Opin Crit Care*. 2014;20(1):77–85.

12. Ferguson ND, Cook DJ, Guyatt GH, Mehta S, Hand L, Austin P, et al. High-frequency oscillation in early acute respiratory distress syndrome. *N Engl J Med*. 2013;368(9):795–805.
13. Malhotra A, Drazen JM. High-frequency oscillatory ventilation on shaky ground. *N Engl J Med*. 2013;368(9):863–5.
14. Young D, Lamb SE, Shah S, MacKenzie I, Tunnicliffe W, Lall R, et al. High-frequency oscillation for acute respiratory distress syndrome. *N Engl J Med*. 2013;368(9):806–13.
15. Goligher EC, Munshi L, Adhikari NKJ, Meade MO, Hodgson CL, Wunsch H, et al. High-frequency oscillation for adult patients with acute respiratory distress syndrome. A systematic review and meta-analysis. *Ann Am Thorac Soc*. 2017;14(Supplement_4):S289–96.
16. Luecke T, Meinhardt JP, Herrmann P, Weisser G, Pelosi P, Quintel M. Setting mean airway pressure during high-frequency oscillatory ventilation according to the static pressure–volume curve in surfactant-deficient lung injury: a computed tomography study. *Anesthesiology*. 2003;99(6):1313–22.
17. Klapsing P, Moerer O, Wende C, Herrmann P, Quintel M, Bleckmann A, et al. High-frequency oscillatory ventilation guided by transpulmonary pressure in acute respiratory syndrome: an experimental study in pigs. *Crit Care*. 2018;22(1):121.
18. Frerichs I, Amato MB, van Kaam AH, Tingay DG, Zhao Z, Grychtol B, et al. Chest electrical impedance tomography examination, data analysis, terminology, clinical use and recommendations: consensus statement of the Translational EIT development study group. *Thorax*. 2017;72(1):83–93.
19. Zhao Z, Moller K, Steinmann D, Frerichs I, Guttman J. Evaluation of an electrical impedance tomography-based Global Inhomogeneity Index for pulmonary ventilation distribution. *Intensive Care Med*. 2009;35(11):1900–6.
20. Zhao Z, Steinmann D, Frerichs I, Guttman J, Moller K. PEEP titration guided by ventilation homogeneity: a feasibility study using electrical impedance tomography. *Crit Care*. 2010;14(1):R8.
21. Guide for the Care and Use of laboratory animals. Washington (DC):National Academies Press (US). 2011.
22. Gong B, Krueger-Ziolek S, Moeller K, Schullcke B, Zhao Z. Electrical impedance tomography: functional lung imaging on its way to clinical practice? *Expert Rev Respir Med*. 2015;9(6):721–37.
23. Frerichs I, Hahn G, Golisch W, Kurpitz M, Burchardi H, Hellige G. Monitoring perioperative changes in distribution of pulmonary ventilation by functional electrical impedance tomography. *Acta Anaesthesiol Scand*. 1998;42(6):721–6.
24. Liu S, Tan L, Moller K, Frerichs I, Yu T, Liu L, et al. Identification of regional overdistension, recruitment and cyclic alveolar collapse with electrical impedance tomography in an experimental ARDS model. *Crit Care*. 2016;20(1):119.
25. Sklar MC, Fan E, Goligher EC. High-frequency oscillatory ventilation in adults with ARDS: past, present, and future. *Chest*. 2017;152(6):1306–17.
26. Ng J, Ferguson ND. High-frequency oscillatory ventilation: still a role? *Curr Opin Crit Care*. 2017;23(2):175–9.
27. Guervilly C, Forel JM, Hraiech S, Demory D, Allardet-Servent J, Adda M, et al. Right ventricular function during high-frequency oscillatory ventilation in adults with acute respiratory distress syndrome. *Crit Care Med*. 2012;40(5):1539–45.
28. Wrigge H, Zinserling J, Muders T, Varelmann D, Gunther U, von der Groeben C, et al. Electrical impedance tomography compared with thoracic computed tomography during a slow inflation maneuver in experimental models of lung injury. *Crit Care Med*. 2008;36(3):903–9.
29. Frerichs I, Hinz J, Herrmann P, Weisser G, Hahn G, Dudykevych T, et al. Detection of local lung air content by electrical impedance tomography compared with electron beam CT (Bethesda, Md: 1985). *J Appl Physiol*. 2002;93(2):660–6.
30. Richard JC, Pouzot C, Gros A, Tourevielle C, Lebars D, Lavenne F, et al. Electrical impedance tomography compared to positron emission tomography for the measurement of regional lung ventilation: an experimental study. *Crit Care*. 2009;13(3):R82.
31. Victorino JA, Borges JB, Okamoto VN, Matos GF, Tucci MR, Carames MP, et al. Imbalances in regional lung ventilation: a validation study on electrical impedance tomography. *Am J Respir Crit Care Med*. 2004;169(7):791–800.
32. Miedema M, de Jongh FH, Frerichs I, van Veenendaal MB, van Kaam AH. Changes in lung volume and ventilation during surfactant treatment in ventilated preterm infants. *Am J Respir Crit Care Med*. 2011;184(1):100–5.

Publisher's Note

Springer Nature remains neutral with regard to jurisdictional claims in published maps and institutional affiliations.

Submit your manuscript to a SpringerOpen[®] journal and benefit from:

- Convenient online submission
- Rigorous peer review
- Open access: articles freely available online
- High visibility within the field
- Retaining the copyright to your article

Submit your next manuscript at ► [springeropen.com](https://www.springeropen.com)

Roubik K, Sobota V, Laviola M. Selection of the Baseline Frame for Evaluation of Electrical Impedance Tomography of the Lungs. In 2015 Second International Conference on Mathematics and Computers in Sciences and in Industry (MCSI) 2015 Aug 17 (pp. 293-297). IEEE.

Selection of the Baseline Frame for Evaluation of Electrical Impedance Tomography of the Lungs

Karel Roubik, Vladimir Sobota, Marianna Laviola

Faculty of Biomedical Engineering
Czech Technical University in Prague
Kladno, Czech Republic
e-mail: roubik@fbmi.cvut.cz

Abstract—Electrical impedance tomography (EIT) is a promising modality for lung ventilation monitoring. It can provide information about the distribution of regional ventilation in predefined regions of interest (ROIs), as well as estimate several ventilatory parameters including tidal volume (V_T) or end-expiratory lung volume (EELV). The approaches for calculation of V_T and EELV are based on the values of global tidal variation (TV) and end-expiratory lung impedance (EELI) obtained by the means of functional EIT (fEIT). For reconstruction of fEIT data, a set of reference measurements, often called as a baseline frame, needs to be determined. The aim of the study is to show how setting of this baseline frame can influence the values of ROI, global TV and EELI and thus affect the estimation of V_T and EELV and the evaluation of lung recruitment as such. In order to study the effect of the baseline frame selection, an animal study (pigs, $n=3$) was conducted. The animals were anaesthetized and mechanically ventilated. Four incremental steps in positive end-expiratory pressure (PEEP), each having a value of 0.5 kPa were performed to reach a total PEEP level of 2.5 kPa. Continuous EIT monitoring was done during this PEEP trial. The obtained data were reconstructed using baseline frames chosen manually at five different PEEP levels. The selection of the baseline frames resulted in different values of global TV and EELI. Thus, when estimating V_T and EELV by means of fEIT, it is necessary to choose one common baseline frame for data reconstruction. However, the effect on the percentage values that express the distribution of regional ventilation is negligible and below clinical significance.

Keywords—electrical impedance tomography; EIT; functional EIT; fEIT; region of interest; ROI; end-expiratory lung impedance; EELI; end-expiratory lung volume; EELV; positive end-expiratory pressure; PEEP; mechanical ventilation; monitoring; respiratory care Introduction

In clinical routine, computed tomography (CT) is considered as the gold standard for evaluation of lung recruitment and lung aeration inhomogeneity. Nevertheless, CT has disadvantages that should be taken into account, including a high dose of ionizing radiation, inaccessibility of CT bedside and impossibility of its continuous usage. Electrical impedance tomography (EIT) does not have these disadvantages; therefore, EIT might be a suitable alternative to CT for the lung monitoring. However, due to the physical principle used, the reconstruction problem of EIT is rather difficult and when compared with CT, the resulting images have a low spatial resolution [1, 2].

Currently, there are two principal types of EIT images: absolute and functional (often also called as “relative”) [3]. Absolute images provide an information about the distribution of complex electrical impedance within the selected cross-section of the chest [4]. Their main advantage is a possibility to evaluate a development of lung tissue or a pulmonary disease and are thus greatly valuable, especially in neonatal intensive care [5, 6]. Unfortunately, to calculate absolute EIT images, precise information about the chest geometry and about the position of electrodes is necessary. Since obtaining these parameters can be troublesome in clinical environment, a concept of functional imaging was developed to circumvent this problem. [7, 8]. In functional EIT (fEIT), the measured data are normalized using a vector of reference measurements [7]. This vector is frequently determined by choosing a reference frame (sometimes called as “baseline frame”) or by calculation of average values over a certain time period [3]. The approach of fEIT eliminates most of the artifacts caused by the chest geometry, but the information about the complex electrical impedance is lost [3]. However, the evaluation of lung ventilation remains feasible. As no further information about the patient’s chest or about the position of electrodes is necessary, fEIT imaging is becoming popular in clinical routine.

The interpretation of information provided by EIT is still rather difficult, even for experienced users [2]. Therefore, several approaches were developed to evaluate lung ventilation. In spatial domain, one of the basic methods is to split the image into the regions of interest (ROIs) and calculate the proportions of ventilation in these regions [9, 10]. Several studies also proved that some useful ventilation parameters can be estimated from fEIT measurements. Linear relationship has been shown between tidal volume (V_T) and global tidal variation (TV) values derived from fEIT when previous calibration is performed [11]. Similarly, good or moderate agreement has been found between end-expiratory lung volume (EELV) and end-expiratory lung impedance (EELI) in [12] and [13], respectively.

As the reconstruction of fEIT images is dependent on the setting of baseline frame, we hypothesized that also parameters derived from fEIT might be influenced by the selection of the baseline frame as well.

The aim of the study is to show how setting of reference measurement (baseline frame) can influence the values of ROI, global TV and EELI and thus affect the estimation of V_T and EELV and the evaluation of lung recruitment as such.

I. METHODS

The study was approved by the local Ethics Committee and is in accordance with Act No. 246/1992 Coll., on the protection of animals against cruelty. The measurements were performed at the accredited animal laboratory of the First Faculty of Medicine, Charles University in Prague.

Three crossbred Landrace female pig (*Sus scrofa domestica*) with a body weight 48 ± 2 kg were used in this study.

A. Anesthesia and preparation

The animals were premedicated with azaperone (2 mg/kg IM). Anesthesia was initiated with ketamine hydrochloride (20 mg/kg IM) and atropine sulphate (0.02 mg/kg IM), followed by boluses of morphine (0.1 mg/kg IV) and propofol (2 mg/kg IV). A cuffed endotracheal tube (I.D. 7.5 mm) was used for intubation. Anesthesia was maintained with propofol (8 to 10 mg/kg/h IV) in combination with morphine (0.1 mg/kg/h IV) and heparin (40 U/kg/h IV). To suppress spontaneous breathing, myorelaxant pipecuronium bromide (4 mg boluses every 45 min) was administered during mechanical lung ventilation. Initially, rapid infusion of 1 000 mL of saline was administered intravenously, followed by a continuous IV administration of 250 mL/h to reach and maintain central venous pressure of 6 to 7 mmHg. Mixed venous blood oxygen saturation (SvO_2), pulmonary artery pressure (PAP) and continuous cardiac output (CO) were measured by Vigilance (Edwards Lifesciences, Irvine, CA, USA) monitor.

B. Ventilation

Conventional ventilator Hamilton G5 (Hamilton Medical AG, Bonaduz, Switzerland) was used in the (S)CMV mode with the following setting: respiratory rate 18 bpm, FiO_2 21 %, I:E 1:2 with initial positive end-expiratory pressure (PEEP) of 0.5 kPa. The initial V_T was set to 8.5 mL/kg of the actual body weight and was titrated to reach normocapnia ($PaCO_2$ 40 ± 1 mmHg). During the study protocol four increasing PEEP steps of 5 cmH₂O were performed. Each PEEP level was maintained at least for 3 minutes.

C. EIT measurements

PulmoVista 500 (Dräger Medical, Lübeck, Germany) was used for the EIT measurements. The electrode belt (size S) was attached to the chest of the animal at the level of the 6th intercostal space. The frequency of the applied current was set to 110 kHz with amplitude of 9 mA. Data were acquired continuously with a frame rate of 50 Hz during the whole PEEP trial.

D. Data Processing

The measured data were pre-processed using Dräger EIT Data Analysis Tool 6.1 (Dräger Medical, Lübeck, Germany).

For each PEEP level, baseline frame was manually chosen among EELI frames and data were reconstructed using these baseline frames as a reference.

The processing of reconstructed data was performed in MATLAB 2014b (MathWorks, Natick, MA, USA). Impedance waveforms were calculated as a sum of pixel values in fEIT images. To obtain the same level of EELI values for the lowest PEEP level, the global minimum value of each impedance waveform was subtracted from all its points. EELI values were determined as local minima on the impedance waveform (more detailed explanation of this approach is given in [14]). Similarly, end-inspiratory lung impedance (EILI) values were determined as local maxima in the impedance waveform. Global TV was calculated for each breath as a difference between EILI and EELI. Four ROIs of equal size were chosen in the fEIT images (Fig 1). This setting is the same as the default definition of zonal ROIs in PulmoVista 500 EIT system. For each ROI, fractional impedance in percentage was calculated. To compare the changes in ROI values, boxplots were created in STATISTICA (StatSoft, Inc., Tulsa, OK, USA).

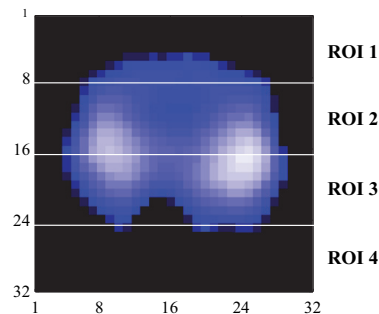


Fig. 1. Determination of the ROIs in the fEIT image.

II. RESULTS

According to the study protocol, data from 3 animals were processed. The impedance waveforms were reconstructed using five manually selected baseline frames, each from different PEEP level. An example of the waveforms is presented in Fig. 2. Both the curves of EELI and EILI are dependent on the baseline frame selection. The differences increase with the incremental PEEP levels at which the baseline frame was chosen.

For each impedance waveform, the values of global TV, as well as the fractional impedance change in selected ROIs were calculated. The results presented in Fig. 2 show, that the values of global TV differ when baseline frames are selected from different PEEP levels. Comparison of ventilation distribution in ROIs for one of the animals is shown in Fig. 2 as well and the comparison of ROIs calculated at two selected PEEP levels using two different baseline frames is in Fig 3. The variation of ROI values computed from the data obtained using baseline frames selected at different PEEP levels is much smaller than the variation in data provided by the EIT system PulmoVista 500 during mechanical ventilation of the animal. When reconstructing a dataset consisting of several measurements

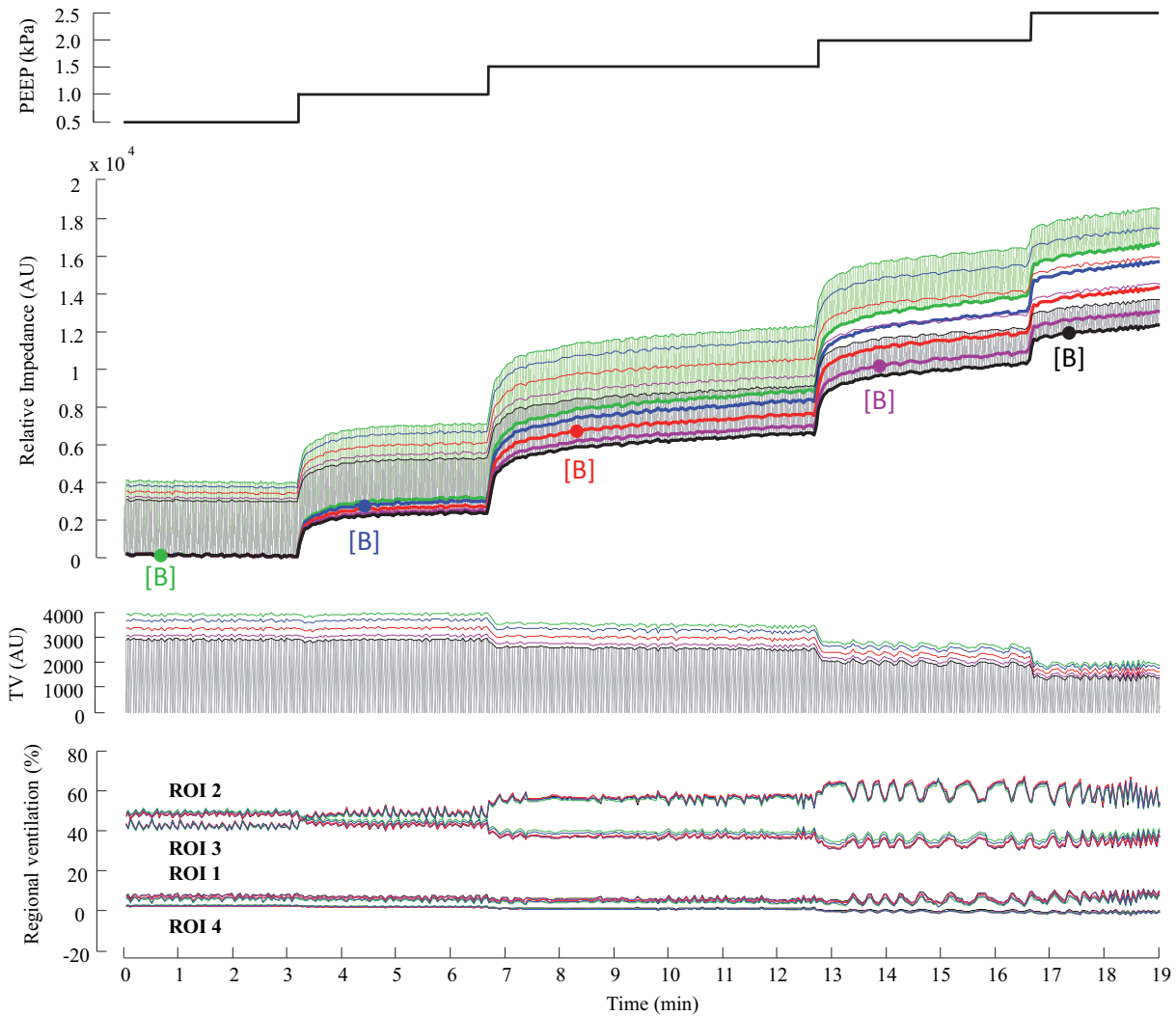


Fig. 2. Processing of impedance waveforms for evaluation of end-expiratory lung impedance (EELI), global tidal variation (TV) and fractional impedance in regions of interest (ROIs) during changes in positive end-expiratory pressure (PEEP). Top graph: PEEP values in time. The second graph from the top: impedance waveforms reconstructed for baseline frames selected for each PEEP level (marked as [B]; green: 0.5 kPa, blue: 1.0 kPa, red: 1.5 kPa, magenta: 2.0 kPa and black: 2.5 kPa). The bold line connects the end-expiratory lung impedance (EELI) points, the thin line connects the end-inspiratory impedance points. Only two complete impedance waveforms (light green for the baseline frame chosen at PEEP level of 0.5 kPa and gray for the baseline frame chosen at PEEP level of 2.5 kPa) are presented for clarity. The second graph from the bottom: comparison of global TV calculated from impedance waveforms that were reconstructed using the selected baseline frames. The complete data for baseline frame chosen at PEEP 2.5 kPa (gray) are presented for clarity. Bottom graph: regional ventilation distribution in selected ROIs in time. The colors of the curves correspond with the color coding of PEEP levels in the second graph from the top.

that follow each other, discontinuities in the impedance waveform were observed when baseline frames were chosen independently for each measurement as depicted in Fig. 4.

III. DISCUSSION

The main findings of the study are that selection of the baseline frame for fEIT data reconstruction has a minor effect on evaluation of ventilation distribution using ROIs whereas it has a substantial effect on evaluation of EELI and thus EELV.

There are small differences in the distribution of ventilation among ROIs when various baseline frames are selected for reconstruction of fEIT data. These differences might be statistically significant, but their magnitudes are in the order of units of percents. These magnitudes are typically smaller than the natural fluctuation in breath-to-breath results provided by the EIT system (see the bottom graph in Fig. 2) and their values are at the edge of clinical significance. Therefore, neglecting of these differences does not affect clinical interpretation of the calculated regional distribution of

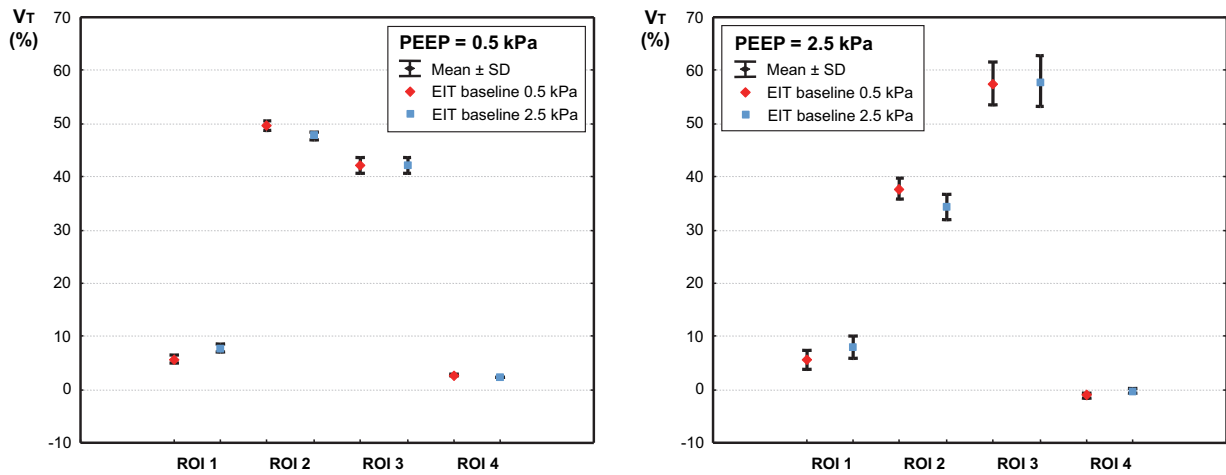


Fig. 3. Comparison of ventilation distribution at two selected PEEP levels (left: PEEP = 0.5 kPa, right: PEEP = 2.5 kPa) calculated from the data that were reconstructed using two baseline frames from different PEEP levels (red: 0.5 kPa, blue: 2.5 kPa).

ventilation. As a result, automated selection of the baseline frame, typically within a segment of EIT data currently analyzed and displayed by the EIT system, may be employed. This makes the evaluation easier without negative influence upon clinical interpretation.

On the other hand, when a long-time evaluation of the EELI (and thus EELV) is desired or when a comparison of two or more segments of EIT records is required, all the evaluated and compared segments should be reconstructed using an identical baseline frame.

The study was performed using the data from three animals. We do not consider this number as insufficient because the studied effect is caused by the reconstruction algorithm and the results were consistent for all pigs.

IV. CONCLUSION

EIT is an interesting method that can offer real time information about ventilation of lungs. Nevertheless, as EIT is not in fact a true imaging modality, the provided information is dependent on the quality and the way of processing.

Selection of the baseline frames at different PEEP levels results in different values of global TV and EELI. Thus, when

estimating V_T and EELV by means of fEIT , it is necessary to choose one common baseline frame for data reconstruction. However, the effect on the percentage values that express the distribution of regional ventilation is negligible and below clinical significance.

ACKNOWLEDGMENT

The authors would like to thank the employees of the animal laboratory of the Department of Physiology, The First Faculty of Medicine, Charles University in Prague, where the animal trial was performed.

The study was supported by grant OP VK CZ.1.07/2.3.00/30.0034, grants VG20102015062 and SGS14/216/OHK4/3T/17.

REFERENCES

- [1] D. Holder. *Electrical impedance tomography: methods, history, and applications*. Philadelphia: Institute of Physics Pub., 2005.
- [2] C. Putensen, H. Wrigge and J. Zinserling, "Electrical impedance tomography guided ventilation therapy," *Curr Opin Crit Care*, vol. 13, pp. 344-50, Jun 2007.
- [3] S. Leonhardt and B. Lachmann. "Electrical impedance tomography: the holy grail of ventilation and perfusion monitoring?" *Intensive Care Med*, vol. 38, issue 12, pp. 1917-1929, 2012.

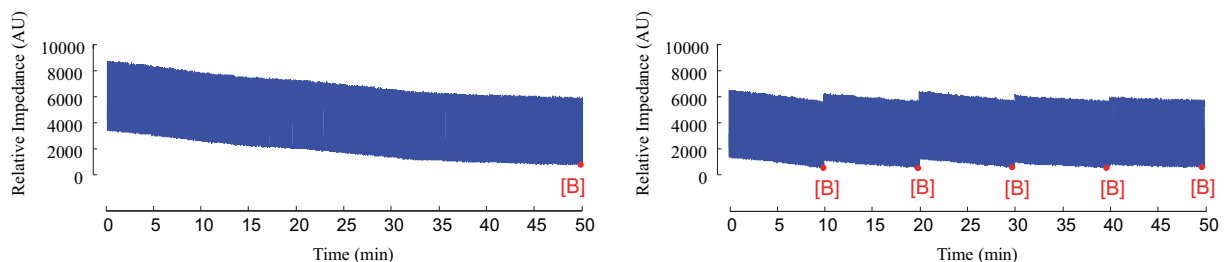


Fig. 4. The effect of baseline setting in a long-term EIT monitoring. Left: one common baseline frame (marked as [B]) was used for the reconstruction of several measurements. Right: each of the measurements was reconstructed using its own baseline frame.

- [4] B. H. Brown Electrical impedance tomography (EIT): a review. *J Med Eng Technol*, vol. 27, issue 3, pp. 97–108, 2003.
- [5] B. H. Brown, "Neonatal lungs – can absolute lung resistivity be determined non-invasively?" *Med Biol Eng Comput*, vol. 40, issue 4, pp. 388-394, 2002.
- [6] K. Buzkova and J. Suchomel. "Use of Electrical Impedance Tomography for Quantitative Evaluation of Disability Level of Bronchopulmonary Dysplasia," *2013 E-Health and Bioengineering Conference (EHB)*, IEEE, 2013.
- [7] D. C. Barber, "Quantification in impedance imaging". *Clin Phys Physiol Meas*, vol. 11, pp. 45–56, 1990.
- [8] G. Hahn, I. Sipinkova, F. Baisch and G. Hellige, "Changes in the thoracic impedance distribution under different ventilatory conditions," *Physiol Meas*, vol. 16, pp. 161–173, 1995.
- [9] S. Pulletz, H. R. van Genderingen, G. Schmitz, G. Zick, D. Schadler, J. Scholz, N. Weiler, and I. Frerichs, "Comparison of different methods to define regions of interest for evaluation of regional lung ventilation by EIT," *Physiol Meas*, vol. 27, pp. 115-27, 2006.
- [10] K. Lowhagen, S. Lundin and O. Stenqvist, "Regional intratidal gas distribution in acute lung injury and acute respiratory distress syndrome assessed by electric impedance tomography," *Minerva Anesthesiol*, vol. 76, issue 12, pp. 1024-35, 2010.
- [11] A. Adler, R. Amyot, R. Guardo, J. H. Bates and Y. Berthiaume, "Monitoring changes in lung air and liquid volumes with electrical impedance tomography," *J Appl Physiol*, vol. 83, issue 5, pp. 1762-1767, 1997.
- [12] J. Hinz, G. Hahn, P. Neumann, M. Sydow, P. Mohrenweiser, G. Hellige and H. Burchardi, "End-expiratory lung impedance change enables bedside monitoring of end-expiratory lung volume," *Intensive Care Med*, vol. 29, issue 1, pp. 37-43, 2003.
- [13] I. G. Bikker, S. Leonhardt, J. Bakker and D. Gommers, "Lung volume calculated from electrical impedance tomography in ICU patients at different PEEP levels," *Intensive Care Med*, vol. 35, issue 8, pp. 1362-1367, 2009.
- [14] J. Suchomel and V. Sobota, "A model of end-expiratory lung impedance dependency on total extracellular body water," *J Phys: Conf Ser*, vol. 434, issue 1, 2013.

Roubik K, Sobota V, Laviola M. Selection of the Baseline Frame for Evaluation of Electrical Impedance Tomography of the Lungs. In 2015 Second International Conference on Mathematics and Computers in Sciences and in Industry (MCSI) 2015 Aug 17 (pp. 293-297). IEEE.

Spontaneous breathing during high-frequency oscillatory ventilation improves regional lung characteristics in experimental lung injury

M. VAN HEERDE¹, K. ROUBIK², V. KOPELENT², M. C. J. KNEYBER^{1,3} and D. G. MARKHORST¹

¹Department of Pediatric Intensive Care, VU University Medical Center, Amsterdam, The Netherlands; ²Faculty of Biomedical Engineering, Czech Technical University in Prague, Kladno, Czech Republic and ³Department of Pediatric Intensive Care, Beatrix Children's Hospital, University Medical Center Groningen, Groningen, The Netherlands

Background: Maintenance of spontaneous breathing is advocated in mechanical ventilation. This study evaluates the effect of spontaneous breathing on regional lung characteristics during high-frequency oscillatory (HFO) ventilation in an animal model of mild lung injury.

Methods: Lung injury was induced by lavage with normal saline in eight pigs (weight range 47–64 kg). HFO ventilation was applied, in runs of 30 min on paralyzed animals or on spontaneous breathing animals with a continuous fresh gas flow (CF) or a custom-made demand flow (DF) system. Electrical impedance tomography (EIT) was used to assess lung aeration and ventilation and the occurrence of hyperinflation.

Results: End expiratory lung volume (EELV) decreased in all different HFO modalities. HFO, with spontaneous breathing maintained, showed preservation in lung volume in the dependent lung regions compared with paralyzed conditions. Comparing DF with paralyzed conditions, the center of ventilation was located at 50% and

51% (median, left and right lung) from anterior to posterior and at 45% and 46% respectively, $P < 0.05$. Polynomial coefficients using a continuous flow were -0.02 (range -0.35 to 0.32) and -0.01 (-0.17 to 0.23) for CF and DF, respectively, $P = 0.01$.

Conclusions: This animal study demonstrates that spontaneous breathing during HFO ventilation preserves lung volume, and when combined with DF, improves ventilation of the dependent lung areas. No significant hyperinflation occurred on account of spontaneous breathing. These results underline the importance of maintaining spontaneous breathing during HFO ventilation and support efforts to optimize HFO ventilators to facilitate patients' spontaneous breathing.

Accepted for publication 3 September 2010

© 2010 The Authors
Journal compilation © 2010 The Acta Anaesthesiologica Scandinavica Foundation

ONCE the mechanisms responsible for ventilator-induced lung injury (VILI) were elucidated, ventilator strategies were sought that could protect the already injured lung from additional harm.^{1,2} Lung-protective ventilation strategies aim at the reversal of atelectasis and avoidance of hyperinflation as well as cyclic opening and closing of lung units during tidal ventilation. High-frequency oscillatory (HFO) ventilation is, at least in theory, a ventilation modality that can achieve optimal lung protection. Several animal studies show that HFO ventilation reduces VILI.^{3,4}

Both experimental and clinical studies emphasize the positive effect of spontaneous breathing during mechanical ventilation on the distribution of inflation and ventilation in the diseased lung.

Spontaneous breathing improves oxygenation, lowers the need for sedatives, improves hemodynamics and reduces the duration of mechanical ventilation and intensive care stay.^{5–8}

In HFO ventilation, more conventional respiratory rates (RR) and tidal volumes, as in spontaneous breathing efforts, are not needed to achieve adequate gas exchange.⁹ Vigorous spontaneous breathing during HFO ventilation in large patients may in fact cause swings in set mean airway pressure (mP_{aw}) that activate alarms, interrupt oscillations and produce significant desaturations. Initial adult HFO ventilation trials recommended muscular paralysis for this reason.^{10,11} The current HFO ventilators' design (3100 A/B, SensorMedics, Yorba Linda, CA) with a fixed fresh gas rate makes it difficult to breathe during HFO ventilation.¹²

In an earlier paper, we reported on this animal experiment focused on work of breathing during HFO ventilation.¹³ We demonstrated that demand flow (DF), instead of a continuous fresh gas flow (CF), facilitated spontaneous breathing. The focus of this part of the experiment was to evaluate the effect of spontaneous breathing during HFO ventilation on lung aeration and ventilation in a porcine model of moderate lung injury with the use of electrical impedance tomography (EIT).

EIT is a noninvasive technique for pulmonary imaging. EIT provides meaningful dynamic information on pulmonary conditions. EIT is able to accurately describe both global and regional lung volume changes over time during mechanical ventilation.¹⁴ Compared with electron beam computed tomography, as an established method to assess changes in local air content, simultaneous EIT measurements correlate quite closely.^{14–16}

Materials and methods

Animal model preparation

The study was approved by the local Animal Welfare Committee. Eight Daland pigs 53 ± 6.5 kg (mean \pm SD) were used. Anesthesia was induced with an intramuscular injection of 0.5 mg atropine, 0.5 mg/kg midazolam and 10 mg/kg ketamine. After induction, propofol 3 mg/kg was injected intravenously before endotracheal intubation with a cuffed tube (inner diameter 8 mm). Anesthesia was maintained with continuous infusions of propofol 4 mg/kg/h and remifentanyl 0.4 μ g/kg/min during instrumentation and lung lavage. To allow spontaneous breathing, propofol dosage was reduced to 2 mg/kg/h, and that of remifentanyl to 0.05–0.1 μ g/kg/min. Spontaneous breathing was suppressed using pancuronium bromide 0.3 mg/kg/h during instrumentation, lung lavage and when necessary according to the experimental protocol. At the end, animals were euthanized using sodium pentobarbital.

During instrumentation, lung lavage and the stabilization period, animals were ventilated using a Servo 900C ventilator (Maquet Critical Care AB, Solna, Sweden) in the volume-controlled mode: RR 20/min, inspiratory pause time 0.6 s, positive end-expiratory pressure 5 cmH₂O, inspiration to expiration ratio 1:2, FiO₂ 1.0, initial tidal volume (V_T) 10 ml/kg and then adjusted to maintain normocapnia (PaCO₂ 38–45 mmHg). Animals were placed in a supine position on a heated table. Temperature

was maintained in the normal range (38–39 °C) using a heating pad.

The left femoral artery was cannulated to measure blood pressure and sample blood. A pulmonary arterial catheter was inserted to sample mixed venous blood. A separate catheter was inserted into the superior vena cava to infuse fluids and anesthetics.

Flow was measured at the proximal end of the endotracheal tube using a hot-wire anemometer (Florian, Acutronic Medical Systems AG, Hirzel, Switzerland). The pressure at the Y-piece in the ventilator circuit (P_{aw}) was sampled using the electronic signal from the internal pressure sensor of the HFO ventilator. The pressure sensor signal was calibrated using a water column. Flow and pressure signals were recorded at 100 Hz and stored on a laptop computer for off-line analysis.

Surfactant deficiency was induced by repeated whole lung lavage. Normal saline 30–40 ml/kg of 37 °C was instilled in the lungs at a pressure of 50 cmH₂O and then directly removed by drainage. The lavage was repeated after one hour.^{17,18}

HFO ventilator

HFO ventilation was applied using the 3100B HFO ventilator (SensorMedics). The HFO ventilator was used in a standard configuration with a CF. In order to facilitate spontaneous breathing, the HFO ventilator was equipped with a custom-made DF system. The DF system is able to respond to fluctuations in mP_{aw} on account of spontaneous breathing. The DF system is programmed to maintain a stable mP_{aw} . During inspiration, fresh gas flow is increased, and during expiration, decreased. The DF system is capable of delivering fresh gas flow from 0 to 160 l/min. A more detailed description of the system is given elsewhere.¹⁹

Study protocol

The study design is depicted in Fig. 1. After 30 min of stabilization on conventional ventilation (CMV) after the last lung lavage, HFO ventilation was initiated. Initial settings: mP_{aw} 20 cmH₂O, proximal pressure amplitude (ΔP) was set to attain normocapnia (38–45 mmHg) and thereafter remained unchanged, oscillatory frequency 5 Hz, inspiration/expiration ratio 1:2, fresh gas flow 20 l/min and FiO₂ 1.0. HFO ventilation was then applied for 30 min in three different modes: (1) continuous fresh gas flow of 20 l/min and spontaneous breathing

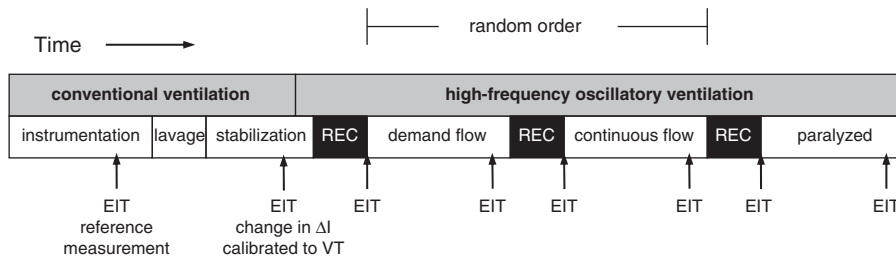


Fig. 1. Study design and electrical impedance tomography analysis. EIT, electrical impedance tomography measurement; rec, recruitment maneuver; ΔI , relative impedance change; V_T , tidal volume of spontaneous breathing.

maintained (CF), (2) DF and spontaneous breathing maintained (DF), both in random order, and in a last step (3) during muscular paralysis (PAR). EIT and physiologic measurements were performed during the last 5 min of every HFO ventilation modality. To avoid the occurrence of lung collapse on account of the preceding HFO ventilation run, a recruitment maneuver was performed preceding each HFO ventilation modality.^{20,21} At the start of the recruitment maneuver, mP_{aw} was increased to 30 cmH₂O for five minutes. mP_{aw} was then reduced in steps of 3 cmH₂O each 3 min until the animals started breathing in a regular pattern.

EIT measurements

EIT measurements were performed using the Göttingen Goe-MF II EIT system (Cardinal Health, Yorba Linda, CA). Sixteen electrodes (Blue Sensor BR-50-K, Ambu, Denmark) were circumferentially applied around the chest at the xyphoid level. A 30-s reference measurement was recorded before lung lavage (Fig. 1). All further measurements were referenced to this measurement. Measurements were performed at a scan rate of 44 Hz for 2 min. A 5 mA peak-to-peak, 50 kHz electrical current was injected at one adjacent electrode pair and the resultant potential differences were measured at the remaining adjacent electrode pairs. Subsequently, all adjacent electrode pairs were used for current injection, thus completing one data cycle. A back-projection algorithm calculated the changes in impedance in time and reconstructed topographic EIT images of 912 pixels representing local impedance changes in a circular plane.²²

EIT data analysis

Both the respiratory and the cardiac components of the EIT signal were identified in the frequency spectra generated from all EIT measurements (Fourier transformation). To eliminate the cardiac signal from the impedance measurements, the cut-off frequency of the low-pass filter was set below the heart rate, 0.67 Hz, 40 beats/min.²³ Figure 2A

depicts the method used for assessing the region of interest of the lungs before lung lavage.²⁴ For comparison of changes in expiratory lung volumes (EELV), the changes in impedance (ΔI) were calibrated to V_T during CMV after the last lung lavage (Fig. 1). For comparison of EELV, the change in EELV at the end of each HFO ventilation modality was referenced to the EELV at completion of the preceding recruitment maneuver. The EIT data were analyzed over three regions of interest, comprising the total area of the lungs and the upper and lower halves of the lungs (Fig. 2B).²⁵

The center of ventilation was determined in order to compare shifts in the distribution of ventilation between the three HFO ventilation modes. The center of ventilation was the point where the sum of fractional ventilation was 50% of the summed fractional ventilation (Fig. 2C).²⁶

To assess the occurrence of regional hyperinflation or recruitment on account of spontaneous breathing, regional filling characteristics of the lungs were calculated as depicted in Fig. 3.^{27,28} To do this, the local relative impedance change was compared with the total relative impedance change of all pixels during inspiration and then fitted to a polynomial function of the second degree: $y = ax^2 + bx + c$. See Fig. 3 for a detailed explanation.

Hemodynamic and respiratory variables

A MATLAB environment was used for data processing (MATLAB 7.04, The Mathworks, Natick, USA). The data processing is described elsewhere.¹³ In short, in order to eliminate HFO ventilator oscillations, the recorded flow and pressure signals were low-pass filtered using a seventh-order Butterworth filter with a cut-off frequency of 2.5 Hz. The filtered flow signal represented the flow change caused by spontaneous breathing of the pigs. From the integrated filtered flow signals, breathing pattern and minute ventilation were determined for each individual breath and averaged over a two-minute period. Arterial and mixed venous blood samples were analyzed using ABL505 and OSM3 hemoximeters

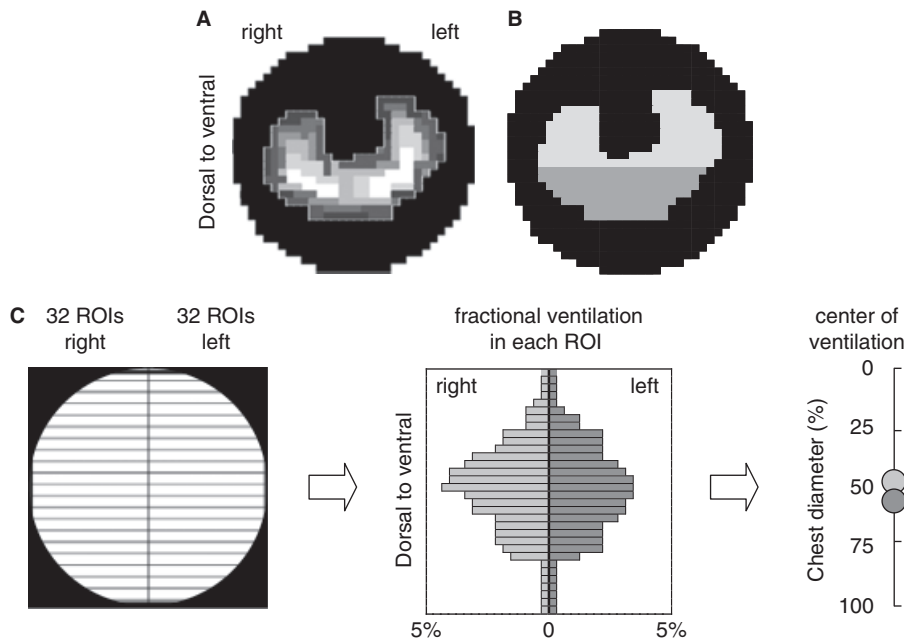


Fig. 2. Electrical impedance tomography analysis. (A) Example of an electrical impedance tomography (EIT) image. Gray areas, within the white line, represent those pixels where the impedance variation exceeded 20% of the maximum pixel variation in the image, corresponding with the lung. (B) EIT image showing the tree regions of interest (ROIs) used for the evaluation of end expiratory lung volume (EELV). The total lung, total gray area. The ventral and dorsal lung regions, the light and dark gray areas, respectively. (C) Example of determination of fractional regional lung ventilation. Each half of the scan is analyzed in 32 ROIs. The 64 values represent the ventral to dorsal profiles of local ventilation in the chest as a percentage of the total ventilation of each half of the EIT image. The center of ventilation was defined as the point where the sum of fractional ventilation was 50% of the summed fractional ventilation.

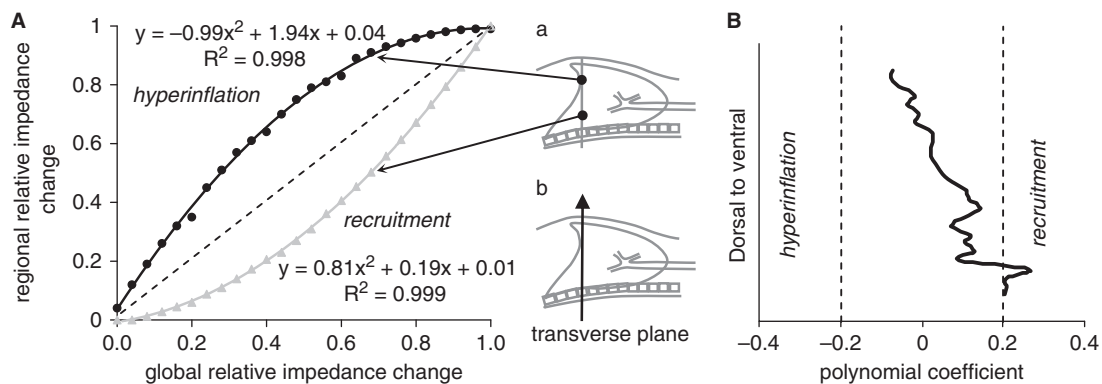


Fig. 3. Determination of regional filling characteristics. (A) Examples of relative impedance change in two individual pixels compared with the relative impedance change of all selected pixels representing the lungs. Both regional and global relative impedance change were calculated as a fraction of 1. Filling characteristics were calculated for every single spontaneous breath beginning at inspiration and ending at end-inspiration and averaged over the 2-min electrical impedance tomography (EIT) recording. ● and ▲ represent the measured data points of one single spontaneous inspiration in two different pixels. The plots were fitted to a polynomial of the second degree, $y = ax^2 + bx + c$, the black and gray lines. The polynomial coefficient of the second degree, a , describes the curve linearity of the plot. A polynomial coefficient a near zero (-0.2 to 0.2), near the dotted line, suggests a homogeneous regional tidal volume change on account of spontaneous breathing. A negative polynomial coefficient a (< -0.2) indicates low late regional filling and suggests local hyperinflation. A positive a (> 0.2) indicates low initial filling and suggests local recruitment. (B) Example of regional filling characteristics in the transverse plane in one animal. Polynomial coefficients of each individual pixel were averaged in each horizontal level in order to evaluate regional filling in the dorsal to ventral direction.

(Radiometer, Copenhagen, Denmark). Continuous arterial blood gas analysis was conducted by the Paratrend 7 (Biomedical Sensors, High Wycombe, UK). Respiratory indices were calculated according to standard formulas.²⁹

Statistical analysis

Data are expressed as median and 25th to 75th interquartile range (IQR) unless otherwise stated.

Parameter comparison for different HFO ventilation modes was performed using repeated measures analysis of variance with Bonferroni's *post hoc* testing. Parameter comparison for the polynomial coefficient was performed using the Wilcoxon signed rank test. In all analyses, a $P < 0.05$ was considered statistically significant. Statistical analysis was performed using SPSS 15 for Windows (SPSS, Chicago, IL).

Results

All animals completed the entire study protocol. Respiratory variables and data on gas exchange are summarized in Table 1. V_T of spontaneous breathing during HFO ventilation with DF was significantly higher, 5.1 ml/kg, compared with the V_T with continuous fresh gas flow, 4.3 ml/kg. Oxygenation improved in all HFO ventilation modes when spontaneous breathing was maintained. When pigs were paralyzed, PaO_2 decreased remarkably during the 30-min experimental period. PaCO_2 decreased using DF. PaCO_2 increased significantly using a continuous fresh gas flow and during muscular paralysis.

Figure 4 depicts the changes in EELV referenced to EELV after the completion of each preceding recruitment maneuver. In all HFO ventilation modalities, a decrease in lung volume was observed. Lung volume was significantly better preserved when spontaneous breathing was maintained. When ventral and dorsal lung regions were considered separately, changes in lung volume were most markedly in the dorsal lung areas.

In Fig. 5, the center of lung ventilation, determined from functional EIT measurements for all HFO ventilation modalities, is shown for the right and the left lung separately. When the animals were breathing spontaneously on HFO ventilation and DF was used, the center of ventilation significantly shifted towards the dependent dorsal parts of both lungs compared with the measurements during muscular paralysis.

Figure 6 summarizes the regional filling characteristics of all animals for both CF and DF. Summarizing all individual results, the polynomial coefficient calculated using HFO ventilation and continuous flow was -0.02 (IQR -0.05 to 0.14 , range -0.35 to 0.32). For measurements using DF, polynomial coefficients were significantly different -0.01 (IQR -0.006 to 0.11 , range -0.17 to 0.23), $P = 0.01$.

Discussion

The present study is the first to investigate the effect of spontaneous breathing during HFO ventilation on lung aeration and the distribution of ventilation. The main results of the animal experiment were that (1) lung volume was best preserved when spontaneous breathing was maintained during HFO ventilation, predominantly in the dorsal-dependent lung zones. (2) The use of DF during HFO ventilation shifted the center of ventilation to the dependent lung zones when compared with HFO ventilation during muscular paralysis. (3) There was no indication that spontaneous breaths during HFO ventilation resulted in regional hyperinflation.

When lung aeration was considered, a positive effect of spontaneous breathing during HFO ventilation was observed. Lung volume at the end of expiration of spontaneous breathing during HFO ventilation, both for CF and DF, was significantly higher compared with the measurements during

Table 1

Respiratory and physiologic variables during different high-frequency oscillatory ventilation modes.

	Spontaneously breathing		
	Continuous flow	Demand flow	Paralyzed
RR (min)	8.5 (7.8–9.4)	7.6 (6.4–9.9)*	
V_T (ml/kg)	4.3 (4.2–4.7)	5.1 (4.2–6.4)*	
MV (l/min)	2.1 (1.9–2.2)	2.2 (1.9–2.4)	
mP_{aw} (cmH ₂ O)	10 (9.9–11)	10 (8.7–11)	10 (9.9–11)
PaO_2 start (mmHg)	460 (454–498)	458 (421–509)	590 (536–611)*
PaO_2 end (mmHg)	493 (455–502)	473 (420–502)	451 (420–489)
ΔPaO_2 (mmHg)	19.9 (19.6–37)	31 (–5.5–84)	–140 (–225 to –53)*
PaCO_2 start (mmHg)	54 (47–58)	55 (51–56)	56 (48–62)
PaCO_2 end (mmHg)	53 (52–54)	49 (46–52)	70 (63–72)*
ΔPaCO_2 (mmHg)	6.3 (–3.0–18)	–5.7 (–4.3 to –7.4)*	9.9 (3.6–22)*, †

Data are expressed as median (IQR), $P < 0.05$;

*vs. continuous flow,

†vs. demand flow.

RR, respiratory rate; V_T , tidal volume of spontaneous breathing; MV, minute ventilation; mP_{aw} , mean airway pressure; PaO_2 start and PaO_2 end, PaO_2 at the start and at the end of the HFO ventilation modality; PaCO_2 start and PaCO_2 end, PaCO_2 at the start and at the end of the HFO ventilation modality; ΔPaO_2 and ΔPaCO_2 , difference in PaO_2 and PaCO_2 at the start and at the end of the HFO ventilation modality.

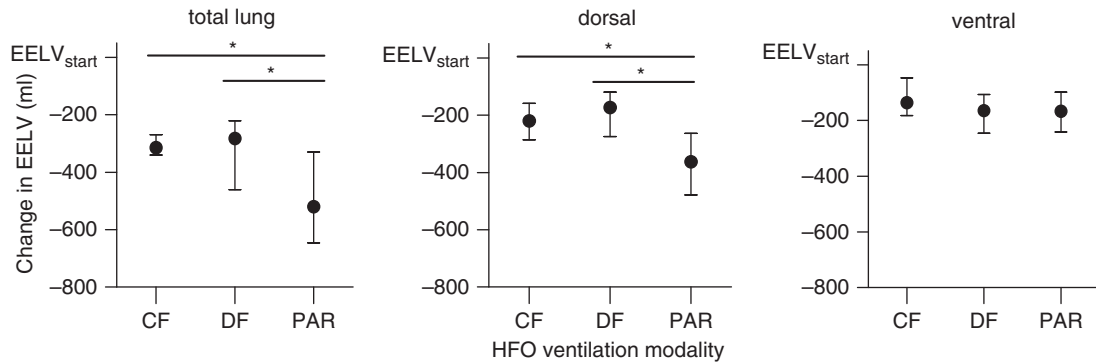


Fig. 4. Change in the end expiratory lung volume (EELV) determined from electrical impedance tomography (EIT) measurements for all high-frequency oscillatory (HFO) ventilation modalities. Data are expressed as median (IQR), *P < 0.05. The EELV at the end of each HFO ventilation modality is referenced to the EELV at the start (EELV_{start}) of the same 30-min experimental run. A comparison of change in EELV was performed for the total lung EIT measurement and for the ventral and dorsal lung zones separately. CF, continuous fresh gas flow; DF, demand flow; PAR, paralyzed.

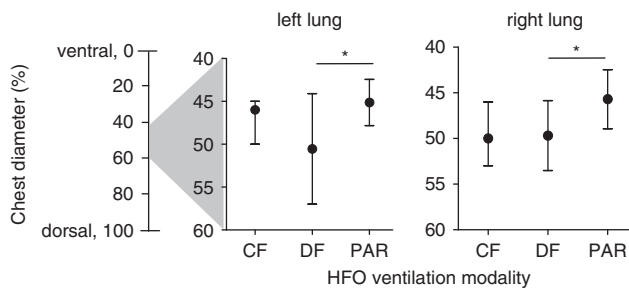


Fig. 5. Ventral to dorsal distribution of lung ventilation. Data are expressed as median (IQR), *P < 0.05. Ventral to dorsal distribution of lung ventilation determined from EIT measurements for all high-frequency oscillatory (HFO) ventilation modalities. The center of ventilation is depicted for the left and right lung separately. EIT, electrical impedance tomography; CF, continuous fresh gas flow; DF, demand flow; PAR, paralyzed.

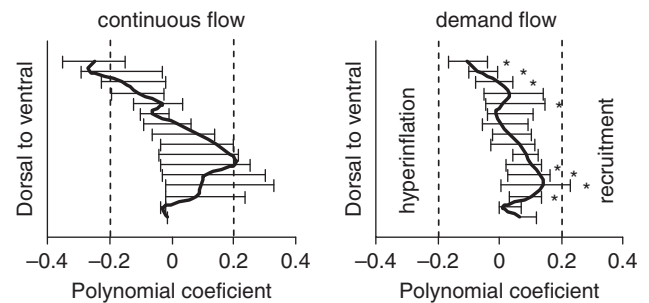


Fig. 6. Polynomial coefficients of regional versus global filling characteristics. Data are expressed as median (range), *P < 0.05. Polynomial coefficients of regional vs. global filling, on account of spontaneous breathing, in the dorsal to ventral direction. Results determined from electrical impedance tomography measurements during high-frequency oscillatory ventilation with continuous flow or demand flow.

muscular paralysis. The maintenance of EELV was most markedly in the dependent dorsal lung areas.

An explanation for the results on lung aeration is that ventilation and aeration are distributed differently when comparing spontaneous breathing and controlled mechanical ventilation.^{6,30} The most important factor responsible is the diaphragm. The diaphragm consists of an anterior tendon plate and a posterior muscle section. An active diaphragm lowers pleural pressure. As a result, transpulmonary pressure increases, enabling better aeration of dependent lung regions close to the diaphragm. In addition, during spontaneous breathing, the active dorsal muscle section of the diaphragm shifts the ventilation to the dorsal lung areas. A positive effect on lung aeration was already observed in several animal and clinical studies, when during mechanical ventilation, spontaneous breathing

contributed only 10–30% to the total minute ventilation.^{6,30–32}

After lung recruitment, a decrease in the lung volume was observed in all HFO ventilation modalities (Fig. 4). The decrease in the lung volume can be explained by the low mP_{aw} that could be applied. Higher mP_{aw} would have prevented lung collapse. However, high mP_{aw} is known to induce apnea in pigs, representing a limitation of the study (personal communication H. Wrigge from the department of Anesthesiology and Intensive Care Medicine of the University of Bonn). The decrease in the lung volume only coincided with a decrease in PaO_2 when pigs were paralyzed. When spontaneous breathing was maintained, the decrease in the lung volume did not lead to a decrease in PaO_2 . Considering the mechanisms of gas exchange during HFO ventilation spontaneous

breathing is not necessary.⁹ The results indicate, however, that a lower mP_{aw} may be required to achieve adequate gas exchange when spontaneous breathing is maintained.

We observed a significant shift in the center of ventilation to the dependent lung zones in favor of HFO ventilation with DF compared with HFO ventilation during muscular paralysis. This observation is in agreement with other studies that investigated the effect of lung recruitment on lung mechanics and the distribution of ventilation.²⁶ Thus, in the HFO ventilation with DF, the spontaneous breathing not only resulted in a better preservation of EELV, it also directed ventilation towards the dependent lung zones. The redirection of ventilation favored gas exchange, indicated by the increase in PaO_2 and decrease in $PaCO_2$ during HFO ventilation with DF.

One of the basic principles of a lung-protective HFO strategy is the application of small tidal volumes, usually below the anatomical dead space.⁹ Spontaneous breathing during HFO ventilation caused considerably larger volumes in our animal model. To assess the occurrence of regional hyperinflation and recruitment, regional filling characteristics of the lungs on account of spontaneous breathing were analyzed (Fig. 6). Regional filling characteristics of the lungs were more homogeneous when DF was used instead of continuous flow. The more homogeneous distribution can be derived from the fact that polynomial coefficients were closer to 0 throughout the lungs when the DF was used.

The cut-off values for the polynomial coefficients to indicate hyperinflation, recruitment or homogeneous filling are arbitrary. In a study describing the regional filling characteristics in mechanically ventilated adults with acute respiratory failure, $PaO_2/FiO_2 < 300$ mmHg, a much broader heterogeneity of regional filling was found.²⁸ In that study, minimal regional polynomial coefficients varied from -2.8 to -0.56 (median -1.16), and maximum coefficients varied from 0.58 to 3.65 (median 1.41). In comparison with these data, the regional filling characteristics we observed were more homogeneous.

Despite the fact that the tidal volumes of spontaneous breathing were higher using DF, there was no indication that this caused hyperinflation. It is an important observation with respect to the earlier discussed shift of the center of ventilation towards the dorsal lung regions when DF was used. This shift is explained by enhanced ventilation of the

dorsal lung regions, rather than hyperinflation of the anterior lung parts during the use of DF.

The interaction between spontaneous breathing and mechanical ventilation differs in various ventilation modes. Modes like airway pressure release ventilation (APRV) or biphasic positive pressure (BIPAP) ventilation allow unrestricted spontaneous breathing. In assist-control ventilation, only some breathing effort is necessary to trigger the ventilation and assist a breath. The presented modification of the HFO ventilator with a DF system allows unrestricted spontaneous breathing. The optimal mode for delivering partial ventilatory support is much discussed.³³ A recent prospective observational study, however, did not demonstrate a difference in outcome when APRV/BIPAP and assist/control ventilation were compared.³⁴

Not all research is in favor of the preservation of spontaneous breathing during mechanical ventilation. Some studies suggest that the use of neuromuscular blocking agents in the early phase of ALI/ARDS may improve oxygenation and reduce inflammation. Gentle spontaneous breathing may be beneficial; it can be argued that vigorous spontaneous respirations are contraindicated for the injured lung. Forceful respiration efforts can impose stress on the lungs and aggravate VILI.^{35,36} During our experiments with only mild lung injury, we observed calm spontaneous respirations with a limited tidal volume of spontaneous breaths. The effects of the HFO ventilator with DF on spontaneous breathing pattern and effort in severe lung injury need further study.

The animal study has limitations. As the application of high mP_{aw} prevented the animals from breathing spontaneously, only mild lung injury could be induced. Therefore, only two single lung lavages with no specific target for lung injury could be performed. With the limited lung lavage experimental conditions are not completely stable.¹⁷ The PaO_2 at the start of HFO ventilation during paralysis indicate that lungs improved during the experiment. Whether similar results would be observed during spontaneous in severe human ARDS, using an open lung strategy with higher mP_{aw} will require further research.

Conclusions

This animal study demonstrates that spontaneous breathing during HFO ventilation preserves lung volume and when DF was used improves ventila-

tion of the dependent lung areas. No significant hyperinflation occurred on account of spontaneous breathing. These results underline the importance of maintaining spontaneous breathing during HFO ventilation and support efforts to optimize HFO ventilators to facilitate patients' spontaneous breathing.

Acknowledgements

Financial support: The study was partly funded by the Ministry of Education, Youth and Sports of the Czech Republic, project number MSM 6840770012.

Conflict of interest: None.

References

1. Froese AB. High-frequency oscillatory ventilation for adult respiratory distress syndrome: let's get it right this time!. *Crit Care Med* 1997; 25: 906–8.
2. Tremblay LN, Slutsky AS. Ventilator-induced lung injury: from the bench to the bedside. *Intensive Care Med* 2006; 32: 24–33.
3. Muellenbach RM, Kredel M, Said HM, Klosterhalfen B, Zollhoefer B, Wunder C, Redel A, Schmidt M, Roewer N, Brederlau J. High-frequency oscillatory ventilation reduces lung inflammation: a large-animal 24-h model of respiratory distress. *Intensive Care Med* 2007; 33: 1423–33.
4. Meyer J, Cox PN, McKerlie C, Bienzle D. Protective strategies of high-frequency oscillatory ventilation in a rabbit model. *Pediatr Res* 2006; 60: 401–6.
5. Neumann PF, Schubert AF, Heuer JF, Hinz JF, Quintel MF, Klockgether-Radke A. Hemodynamic effects of spontaneous breathing in the post-operative period. *Acta Anaesthesiol Scand* 2005; 49: 1443–8.
6. Putensen C, Mutz NJ, Putensen-Himmer G, Zinserling J. Spontaneous breathing during ventilatory support improves ventilation-perfusion distributions in patients with acute respiratory distress syndrome. *Am J Respir Crit Care Med* 1999; 159: 1241–8.
7. Putensen C, Zech S, Wrigge H, Zinserling J, Stuber F, von Spiegel T, Mutz N. Long-term effects of spontaneous breathing during ventilatory support in patients with acute lung injury. *Am J Respir Crit Care Med* 2001; 164: 43–9.
8. Varelmann D, Muders T, Zinserling J, Guenther U, Magnusson A, Hedenstierna G, Putensen C, Wrigge HS. Cardiorespiratory effects of spontaneous breathing in two different models of experimental lung injury: a randomized controlled trial. *Crit Care* 2008; 12: R1351–63.
9. Pillow JJ. High-frequency oscillatory ventilation: mechanisms of gas exchange and lung mechanics. *Crit Care Med* 2005; 33: S135–41.
10. Derdak S. High-frequency oscillatory ventilation for acute respiratory distress syndrome in adult patients. *Crit Care Med* 2003; 31: S317–23.
11. Higgins J, Estetter B, Holland D, Smith B, Derdak S. High-frequency oscillatory ventilation in adults: respiratory therapy issues. *Crit Care Med* 2005; 33: S196–203.
12. van Heerde M, van Genderingen HR, Leenhoven T, Roubik K, Plötz FB, Markhorst DG. Imposed work of breathing during high-frequency oscillatory ventilation: a bench study. *Crit Care* 2006; 10: R231–7.
13. van Heerde M, Roubik K, Kopelent V, Plötz FB, Markhorst DG. Demand flow facilitates spontaneous breathing during high-frequency oscillatory ventilation in a pig model. *Crit Care Med* 2009; 37: 1068–73.
14. Richard JC, Pouzot C, Gros A, Tourevieille C, Lebars D, Lavenne F, Frerichs I, Guerin C. Electrical impedance tomography compared to positron emission tomography for the measurement of regional lung ventilation: an experimental study. *Crit Care* 2009; 13: R821–9.
15. Hinz J, Moerer O, Neumann P, Dudykevych T, Frerichs I, Hellige G, Quintel M. Regional pulmonary pressure-volume curves in mechanically ventilated patients with acute respiratory failure measured by electrical impedance tomography. *Acta Anaesthesiol Scand* 2006; 50: 331–9.
16. Schibler A, Calzia E. Electrical impedance tomography: a future item on the 'Christmas wish list' of the intensivist? *Intensive Care Med* 2008; 34: 400–1.
17. Grotjohan H, van der Heijde R. Experimental models of the respiratory distress syndrome: lavage and oleic acid. Rotterdam: Erasmus University, 2006.
18. Lachmann B, Robertson B, Vogel J. In vivo lung lavage as an experimental model of the respiratory distress syndrome. *Acta Anaesthesiol Scand* 1980; 24: 231–6.
19. van Heerde M, Roubik K, Kopelent V, Plötz FB, Markhorst DG. Unloading work of breathing during high-frequency oscillatory ventilation: a bench study. *Crit Care* 2006; 10: R1031–7.
20. Lachmann B. Open up the lung and keep the lung open. *Intensive Care Med* 1992; 18: 319–21.
21. Tingay DG, Mills JF, Morley CJ, Pellicano A, Dargaville PA. The deflation limb of the pressure-volume relationship in infants during high-frequency ventilation. *Am J Respir Crit Care Med* 2006; 173: 414–20.
22. Brown BH. Electrical impedance tomography (EIT): a review. *J Med Eng Technol* 2003; 27: 97–108.
23. Wolf GK, Grychtol B, Frerichs I, van Genderingen HR, Zurakowski D, Thompson JE, Arnold JH. Regional lung volume changes in children with acute respiratory distress syndrome during a derecruitment maneuver. *Crit Care Med* 2007; 35: 1972–8.
24. Hahn G, Frerichs I, Kleyer M, Hellige G. Local mechanics of the lung tissue determined by functional EIT. *Physiol Meas* 1996; 17 (Suppl. 4A): A159–66.
25. van Genderingen HR, van Vught AJ, Jansen JR. Estimation of regional lung volume changes by electrical impedance tomography during a pressure-volume maneuver. *Intensive Care Med* 2003; 29: 233–40.
26. Frerichs I, Dargaville PA, van GH, Morel DR, Rimensberger PC. Lung volume recruitment after surfactant administration modifies spatial distribution of ventilation. *Am J Respir Crit Care Med* 2006; 174: 772–9.
27. Frerichs I, Dudykevych T, Hinz J, Bodenstern M, Hahn G, Hellige G. Gravity effects on regional lung ventilation determined by functional EIT during parabolic flights. *J Appl Physiol* 2001; 91: 39–50.
28. Hinz J, Gehoff A, Moerer O, Frerichs I, Hahn G, Hellige G, Quintel M. Regional filling characteristics of the lungs in mechanically ventilated patients with acute lung injury. *Eur J Anaesthesiol* 2007; 24: 414–24.
29. Guyton AC, Hall JE. Textbook of medical physiology, 11th edn. Philadelphia: Elsevier Saunders, 2006.
30. Neumann P, Wrigge H, Zinserling J, Hinz J, Maripuu E, Andersson LG, Putensen C, Hedenstierna G. Spontaneous breathing affects the spatial ventilation and perfusion

- distribution during mechanical ventilatory support. *Crit Care Med* 2005; 33: 1090–5.
31. Wrigge H, Zinserling J, Neumann P, Defosse J, Magnusson A, Putensen C, Hedenstierna G. Spontaneous breathing improves lung aeration in oleic acid-induced lung injury. *Anesthesiology* 2003; 99: 376–84.
 32. Wrigge H, Zinserling J, Neumann P, Muders T, Magnusson A, Putensen C, Hedenstierna G. Spontaneous breathing with airway pressure release ventilation favors ventilation in dependent lung regions and counters cyclic alveolar collapse in oleic-acid-induced lung injury: a randomized controlled computed tomography trial. *Crit Care* 2005; 9: R780–9.
 33. Seymour CW, Frazer M, Reilly PM, Fuchs BD. Airway pressure release and biphasic intermittent positive airway pressure ventilation: are they ready for prime time? *J Trauma* 2007; 62: 1298–308.
 34. Gonzalez M, Arroliga AC, Frutos-Vivar F, Raymondos K, Esteban A, Putensen C, Apezteguia C, Hurtado J, Desmery P, Tomicic V, Elizalde J, Abroug F, Arabi Y, Moreno R, Anzueto A, Ferguson ND. Airway pressure release ventilation versus assist-control ventilation: a comparative propensity score and international cohort study. *Intensive Care Med* 2010; 36: 817–27.
 35. Forel JM, Roch A, Marin V, Michelet P, Demory D, Blache JL, Perrin G, Gannier M, Bongrand P, Papazian L. Neuro-muscular blocking agents decrease inflammatory response in patients presenting with acute respiratory distress syndrome. *Crit Care Med* 2006; 34: 2749–57.
 36. Forel JM, Roch A, Papazian L. Paralytics in critical care: not always the bad guy. *Curr Opin Crit Care* 2009; 15: 59–66.

Address:
Dr *Marc van Heerde*
Department of Pediatric Intensive Care
VU University Medical Center
Room 8D12
PO Box 7057
1007 MB Amsterdam
The Netherlands
e-mail: m.vanheerde@vumc.nl